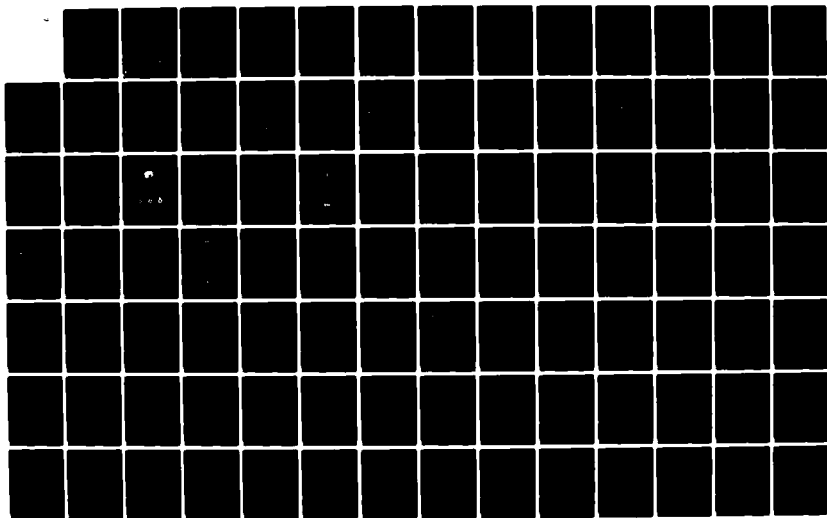


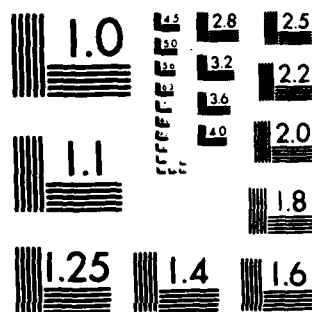
AD-A138 632 ANALYSIS OF SPACECRAFT CHARGING PARTICLE BEAMS AND
GEOPHYSICAL DATA BASES... (U) ARMY SIGNALS WARFARE LAB
VINT HILL FARMS STATION VA K H BHAVNANI ET AL.

1/2

UNCLASSIFIED 31 JUL 83 AFGL-TR-83-0140 F19628-80-C-0127 F/G 22/2

NL





MICROCOPY RESOLUTION TEST CHART
NATIONAL BUREAU OF STANDARDS-1963-A

12

AFGL-TR-83-0140

AD A138632

ANALYSIS OF SPACECRAFT CHARGING, PARTICLE BEAMS
AND GEOPHYSICAL DATA BASES

Krishin H. Bhavnani
William J. McNeil
Maurice F. Tautz

RADEX, Inc.
192 Log Hill Road
Carlisle, MA 01741

Final Report
May 1980 - May 1983

31 July 1983

Approved for public release; distribution unlimited

DTIC
ELECT
MAR 7 1984
A

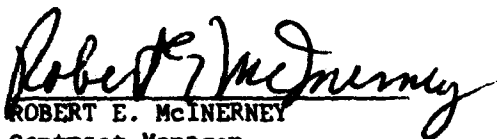
DTIC FILE COPY

AIR FORCE GEOPHYSICS LABORATORY
AIR FORCE SYSTEMS COMMAND
UNITED STATES AIR FORCE
HANSCOM AFB, MASSACHUSETTS 01731

84 03 06 039

This report has been reviewed by the ESD Public Affairs Office (PA) and is releasable to the National Technical Information Service (NTIS).

This technical report has been reviewed and is approved for publication


ROBERT E. MCINERNEY
Contract Manager


ROBERT E. MCINERNEY
Branch Chief

FOR THE COMMANDER


EUNICE C. CRONIN
Division Director

Qualified requestors may obtain additional copies from the Defense Technical Information Center. All others should apply to the National Technical Information Service.

If your address has changed, or if you wish to be removed from the mailing list, or if the addressee is no longer employed by your organization, please notify AFGL/DAA, Hanscom AFB, MA 01731. This will assist us in maintaining a current mailing list.

Do not return copies of this report unless contractual obligations or notices on a specific document requires that it be returned.

Unclassified

SECURITY CLASSIFICATION OF THIS PAGE (When Data Entered)

REPORT DOCUMENTATION PAGE		READ INSTRUCTIONS BEFORE COMPLETING FORM
1. REPORT NUMBER AFGL-TR-83-0140	2. GOVT ACCESSION NO. AD-A138632	3. RECIPIENT'S CATALOG NUMBER
4. TITLE (and Subtitle) ANALYSIS OF SPACECRAFT CHARGING, PARTICLE BEAMS AND GEOPHYSICAL DATA BASES		5. TYPE OF REPORT & PERIOD COVERED Scientific-Final May 1980-May 1983
		6. PERFORMING ORG. REPORT NUMBER
7. AUTHOR(s) Krishin H. Bhavnani William J. McNeil Maurice F. Tautz		8. CONTRACT OR GRANT NUMBER(s) F19628-80-C-0127
9. PERFORMING ORGANIZATION NAME AND ADDRESS RADEX, Inc. 192 Log Hill Road Carlisle, MA 01741		10. PROGRAM ELEMENT, PROJECT, TASK AREA & WORK UNIT NUMBERS 9993XXXX
11. CONTROLLING OFFICE NAME AND ADDRESS Air Force Geophysics Laboratory Hanscom AFB, Massachusetts, 01731 Contract Monitor: Robert E. McInerney/RMY		12. REPORT DATE 31 July 1983
		13. NUMBER OF PAGES 121
14. MONITORING AGENCY NAME & ADDRESS (if different from Controlling Office)		15. SECURITY CLASS. (of this report) Unclassified
		15a. DECLASSIFICATION/DOWNGRADING SCHEDULE
16. DISTRIBUTION STATEMENT (of this Report) Approved for public release; distribution unlimited		
17. DISTRIBUTION STATEMENT (of the abstract entered in Block 20, if different from Report)		
18. SUPPLEMENTARY NOTES Tech, Other		
19. KEY WORDS (Continue on reverse side if necessary and identify by block number) SPACECRAFT CHARGING SCATHA GEOMAGNETIC FIELD ELECTRON-ION BEAMS GRAPHICS PARTICLE TRACKING MATERIALS CHARGING CONTOUR ATMOSPHERIC DENSITY NASCAP ISOMETRIC ATMOSPHERIC WINDS PLASMAS IONIZATION ROCKET SPHERE		
20. ABSTRACT (Continue on reverse side if necessary and identify by block number) This report documents investigations and computer programs developed for study of spacecraft charging, ionization effects of beams, and analyses of geophysical data bases. Spacecraft charging studies have been performed utilizing NASCAP and the associated program MATCHG. → (over)		

DD FORM 1473
1 JAN 73

EDITION OF 1 NOV 65 IS OBSOLETE

1

Unclassified

SECURITY CLASSIFICATION OF THIS PAGE (When Data Entered)

Unclassified

SECURITY CLASSIFICATION OF THIS PAGE(When Data Entered)

The present ~~SCAT~~ operational system at AFGL, and procedures for representing spacecraft models and environmental parameters are described. Specific SCATHA satellite charging events were simulated in detail. Special studies of HELIOS 1, GEOS, and a simple Space Based Radar are also described.

Investigations for plasma definition and for determining threshold conditions for materials charging are summarized.

Ionization and charging characteristics due to electron and ion beam currents are simulated for simple spherical or cylindrical symmetries, and includes flight simulation predictions.

Particle trajectory studies were conducted for some basic electric field configurations, as well as for tracking particle beams in the geomagnetic field.

Atmospheric density and winds have been determined for a series of rocket sphere flights in the lower thermosphere. Analytical and data processing procedures are described.

An interactive graphics program (SUATEK) has been advanced. This system as well as some three-dimensional plotting packages, now available on-line, are summarized.

ACKNOWLEDGEMENTS

The guidance and encouragement of our Contract Monitor, Mr. Robert E. McInerney of the Data Systems Branch, as he coordinated our efforts in numerous phases of spacecraft charging, plasma and beam interactions, atmospheric structure, and graphical systems for their study, is greatly appreciated.

Drs. Herb A. Cohen, Shu T. Lai, Al G. Rubin, and Bert M. Shuman of the Spacecraft Interactions Branch, and Dr. C. Russ Philbrick of the Atmosphere Structure Branch have gratifyingly involved and guided the authors in the conduct and dissemination of many fine investigations in their respective fields. The collaboration of Dr. Nick A. Saflekos of SWRI (formerly with Boston College) was invaluable.

Thanks are also due to Art L. Besse, Nelson A. Bonito, Bob J. Raistrick, Dwight P. Sipler and other AFGL investigators whose support and interest contributed to a number of aspects of our work.



Accession For	
NTIS GRA&I	<input checked="" type="checkbox"/>
DTIC TAB	<input type="checkbox"/>
Unannounced	<input type="checkbox"/>
Justification	<input type="checkbox"/>
By	
Date (MM/DD/YY)	
Avail. and/or	
Special	
A-1	

TABLE OF CONTENTS

	<u>Page</u>
1.0 Spacecraft Charging	11
1.1 Operational System and Simulation Procedures	13
1.2 Plasma Environment Specification	16
1.3 Materials Charging Studies	22
1.4 Special Simulations.	26
1.5 Extended Simulation Studies.	40
References	52
2.0 Ionization and Charging Effects of Beam Currents.	53
2.1 The PLAS3 Model.	55
2.2 Method of Approach and Results	59
2.3 Extensions of the Model.	63
2.4 Flight Simulation.	64
References	66
3.0 Particle Tracking Studies	67
3.1 Particle Tracking near Charged Surfaces.	67
3.1.1 Quadrupole Model.	68
3.1.2 Circular Double Disk Model.	70
3.1.3 Circular Cap Model.	71
3.2 Evaluation of Geomagnetic Field Models	75
References	79

TABLE OF CONTENTS (continued)

	<u>Page</u>
4.0 Atmospheric Density and Winds from Accelerometer Data . . .	80
4.1 Telemetry Data Compaction and Splicing	82
4.2 Sensor Calibrations.	84
4.3 Trajectory Evaluation and Integration.	84
4.4 Evolving Resource and Profile Files.	85
4.5 Signal Demodulation and Conditioning	88
4.6 Sensor Orientation and Winds	90
4.7 Resolution of Density-Temperature Profiles	93
4.8 Tabular and Graphical Presentations.	97
4.9 Comparison with Other Concurrent Experiments	97
4.10 Evaluation of Reliability of Results	100
4.11 Auxiliary Associated Phenomena	102
References	103
 5.0 Interactive Graphics Systems for AFGL Applications. . . .	 104
5.1 Graphical Functions.	104
5.2 Analytical Functions	107
5.3 Data Base Structure.	107
5.4 Implementation of the Internal File Processing . . .	110
5.5 Implementation of the Interactive Modules.	110
5.6 Three Dimensional Graphical Systems.	113
5.6.1 Contour Plotting.	116
5.6.2 Isometric Plotting.	119
References	121

LIST OF FIGURES

	<u>Page</u>
1.1 NASCAP Simulation Operational System.	15
1.2 1 and 3-grid NASCAP Models of SCATHA.	17
1.3 ALLES Fits to SC9 Spectra	19
1.4 Plasma Parameter History for Day 114 Eclipse.	21
1.5 MATCHG Potentials - Time History (Day 113/81)	23
1.6 Threshold Conditions for Charging for ASTROQ.	25
1.7 Helios Model and Boom Potentials vs Rotation Angle.	27
1.8 (a) GEOS Model; (b) GEOS Potentials.	29
1.9 (a) Space Based Radar Model; b) SBR Potentials	32
1.10 SCATHA Potential Measured over a Five Month Span.	41
1.11 NASCAP Simulation for Eclipse of Day 114/79	43
1.12 Potential Contours at 27368 sec. UT on Day 114/79	44
1.13 Electron and Ion Phase Space Distributions for Day 113.	45
1.14 Corrected Electron Density and Temperature for Day 113.	47
1.15 NASCAP Simulation for Eclipse of Day 113/81	48
 2.1 Schematic of Ionization Process	 54
2.2 Charge, Field and Potential Profiles for High Current	60
2.3 Potential and Field Profiles for a Current Sweep.	61
2.4 Effect of Mean Ionization Length.	62
2.5 Flight Simulation Charging Characteristics.	65
 3.1 Potential Contours and Particle Trajectories - Quadrupole	 69
3.2 Potential Contours and Particle Trajectories - Double Disk.	72
3.3 Particle Beam Trajectory in the Geomagnetic Field	78

LIST OF FIGURES (continued)

	<u>Page</u>
4.1 Coordinate Systems for the Rocket Sphere.	81
4.2 Schematic of the Rocket Sphere Processing System.	83
4.3 Resource File (sample segment).	86
4.4 Processing System for Density, Temperature, Winds	87
4.5 Z-sensor and XY-sensor Accelerations.	89
4.6 Determination of Spin Phase and Crosstrack Wind	92
4.7 Composite Estimate for In-track Wind Profile.	94
4.8 Density-Temperature Profiles from ρC_d and V_R	95
4.9 Solved Density Ratio and Temperature Profiles	96
4.10 Plot of Geographic Wind Vector Profile.	99
5.1 SUATEK - Menu of Facilities	105
5.2 Description of Activatable SUATEK Options	106
5.3 General Specification for a SUATEK File	108
5.4 Summary Guide for SUATEK Interactive Input.	111
5.5 Sample Deck Set-up for a) Pen-and-Ink b) Microfiche Plots . .	114
5.6 SUAMRG Options and Sample Execution	115
5.7 SUACON - Interactive Contouring User Guide.	117
5.8 ISOTEK - Interactive Isometric Usage Sample	120

LIST OF TABLES

	<u>Page</u>
1.1 NASCAP Results for Space Based Radar Charging	34
1.2 Worst Case Study - Summary Cases 1 to 4	36
1.2 Worst Case Study - Summary Cases 5 to 8	37
3.1 Geomagnetic Field Models for Particle Trajectories.	76
4.1 Summary of Atmosphere and Wind Profile (AC13)	98
4.2 Solution Sensitivity Error Analysis (AC13).	101

1.0 Spacecraft Charging

Magnetospheric substorms at high altitudes are characterized by hot tenuous plasmas which can charge a satellite negatively to many kilovolts. The reliable estimation of the charging effects on present and future space vehicles has been a concern of the Air Force and NASA for several years, and a subject of considerable R&D activity. The inclusion of all factors that are significant for spacecraft charging presents a formidable problem. Complex three dimensional geometries with diverse surface materials and internal electrical properties have to be taken into account. The surface-plasma interaction which involve secondary emission, backscattering, photoemission and charge transport must be considered in detail. The magnetostatic environment may include solar, magnetic field, substorm and space charge effects. Charging dynamics can exist due to varying photoemission over a rotating or eclipsing satellite, changing plasma conditions, active control by electron or ion beams, and switching of electrically connected satellite configurations. Investigators at AFGL are widely involved in SCATHA satellite and other plasma physics research experiments.

For a number of years the analytical tool which most comprehensively represents these processes has been the NASCAP program developed by S-CUBED.^(1,4) This program represents an attempt to realistically simulate and depict spacecraft charging by numerically solving the full three dimensional problem. The NASCAP model uses a quasi-static Vlasov equation approximation to obtain surface charging fluxes, given potential distributions and the ambient environment conditions. Following calculation of

dielectric charge transport and surface charge distributions, the spatial potential problem (Laplace's equation) is solved using a finite element, nested-mesh technique. The iterative cycle then returns to the Vlasov flux charging equation. Elaborate plasma and material characteristics may be formulated in NASCAP, along with complex geometries and electrical connectivities of the surfaces.

Thus NASCAP is a major evolving engineering level program, as well as a tool for research on plasma sheath models and spacecraft charging experiments such as SCATHA. The NASCAP program was installed at AFGL in 1978 for the purpose of verification and validation, and as a means of support for investigations of charging phenomena.

Since installation, the program has been run extensively to analyze charging effects and to carry out simulation studies for SCATHA and other space vehicles. The early work focused on the identification of program bugs and computational instabilities. These studies were served by examining the charging behavior of simple objects such as NASCAP quasispheres and cylinders. Further testing of the NASCAP program was done by calculating sunlight charging of quasi-spheres for fixed sun direction and rotational motion.⁽³⁾ Preliminary SCATHA simulations were completed assuming simplified plasma environments.^(6,8) These runs included quasispheres, 2-grid and 4-grid SCATHA models. The effect of electron emitter beams on SCATHA charging was also examined.⁽⁷⁾ The most recent SCATHA simulations have implemented time dependent specification of the plasma environment and of solar flux.^(9,15)

1.1 Operational System and Simulation Procedures

The NASCAP source code is provided by S-CUBED on magnetic tape in blocked EBCDIC format. A number of steps are necessary in order to set up the system at AFGL:

- a) read the source tape and convert to CDC compatible format
- b) convert the NASCAP routines to UPDATE format and compile
- c) form a segmented version of the program which is small enough to fit on the CDC 6600

The final segmented binary file requires 276 K₈ to run. Also contained on the source tape are three NASCAP auxiliary programs:

PLOTREAD - reads plot files created by NASCAP and outputs microfiche

TERMTALK - reads the results files created by NASCAP, giving access to summary information.

MATCHG - uses NASCAP algorithms to calculate charging of material surfaces.

In addition, S-CUBED provides an auxiliary file, NASFILES, which contains default values for the surface material parameters, and object definition specifications for SCATHA models.

A number of major revisions of the NASCAP code and its auxiliary programs have been installed on the CDC-6600 system.

A comprehensive system has been implemented to facilitate program maintenance and operational logistics. Considerations provided for at AFGL are:

- a) coordination and compatibility with the UNIVAC 1100 version of NASCAP at S-CUBED)
- b) prompt revision of source, relocatable, and absolute codes
- c) tape storage of source codes and results files
- d) generation of microfiche plots using the auxiliary program PLOTREAD
- e) maintenance and modification of auxiliary programs MATCHG and TERMTALK.
- f) availability of SUATEK plotting routines for display of MATCHG and TERMTALK results
- g) maintenance and modification of program ALLES which calculates Maxwellian fits to spectra, for input to NASCAP
- h) generation of tapes and associated materials for external distribution of programs

The NASCAP simulation of a complex charging event entails considerable operational management. Input files containing the material parameters and the object definition information are required. A flux definition file, which describes the plasma environment, must be constructed. Provision for inputting the flux files to the auxiliary MATCHG program for trial run testing is advantageous. It is necessary to form a run options file from the NASCAP keyword list, in accordance with the rules of syntax and precedence. The run options file may contain repetitive modules for generating variable sunlight intensity or rotational motion. Special card blocks may be needed for specification of onboard beam emitter or detector characteristics. After completion of a NASCAP run the printed output and microfiche must be examined and interpreted, and the restart files either archived or reset for a continuation run. Inspection of the restart file information and plotting of summary and comparative results is made available through the auxiliary TERMTALK program. Figure 1.1 shows a schematic of the AFGL operational system for a NASCAP simulation study.

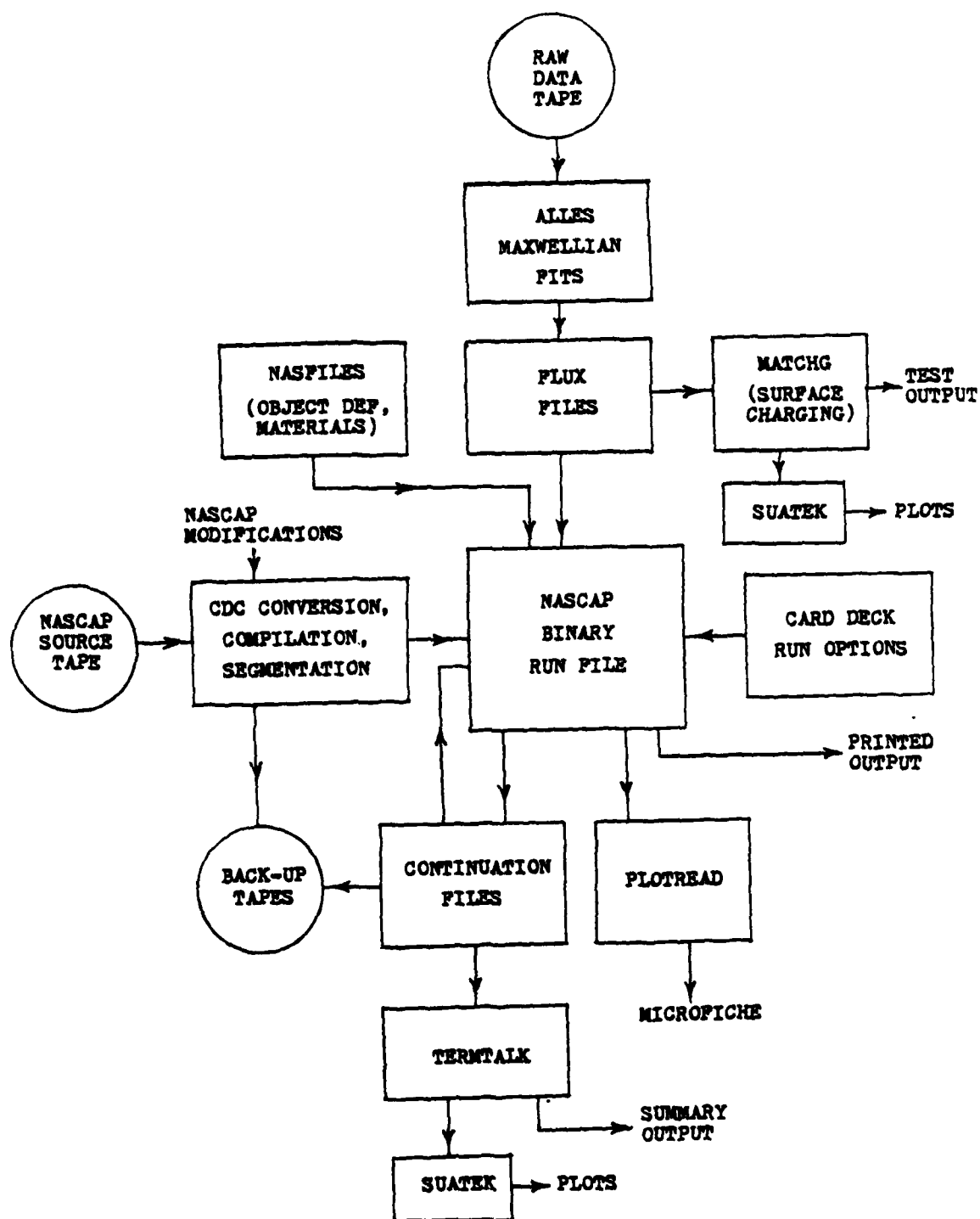


Figure 1.1 NASCAP Simulation Operational System

In the SCATHA simulations, the ambient plasma has been represented by single or double Maxwellian fits to measured data, as determined by the ALLES program. The material properties have been set to default values provided by S-CUBED. For the vehicle object specification, the 1, 2, 3 and 4-grid models of the SCATHA satellite have all been utilized.

The 1-grid and 3-grid models of SCATHA are shown in Fig. 1.2. The main difference between these two models is that the 3-grid version has a more detailed representation of the external booms. Since the computation time goes up rapidly with grid size, most of the analysis has been done with the 1-grid model.

1.2 Plasma Environment Specification

The accurate simulation of charging events requires a detailed representation of the ambient plasma. This is, in itself, a difficult problem and a substantial effort has been applied to the development of a program, ALLES, to generate parameter files to specify the environment. The program makes double Maxwellian fits to measured spectra data, with the plasma temperatures and densities as the floating parameters.

Plots of the individual fits versus the data, and summary plots of the fit parameters versus time are available. The following describes the fitting procedures that were used in the analysis of the day 114 (1979) charging event,⁽⁹⁾ based on spectra obtained from the SC9 experiment.

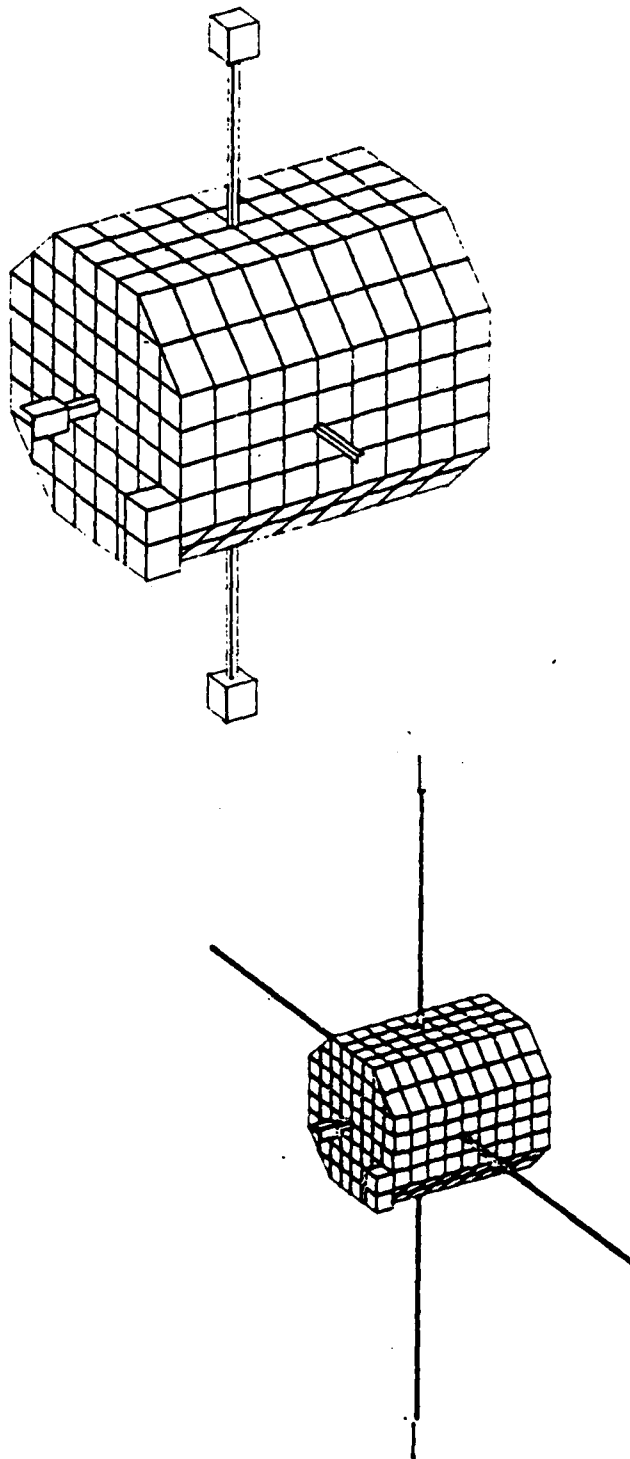


Figure 1.2 NASCAP 1-grid and 3-grid Models of SCATHA

The SC9 plasma data resides on magnetic tape in the form of electron and ion detector counts. The data was recorded at 16 sec intervals and the counts are distributed into 64 energy bins ranging from 0 to 80 KeV. In ALLES the raw counts are converted to phase space distribution functions f (units are sec^3/cm^6) by multiplying by appropriate calibration and phase space factors. Figure 1.3 shows a typical spectrum (UT=27368 secs). The lower two plots give $\ln(f)$ for the electrons (left) and ions (right). The upper plots give expanded views of the low energy region (0-10KeV).

In the analysis, the 15 lowest energy bins are disregarded. Also, the data points are corrected for the shift in the spectra due to vehicle charging. In the plots, the circles show the shifted points and the crosses denote the unshifted distribution. The method employed to fit the shifted spectra is outlined below:

- 1) The spectra are first split into high and low regions (the low energy range extends from vehicle ground plus 2 KeV up to the separation cut which was set at 15 KeV).
- 2) The high energy range (>15 KeV) is fitted with a single Maxwellian function.
- 3) This high energy fit is extrapolated back into the low region and subtracted from the data.
- 4) A second Maxwellian is fitted to the difference spectrum in the low energy region.

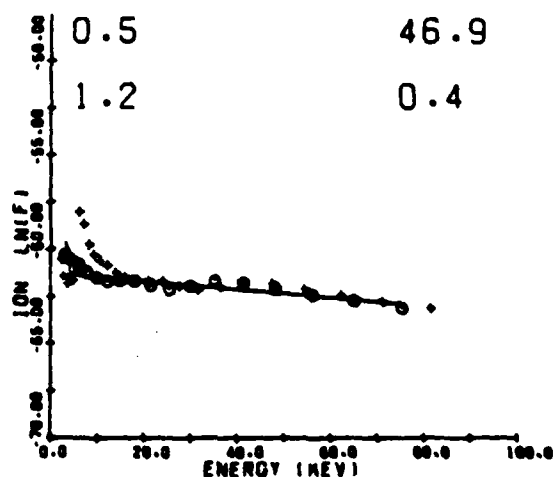
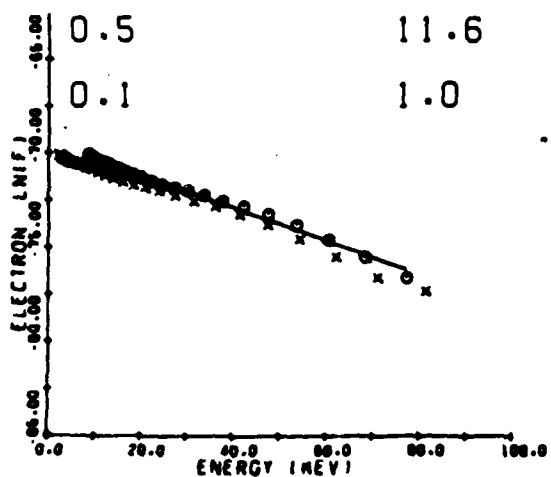
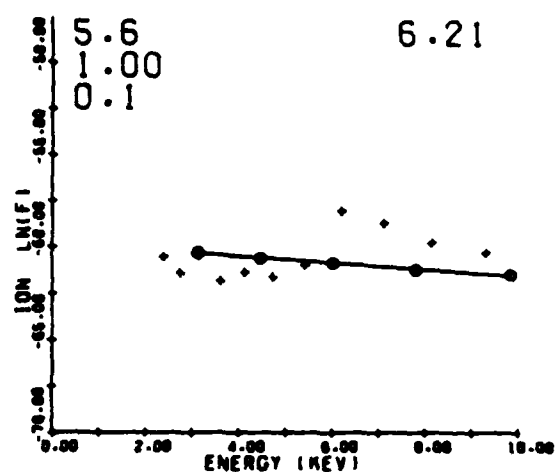
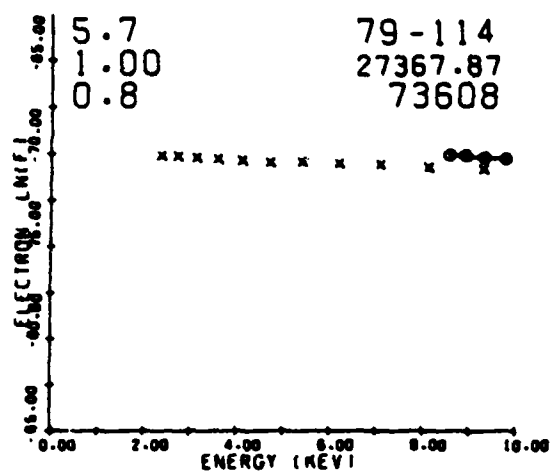


Figure 1.3 ALLES Fits to SC9 Spectra at 27368 sec. UT

A virtue of the above method is that it clearly separates the fits into high and low energy components. However, when the method was applied, it was found the the solutions reached could be very sensitive to the location of the separation cut. Moreover, sometimes no reasonable physical values were obtained from the fit. To remedy this situation, a second level of analysis was employed. The results from the above method were input as starting values for a general least squares fitting routine (if the first method fails, the values from the last previous successful case are input). This additional least squares fitting was invoked whenever it could improve the RMS error of the fit.

A typical fit to the data is displayed by the solid lines in the lower plots of Figure 1.3. The numbers in the upper corners give the fit parameters (temperatures and densities corresponding to the low and high regions). The solid lines in the upper plots show low energy single Maxwellian fits for comparison which were not used in the NASCAP simulation.

In Figures 1.4 (a)-(d) we summarize the derived plasma parameters for the day 114 full eclipse period. Although there are some fluctuations, the temperatures and densities are seen to be relatively flat over this time period.

Before being used for NASCAP simulations, a further change was made to the double Maxwellian fit parameters. The electron densities were renormalized to the ion densities to provide for charge neutralization and a correction was made for the O_2 content of the plasma.

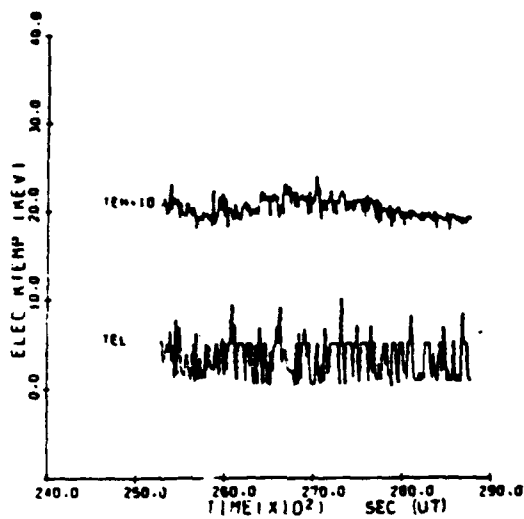


Fig. 4a. Electron temperatures
vs. UT

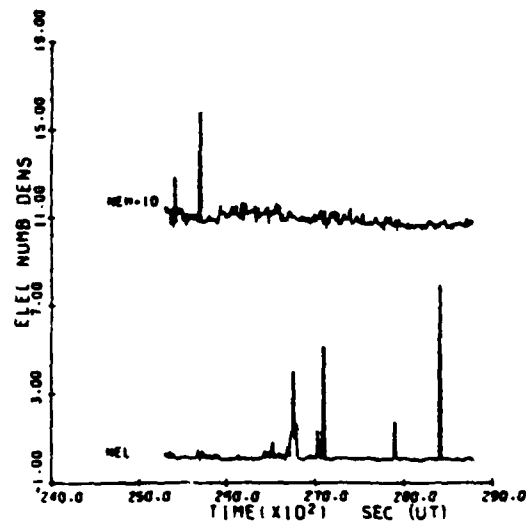


Fig. 4b. Electron number densities
(cm^{-3}) vs. UT

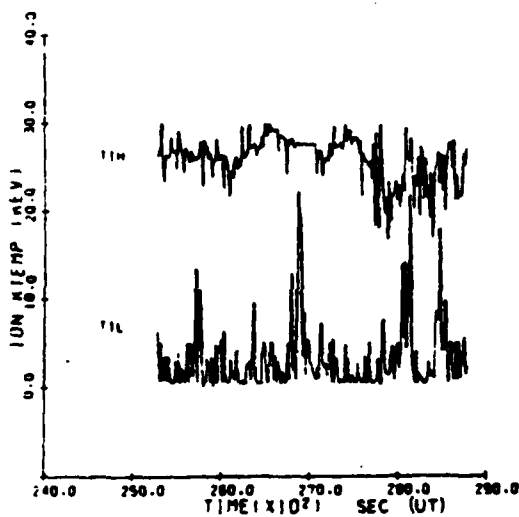


Fig. 4c. Ion temperatures
vs. UT

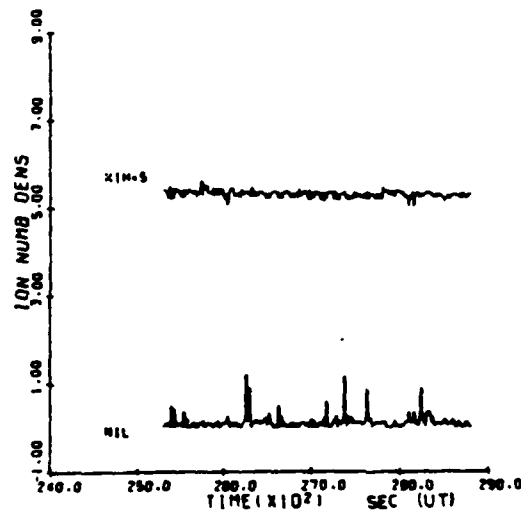


Fig. 4d. Ion number densities
(cm^{-3}) vs. UT

Figure 1.4 Plasma Parameters for Full Eclipse Period (Day 114/79)

1.3 Materials Charging Studies

The auxiliary program MATCHG provides an effective instrument for studying the interactions between a vehicle surface and a given plasma environment. The code calculates the equilibrium potential for any material, from the current balance equation, for cases where surface conductivity, photoemission, and multi-dimensional effects may be neglected. The MATCHG program has been run extensively to investigate the eclipse charging behavior of many different materials.⁽⁵⁾ The code has been utilized for sensitivity studies of the material properties, comparisons of the potentials for single and double Maxwellians, testing of alternate formulations for secondary emission equations, and various other studies of the surface-plasma interaction. The MATCHG code has been adapted so that it can read in the NASCAP flux definition files. In this way, the ALLES fits to spectra data can be input to MATCHG and time histories of the eclipse charging voltages can be produced. The results can be used to compare the effects of different fitting methods on the charging strength, or for making trial passes through the data, before employing the NASCAP code which consumes much more computer time. Figure 1.5 shows a time history of the MATCHG equilibrium voltages, corresponding to ALLES fits to the day 113, 1981 spectra data.⁽¹⁵⁾ Time histories can also be generated for all of the contributing currents at the material surface (primary plasma currents, secondary emission and backscatter currents, and bulk conductivity currents). This information can be quickly obtained and gives an indication of the relative importance of these effects throughout the charging simulation.

A series of MATCHG runs have been done to investigate systematically the threshold conditions for materials charging based on the current balance condition.⁽¹⁴⁾ The dynamics of the charging

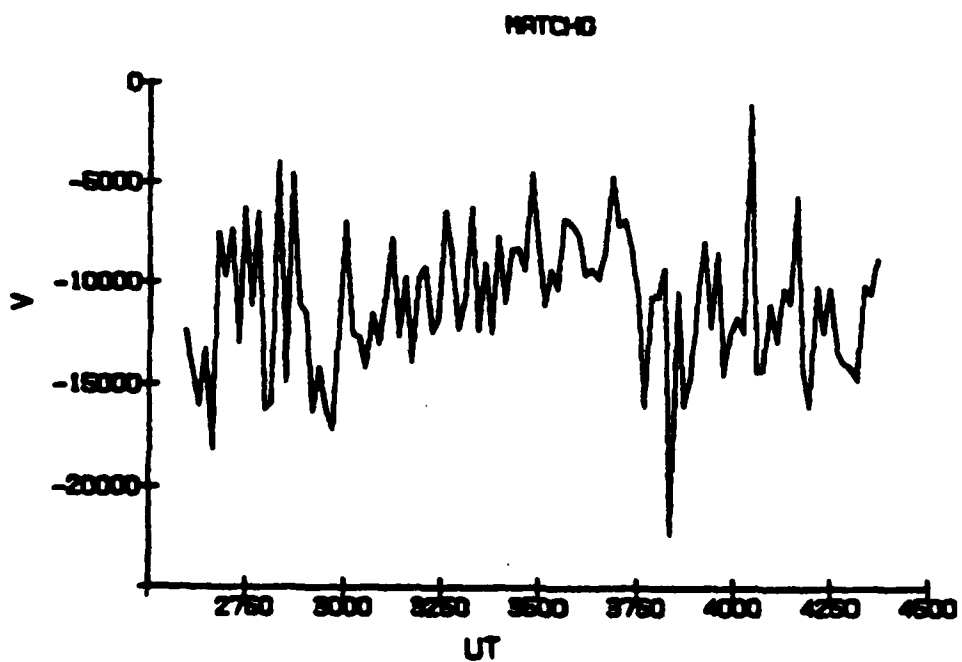


Figure 1.5 MATCHG Potentials versus UT for
Single Maxwellian Fits (Day 113/81)

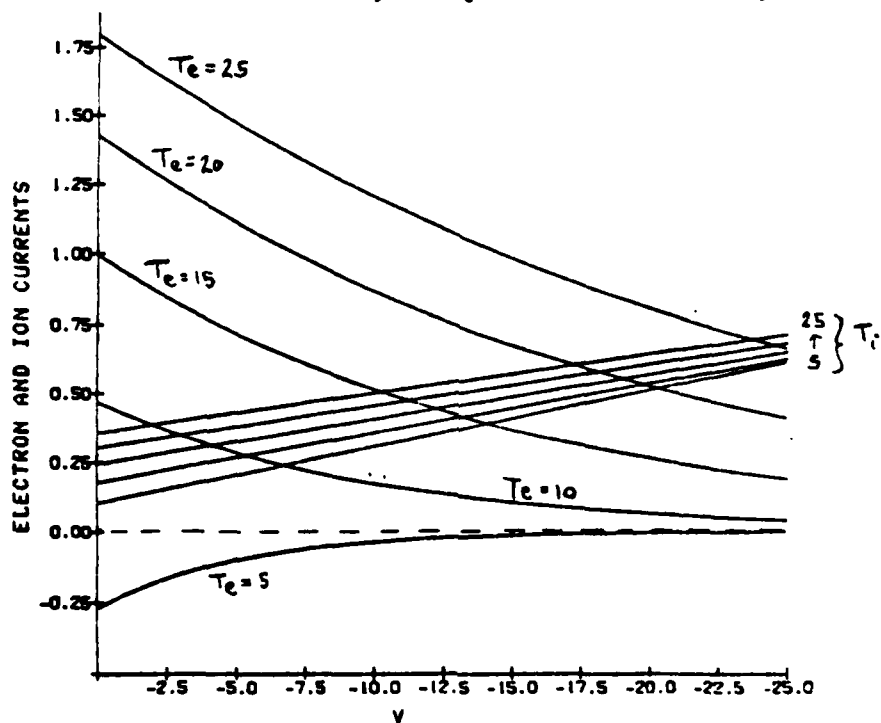
is illustrated in Figure 1.6(a) which shows the MATCHG electron and ion currents $-J_e(V)$ and $J_i(V)$ versus V for ASTROQ material. Each curve corresponds to a different Maxwellian temperature ($T_e, T_i = 5, 10, 15, 20, 25$). The plasma densities are taken as $n_e = n_i = 1$. The intersection of any two curves determines the equilibrium voltage V . The curve for $-J_e(V)$ with $T_e = 5$ lies below the origin and hence can never intercept a $J_i(V)$ line. This is an example of a case where the electron temperature is below the threshold and no charging can occur. The remaining $-J_e(V)$ curves start above the $J_i(V)$ lines at $V=0$ and charging takes place.

We have examined the threshold conditions for charging of a surface material immersed in a Maxwellian plasma. The threshold relations depend on the plasma temperatures and densities and on the material properties through the secondary emission coefficients $\delta^S(T_e), \delta^S(T_i)$ and the backscatter ratio $\delta^B(T_e)$. For a single Maxwellian plasma, the necessary condition for charging is that the electron temperature must be greater than the threshold temperature defined by

$$\delta(T_e) = -1 + \delta^S(T_e) + \delta^B(T_e) = 0$$

The values of this threshold function, calculated by MATCHG, are shown in Figure 1.6(b) for five different NASCAP materials. For a multi-Maxwellian plasma at least one of the electron temperatures must be above threshold and the net electron induced current must be negative. To arrive at necessary and sufficient conditions for charging, one has to take into account the ions as well as the electrons. Explicit formulas have been given for single and double Maxwellians. For a double Maxwellian, the threshold condition defines a linearly bounded region in the density space (n_{e1}, n_{e2}) .

a) $J_e(V)$ AND $J_i(V)$



b) $\delta(T_e) = -1 + \delta^S(T_e) + \delta^B(T_e)$

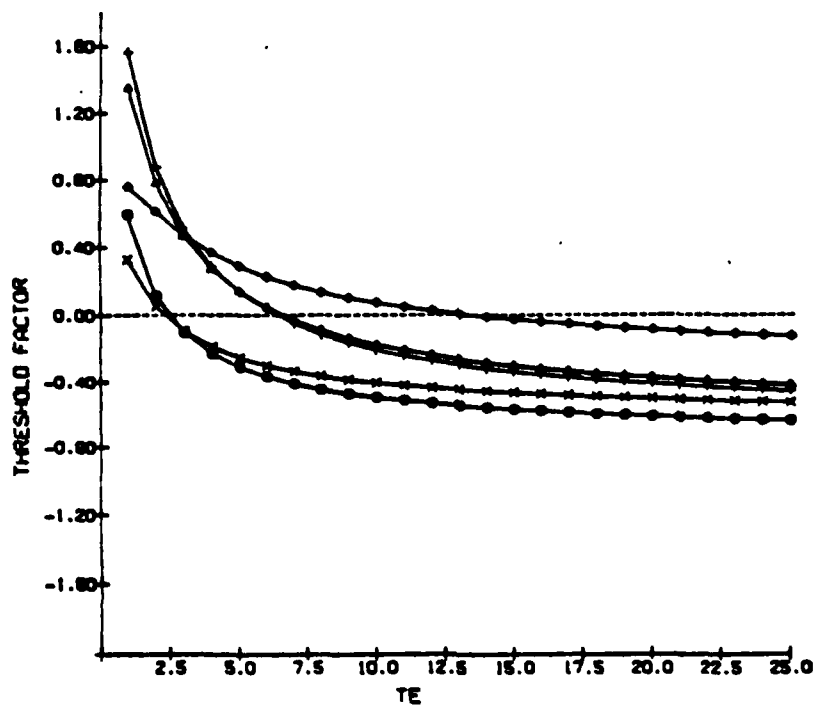


Figure 1.6 Threshold Conditions for Charging for ASTROQ Material

1.4 Special Simulations

The NASCAP model has been applied to several different space vehicles. A simple geometry was configured in order to represent the Helios 1 satellite and its external antenna boom.⁽¹⁰⁾ The NASCAP configuration that was used is shown in Figure 1.7. The satellite body is a 2x2 mesh cube. Attached is a single 16-segmented cylindrical boom (radius = 7mm) which is connected to a separate conductor (other than the vehicle ground) through a 200 pf condenser (the Helios antenna capacitance). In order to scale the system to correspond to the Helios dimensions, the mesh size was set to 1 meter.

Figure 1.7 also shows the boom potentials calculated during one cycle of the NASCAP rotate mode. Two curves are given: one for a cell at the base of the boom, and one for a cell at the boom tip. As can be seen, there is only a small variation of potential (≈ 1 volt) along the boom. Both curves show the expected spin modulation. When the boom is perpendicular to the sun direction ($\phi = +90^\circ, -90^\circ$), the photo current is a maximum and the voltage goes positive. When the boom is aligned with the sun ($\phi = 0^\circ, -180^\circ$) the cells go a few volts negative.

A comparison of Figure 1.7 with the Helios measurements of boom potential indicate that the amplitude of the oscillations are of the right order of magnitude. Considering the very simplified model that has been employed here, the above agreement is satisfactory. It demonstrates that the NASCAP program can successfully predict the spin modulated potential variations on a rotating boom, and that the details of the model are not significant for this case.

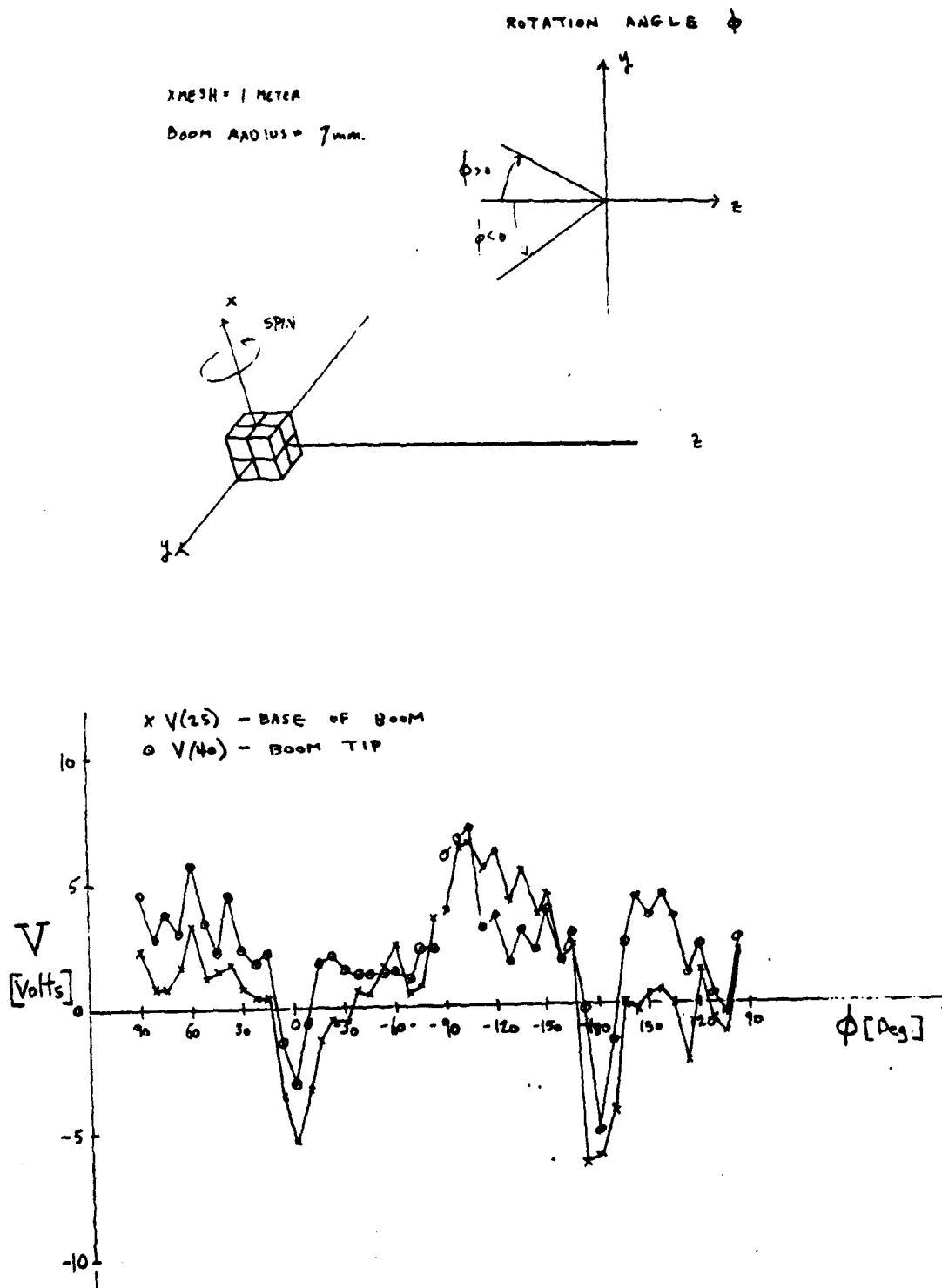


Figure 1.7 Helios Model and Boom Potentials vs Rotation Angle

The NASCAP program has been used to configure a model of the GEOS spacecraft and SPA sensor unit.⁽¹³⁾ The GEOS satellite consists of a cylindrical body with projecting booms. The Suprathermal Plasma Analyzer detector is mounted on one of the booms. The corresponding NASCAP model is described in Figure 1.8(a). The main features of the model are:

- a) The satellite body is built up from 5 vertically stacked 8x4 mesh octagons. The mesh size was taken as .2 m so the effective diameter is $8 \times .2 = 1.6$ m and the height is $5 \times .2 = 1.0$ m.
- b) Two external cylindrical booms of length $11 \times .2 = 2.2$ m extend out from the top of the satellite body.
- c) The SPA sensor unit is represented by a 1x1x1 mesh cube. The effective dimensions are thus 20x20x20 cm, which is slightly larger than actual size. The SPA cube was put on a separate conductor to allow for independent biasing.
- d) The lower 3 mesh units (.6m) of the satellite body is covered with the material Indox.
- e) All other surfaces (the top of the satellite, the booms, the SPA unit) are covered with Goldpd.

Sunlight charging of a GEOS satellite model for three representative voltages on the SPA detector were studied.

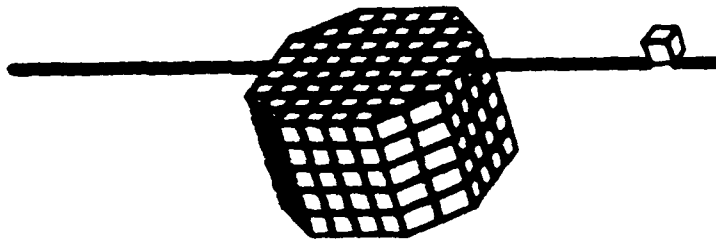


Figure 1.8(a) NASCAP Model of GEOS Satellite

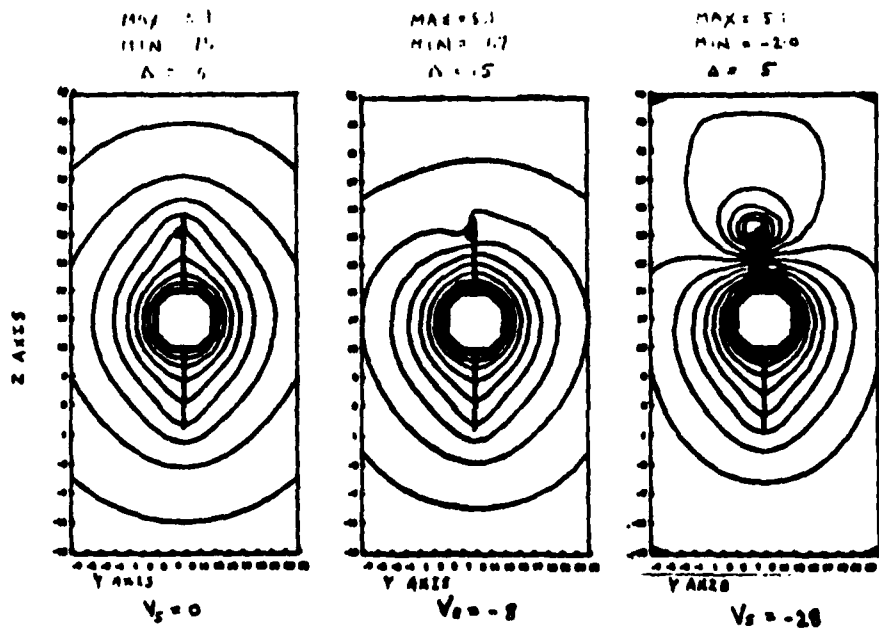


Figure 1.8(b) GEOS Potential Contours (Top View)

The primary questions to be examined were:

- 1) Are the local electrostatic fields around the detector significantly perturbed by changes in sensor bias?
- 2) Are the trajectories of low energy particles near the SPA instrument significantly altered by the sensor bias?

When the model is exposed to the expected plasma environment and sunlight, the vehicle frame potential goes a few volts positive. If the bias on the SPA surface is varied from 0 to -28 volts, the local field near the unit is modified and there is a significant change in the low energy trajectories. Figure 1.8(b) shows a top view of the potential contours around the GEOS model. The influence of the detector biasing on the contours is clearly evident.

The proposed Space Based Radar structure was modeled by NASCAP.⁽¹²⁾ The SBR vehicle is composed of three main components:

- 1) the lower side package (LSP) consisting mainly of the large antenna array.
- 2) the upper side package (USP) consisting of two gimbaled solar arrays.
- 3) the mast connecting LSP to USP.

The corresponding NASCAP model is given in Figure 1.9(a). The mesh size is 8 meters. The large antenna (LSP) is represented by an octagon of diameter 8 meshes = 64 meters (actual diameter = 71 meters).

The mast is a boom cylinder of diameter 2 meters and length 12 meshes = 96 meters (actual length 102.5 meters). The solar arrays (USP) are represented by a 2x2 mesh = 16 meter x 16 meter square.

The surface material on the large antenna (LSP) is mainly KAPTON with a small amount of ALUMINUM edge tape and the USP solar array is assumed to be borosilicate glass.⁽¹⁾ For the NASCAP model we have assumed that the LSP and the mast are covered with KAPTON and the USP with SOLAR material.

The SBR will be in polar orbit going through the auroral region at altitude $\approx 10,000$ km. The LSP antenna always points earthward, while the gimballed solar arrays align themselves with the sun direction. Relative to a coordinate system fixed on the SBR the sun appears to rotate through 360° on each orbit. We chose two representative positions, at $+45^\circ$ and -45° , for the NASCAP simulations.

Two test plasma cases were set up:

- 1) a "cool" plasma with $T_e=5$, $T_i=10$
- 2) a "hot" plasma with $T_e=10$, $T_i=20$

The densities were assumed to be 1 cm^{-3} . In the cold plasma the materials ALUMINUM and KAPTON would charge (in eclipse) but SOLAR would not. For the hot plasma all the materials would charge.

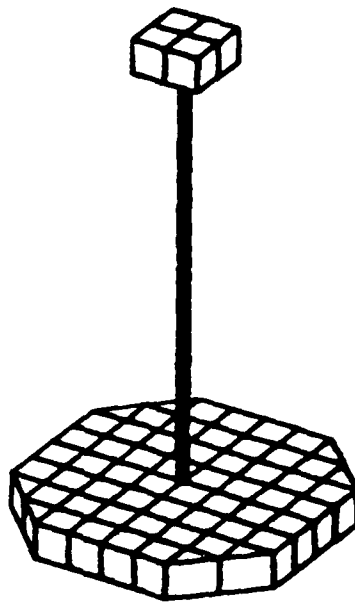


Figure 1.9(a) NASCAP Model of Space Based RADAR

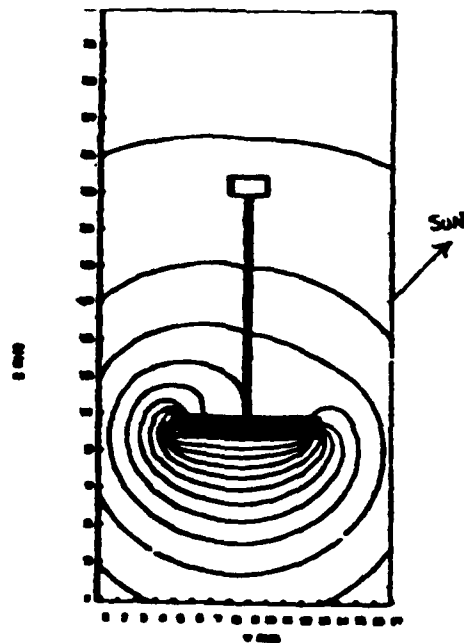


Figure 1.9(b) Potential Contours for 45° Sun Direction

The NASCAP runs that were considered are summarized in Table 1.1. The vehicle ground voltage and the potentials on selected surface cells are listed.

For case (1), the cool plasma is used and the sun is at angle $+45^{\circ}$. The vehicle ground charges to -1.8 KV. The potential contour plots indicate that charge builds up on the shade side of the LSP. The solar array does not charge and therefore the field lines are unperturbed near the USP.

Case (2) is the same as case (1) except that the hot plasma replaces the cool plasma. The vehicle ground thus increases to -5.1 KV. The potential contours are similar to those of case (1) but now the USP charges up and perturbs the potential lines in its vicinity.

Case (3) differs from case (2) in that the sun angle is changed from $+45^{\circ}$ to -45° . Here the contour lines build up on the topside of the LSP, which is now in the shade. The vehicle ground is about the same as for case (2).

The simplified NASCAP model of the SBR provides a possible scenario for vehicle charging. As it follows a polar orbit, the top and bottom sides of the LSP revolve into and out of the sunlight. If there is a low density ambient plasma present, with electron temperature greater than 3KeV , then the shade side of the LSP can charge up to the equivalent eclipse equilibrium voltage. If the plasma temperature is high enough ($\approx 6\text{KeV}$), then the shade side of the USP will charge. The potential contours are of the type shown in Figure 1.9(b).

TABLE 1.1 NASCAP RESULTS FOR SBR CHARGING

			CASE (1)	CASE (2)	CASE (3)
PLASMA			cool	hot	hot
SUN ANGLE			+45°	+45°	-45°
ITERATION STEP			17	15	15
TIME			1.02×10^5	3.2×10^4	3.2×10^4
	CELL#	MATERIAL	V	V	V
GROUND VOLTAGE	-1		-1803	-5149	-5174
LARGE ANTENNA LSP, bottom	2	KAPTON	-2681	-7467	-3010
LARGE ANTENNA LSP, top	1	"	-1329	-3802	-7468
MAST- bottom middle top	161	"	-1006	-3795	-7468
	166	"	-735	-2298	-3297
	172	"	-473	-2638	-2523
SOLAR ARRAY USP, bottom	65	SOLAR	-489	-3007	-2407
SOLAR ARRAY USP, top	64	SOLAR	-408	-1922	-3008

SCATHA charging in sunlight has been studied for a "worst case" plasma environment, based on SC5 measurements.^(2,11) In the NASCAP simulations an averaged double Maxwellian fit to the plasma spectrum was used. Due to uncertainties in the environment parameters we have not attempted to predict absolute potentials with NASCAP but, instead, have looked at the behavior of SCATHA charging, under a variety of input conditions, for comparative studies. The results of the NASCAP runs are given in Tables 1.2 and 1.3. The cases that have been considered are labelled from 1 to 8 as indicated.

Cases (1) and (2) compare eclipse charging for the 1-grid SCATHA model using secondaries of normal incidence (NORMAL) or with an isotropic distribution (ANGLE). It can be seen that the ground voltage is decreased from -10.9 KV to -7.0 KV when ANGLE replaces NORMAL. This reduction is due to the fact that more secondaries are emitted when the particles impinge on a surface isotropically. The ANGLE result is in good agreement with the voltage that was actually measured (≈ -8 KV) in the eclipse that occurred about 25 minutes later.

Cases (3) and (4) again make the comparison between NORMAL and ANGLE secondaries, but for a sunlight environment. Here the SPIN mode of NASCAP, set to give spin averaged illumination around the X-axis, has been employed. Again there is a large difference (-3.2 to -.74 KV) between NORMAL and ANGLE results for the ground voltage. The voltage for the ANGLE calculation is about a factor of two greater than the maximum measured sunlight potential (-.34 KV).

In the preceding runs, it was assumed that there was no biasing of the conductors 2 and 3 of the 1-grid model. To be consistent with the S-CUBED configuration, these conductors were biased to zero volts relative to conductor 1. Case (5) was run to test

TABLE 1.2 SUMMARY CASES 1 to 4 (WORST CASE)

		ECLIPSE		SPIN		
	CELL	MATERIAL	NORMAL	ANGLE	NORMAL	ANGLE
SC1-1	-1	GROUND	-10,886	-7039	-3155	-736
	-2	BOOMTIPS	-14,473	-9885	-1496	-498
	-4	REF BAND	-11,512	-7559	-2576	-1114
	279	KAPTON	-14,450	-9891	-2122	-614
	311	SOLAR	-15,160	-9731	-2136	-612
	309	INDOX	-10,890	-7039	-3155	-736
	419	GOLD	-11,860	-7695	-2108	-612
SC1-2	135	KAPTON	-14,450	-9891	-2174	-802
	352	GOLD	-10,890	-7039	-3155	-736
SC1-3	353	TEFLON	-13,250	-8168	-13,220	-8145
	362	KAPTON	-14,450	-9891	-14,440	-9865
	363	ASTROQ	-10,930	-7060	-3455	-1081
BOTTOM	2	WHITEN	-11,550	-7722	-5285	-2791
TOP	359	GOLDPO	-10,890	-7039	-3155	-736
JOB			TZWCEGR	TZWCE2F	TZWCS13	TZWCSAY
STEP			50	40	20	26
Δ (step)			-169	-145	-1	-7
CASE			1	2	3	4

TABLE 1.3 SUMMARY CASES 5 to 8 (WORST CASE)

	CELL	MATERIAL	SPIN		ROTATE	
			1-grid	3-grid	1-grid	3-grid
SC1-1	-1	GROUND	-689	-1371	-1231	-1908
	-4	REF BAND	-1087	-1639	-1540	-2123
	279/280	KAPTON	-585	-1477	-1453	-2244
	311	SOLAR	-583	-1284	-1389	-1734
	309/310	INDOX	-689	-1371	-1231	-1908
SC1-2	419	GOLD	-584	-1638	-1603	-2123
	135	KAPTON	-777	-1514	-1230	-1959
	352	GOLD	-689	-1371	-1230	-1908
SC1-3	353/354	TEFLON	-8153	-8163	-8601	-8675
	362/363	KAPTON	-9880	-9894	-10,360	-10,410
	363/364	ASTROO	-1035	-1704	-1566	-2222
BOTTOM	2	WHITEN	-2818	-3355	-3340	-3887
TOP	359	GOLDPD	-689	-1371	-1230	-1908
JOB			TZWCS3H	TZWCSBG	TZWCR3X	TZWCTIF
STEP			20	35	77(229)	51(225)
$\Delta V(\text{step})$			-19	-32	+40	-113
CASE			5	6	7	8

the effect of this change. By comparing cases (4) and (5) we see that this modification makes negligible difference to the charging. On subsequent runs, the zero biasing of conductors 2 and 3 was maintained.

Figure 1.2 shows the NASCAP 1-grid model of SCATHA and the corresponding 3-grid model. The only difference between the models is that the external booms have been modified. In the 3-grid model the booms extend out to actual length, and the surface material is changed from BOOMAT to KAPTON. The cell numbering differs slightly for the two models. In column 1 of Table 1.2 both numbers are given (1-grid first), where differences occur.

The 3-grid model was run in eclipse, and it was found to give virtually the same potentials as for the 1-grid model (case 2). This result is expected since the plasma is strong enough to charge the surface cells independently. The situation can be quite different in a weak plasma where the "boot strap" mechanism (charging cells influencing neighboring non-charging cells) can lead to substantial deviations in the potentials obtained from the two models.

Cases (5) and (6) compare the results for sunlight charging (in the SPIN mode) with the 1-grid and 3-grid models. It is evident that the 3-grid model charges higher (-1.37 KV versus -.69 KV). This result holds true also for cases (7) and (8) which make the same comparison relative to the ROTATE mode (-1.9 KV versus -1.23 KV). The potential contours for the 3-grid model are quite different in the region of the booms from those of the 1-grid model. Otherwise, the main features of the charging are the same i.e. the WHITEN cells in the bottom shade and the SC1-3 patch in the top-side shade are at the highest potentials.

By comparing cases (5) and (7) to cases (6) and (8) we see that the vehicle ground tends to be higher for the rotate mode than with SPIN for both the 1-grid model (-1.23 KV versus -.69 KV) and the 3-grid model (-1.91 KV versus -1.37 KV). This behavior is consistent with earlier NASCAP studies⁽³⁾ which gave the same result for a uniform quasisphere.

The NASCAP comparative runs illustrate the following characteristics of SCATHA charging:

- 1) The ANGLE mode for secondary emission produces less charging than NORMAL.
- 2) The 1-grid model charges up less than the 3-grid model.
- 3) The biasing of conductors 2 and 3 on the 1-grid model has little effect
- 4) The SPIN mode tends to give lower charging than for ROTATE.

In the ROTATE runs, the amplitude of the spin modulation can depend on the DVLIM parameter which may have to be adjusted from the default value.

The NASCAP calculation of the vehicle ground potential in sunlight is ≈ -1300 V (average over cases (5) to (8)), which is higher than the maximum measured value of -340 V. The eclipse charging result of ≈ 7.0 KV (from case(2)) is less than the estimated value of -16 KV (from Table 1). On the other hand the NASCAP result is quite close to the actual measured voltage of ≈ 8 KV for the eclipse which occurred later. The SSPM results for sunlight charging are mixed; the calculated voltages are found to be high for GOLD and SOLAR, low for QUARTZ, and in rough agreement with the KAPTON and TEFLON samples.

1.5 Extended Simulation Studies

The P78-2 SCATHA satellite was launched in January 1978, into a near-geosynchronous orbit. The satellite carries thirteen separate experimental payloads for analyzing spacecraft charging effects. The data from the UCSD charged Particle Experiment (SC9) was used to determine periods of strong eclipse charging, by looking for sharp peaks in the high resolution electrostatic analyser (ESA) ion count measurements. The channel number of the peak gives an estimation of the shift in energy due to particle acceleration into the detector, and thus of the spacecraft potential. This effect is clearly evident in the upper-right plot of Figure 1.3 where there is a clear peak in the ion distribution function at about 6.2 KeV corresponding to vehicle charging of 6.2 Kv. Figure 1.10 gives a summary of the spacecraft potential versus UT for the most active charging days of the 1979 eclipse seasons. The "worst case" charging event occurred on day 114, 1979 and this was chosen for a NASCAP simulation study.⁽⁹⁾

On day 114, the SCATHA satellite was in full eclipse from UT=26055 to UT=28868. The NASCAP simulation runs were started at UT=25950, with the vehicle initially uncharged and the sun intensity equal to zero. This procedure approximates the actual situation where the vehicle was charged slightly (≈ 400 volts) in sunlight and the sun intensity rapidly decreased to zero.

The NASCAP 1-grid model (see Figure 1.2) was used to represent the SCATHA satellite. The charging simulation was carried out in the UPDATE mode. That is, on each time-step, the program searches an input file for the most recent spectrum and updates the flux description to the corresponding double Maxwellian fit.

SPACECRAFT GROUND POTENTIAL

1979

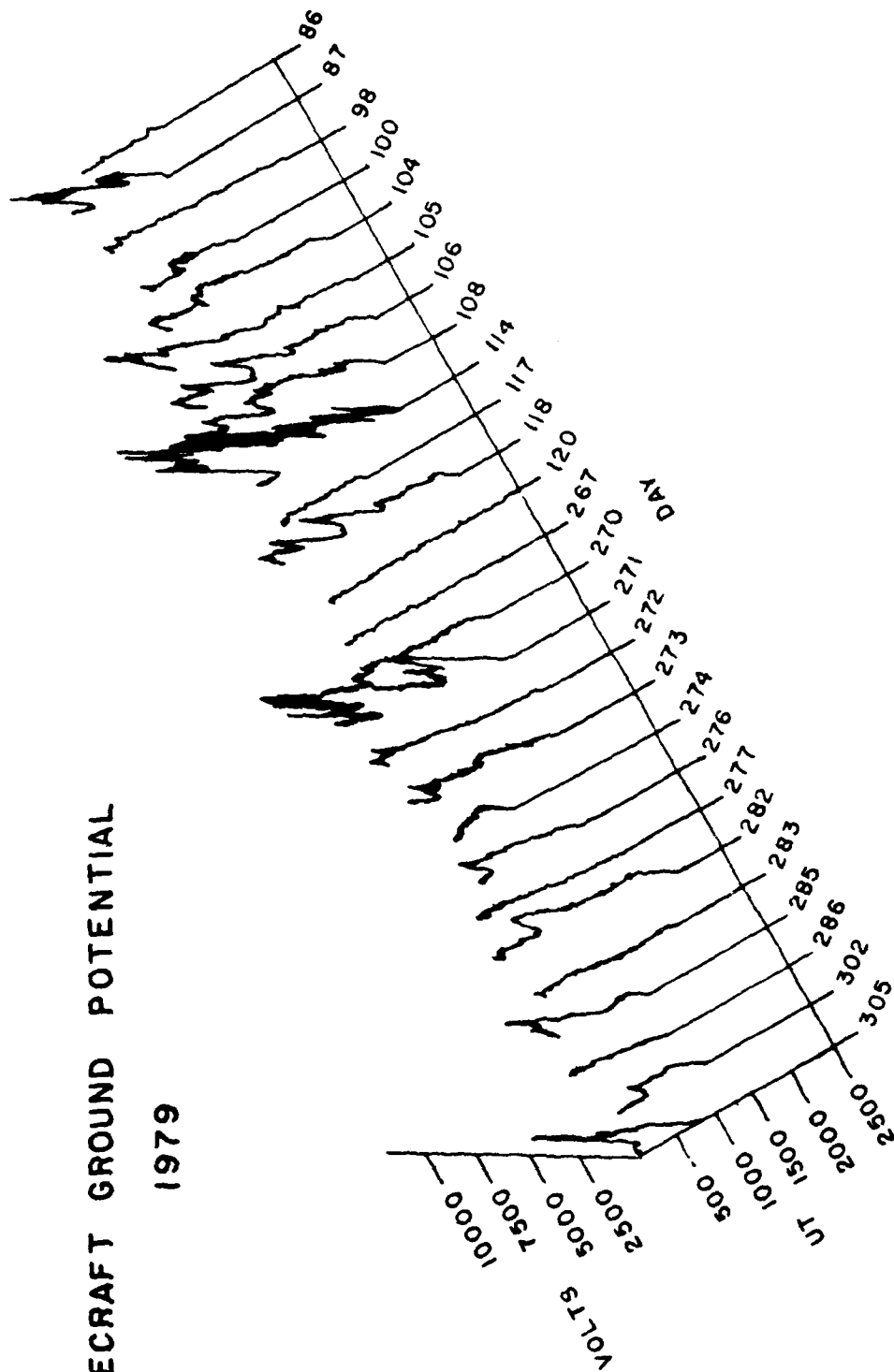


Figure 1.10 Spacecraft Potential Measured over a Five Month Span

Figure 1.11 displays the NASCAP results for the complete pass through the data. As can be seen from the plot, the overall agreement with the measured SC9 voltages is quite good. The potential contours, for a point mid-way through the second pass run, are shown in Figure 1.12. Near the surface, the contour lines tend to follow the satellite geometry, with some deviations due to the booms. Beyond a few meters from the satellite, the monopole field dominates.

The most complex NASCAP simulation that has been attempted is the day 113 (1981) case, where transit into and out of eclipse was considered.⁽¹⁵⁾ Here, in addition to the temporal plasma environment, we have time dependent sun illumination in the penumbra regions.

The SC9 instrument sweeps through 64 energy channels ($0 < E < 82$ KeV). The measurements were made once every 17 seconds during the day 113 eclipse period. The ALLES program reads the SC9 data from magnetic tape, converts the electron and ion counts to the corresponding phase space distribution functions, and makes Maxwellian fits to each spectrum. Figure 1.13 shows the SC9 distribution functions versus UT.

To obtain an overview of the charging strength of the day 113 plasma environment, a number of trial runs were done with the auxiliary program MATCHG. The MATCHG program was adapted so that it could read in the spectrum fits, one-by-one, and calculate the equilibrium potential for each of them. The surface material was chosen to be SOLAR, which is the most prevalent cell on the NASCAP model of SCATHA. From previous work it has been found that SOLAR is a good indicator of the eclipse charging behavior of the 1-grid model i.e. when SOLAR charges, the NASCAP model does so also, usually reaching a value $\approx 30\%$ below that of MATCHG.

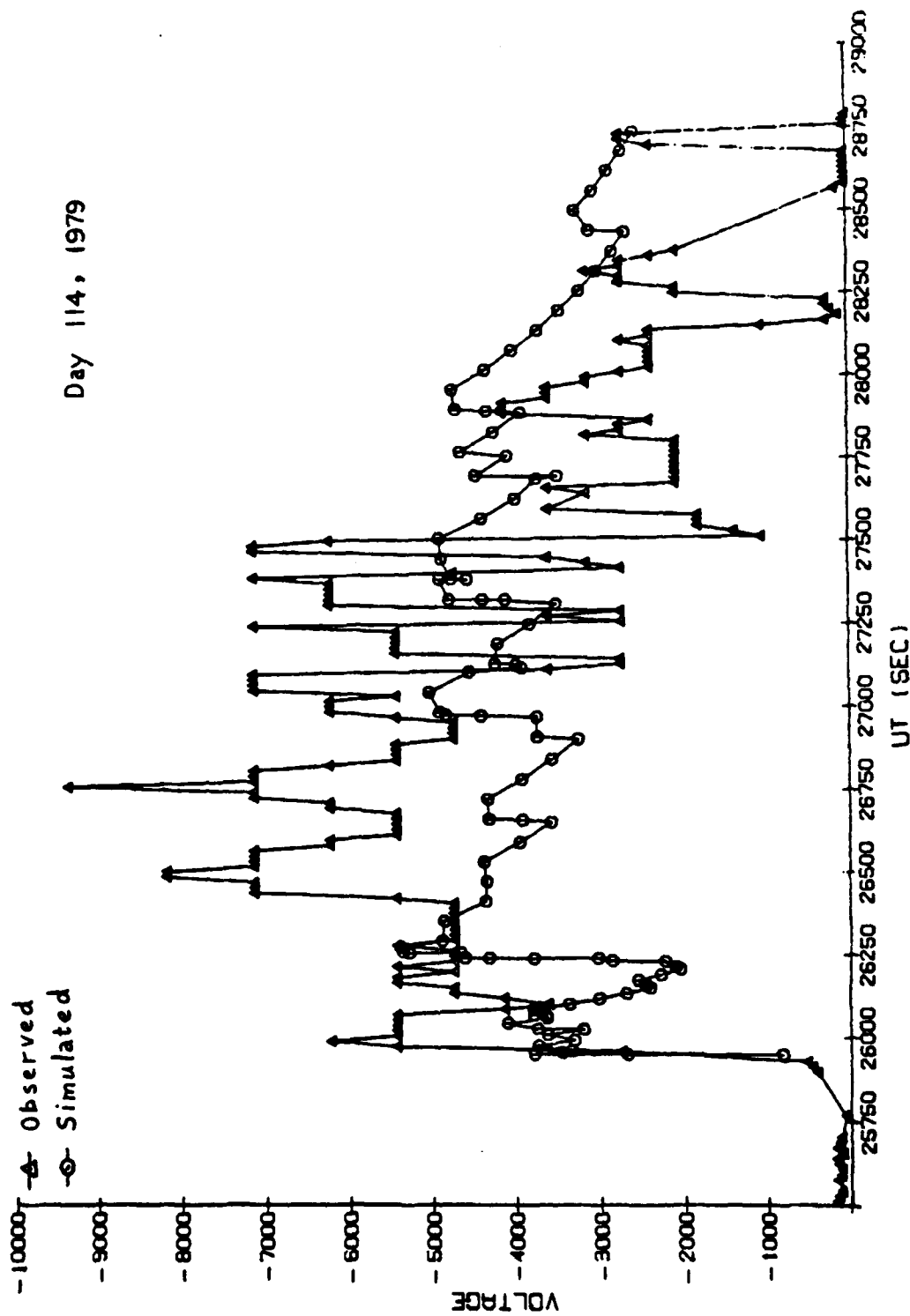


Figure 1.11 Comparison of simulated (2nd pass) and observed ground potentials

POTENTIAL CONTOURS ALONG THE X-Z PLANE OF Y=9
 VMIN=-6.0581E+03 VMAX=-.6187E+02 DV=-5.0000E+02

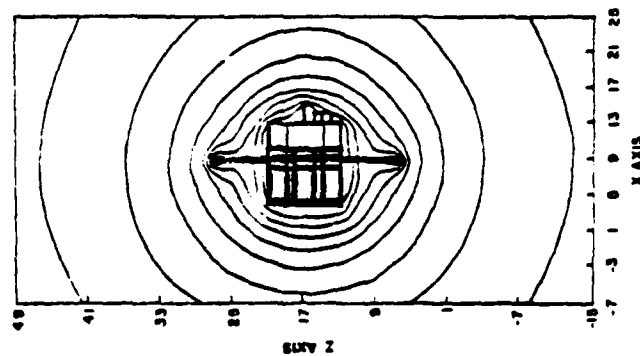


Fig 1.12a X-Z plane

POTENTIAL CONTOURS ALONG THE Z-Y PLANE OF X=9
 VMIN=-5.4130E+03 VMAX=-.61870E+02 DV=-5.0000E+02

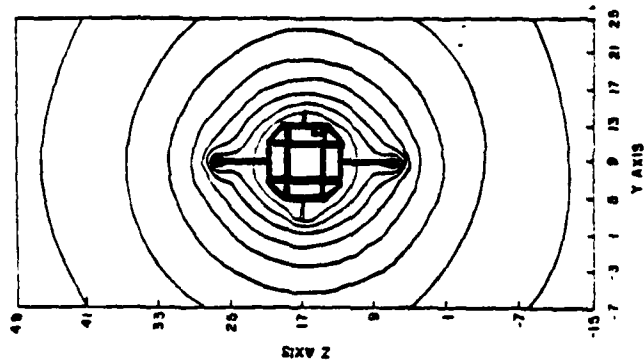


Fig 1.12b Z-Y plane

POTENTIAL CONTOURS ALONG THE X-Y PLANE OF Z=7
 VMIN=-5.5510E+03 VMAX=-.12948E+03 DV=-5.0000E+02

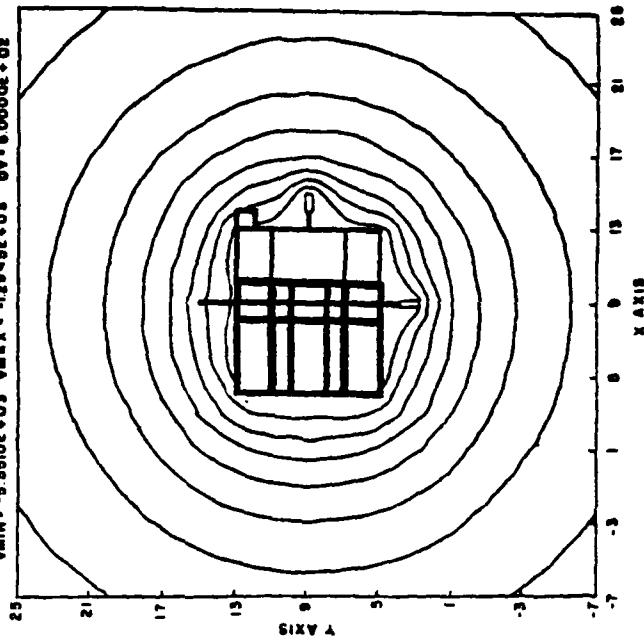
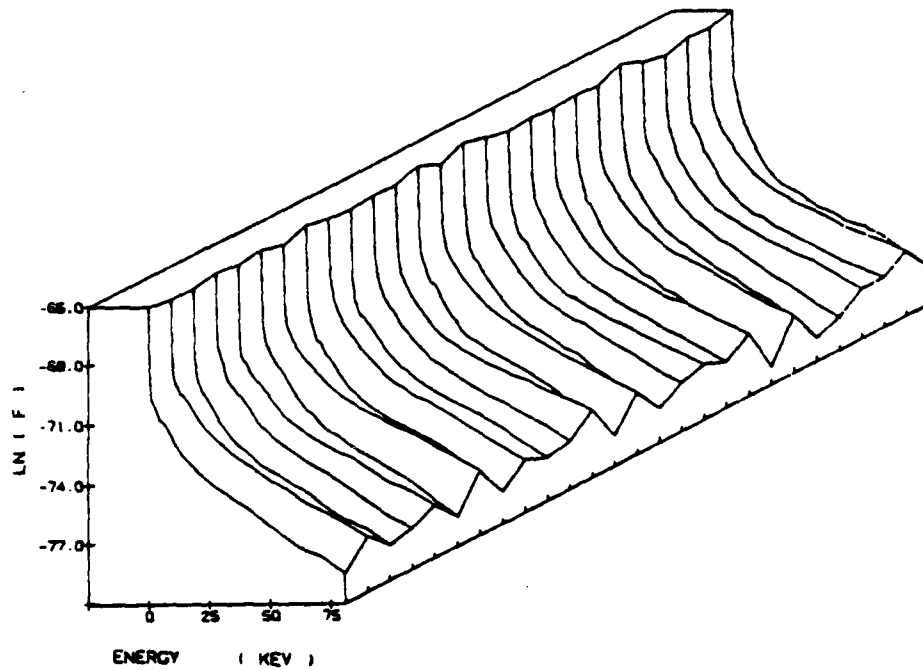


Fig 1.12c X-Y plane

Potential contours for SCATHA model at 27368 sec. UT

1981 0 113 UT= 4021.- 4463. SCATHA SCS ELECTRON



1981 0 113 UT= 4021.- 4463. SCATHA SCS ION

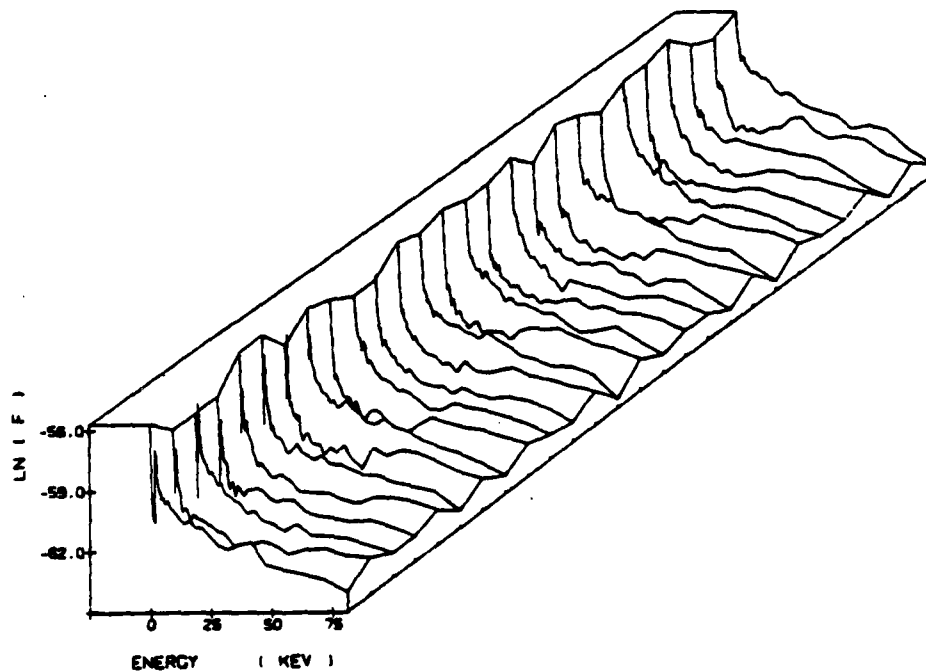


Figure 1.13 Electron and Ion Phase Space Distribution Functions for Day 113

These studies indicated that adequate charging voltages in the eclipse region could be obtained by using the single Maxwellian fits from ALLES. Figure 1.5 gives the MATCHG equilibrium potentials versus UT corresponding to these fits. In order to reduce fluctuations, the electron densities and temperatures were smoothed using a ten point running average. The final input temperatures and densities are given in Figure 1.14.

To conserve computing time, the NASCAP 1-grid model of SCATHA was employed. This model gives an adequate representation of the vehicle geometry and surface materials (the material properties were assumed to have the default values set by S-CUBED). However, the booms are truncated and this will lead to some inaccuracy in the sunlight regions. Also, to save time, the sun illumination was represented by the SPIN approximation, rather than ROTATE. Again this will introduce uncertainties into the calculation of sunlight effects.

The NASCAP simulations were carried out in the UPDATE mode i.e. on each iteration the program searches an input file containing the spectra fits and picks out the one that is closest (earlier) to the current time. Also, by means of RDOPT cards, the sun intensity is adjusted on each step to define the variation in sun illumination in the entrance and exit penumbra regions. The NASCAP time-step was set to 17 secs, which is the interval between SC9 measurements, so that each spectra would be sampled at least once during the run. A complete pass through the data -- into and out of eclipse -- takes about 6 hours running time on the CDC 6600, using the 1-grid model.

The vehicle frame potential, as determined from SC9 measurements, is plotted versus UT in Figure 1.15. The circles represent the measured voltages in KV. The solid line in the figure gives the sunlight intensity during passage through eclipse. The voltage

DAY 113 PLASMA

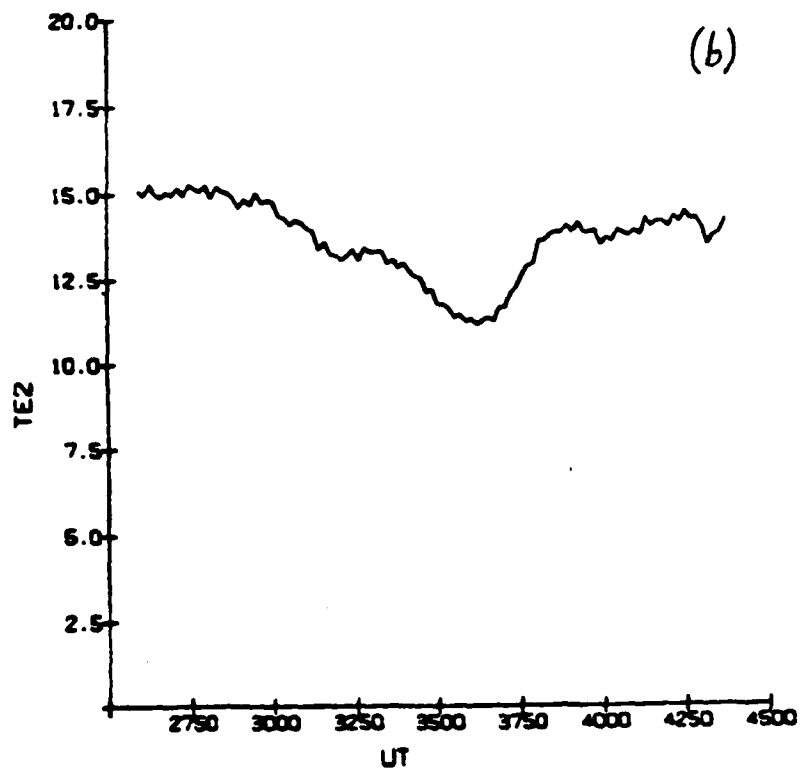
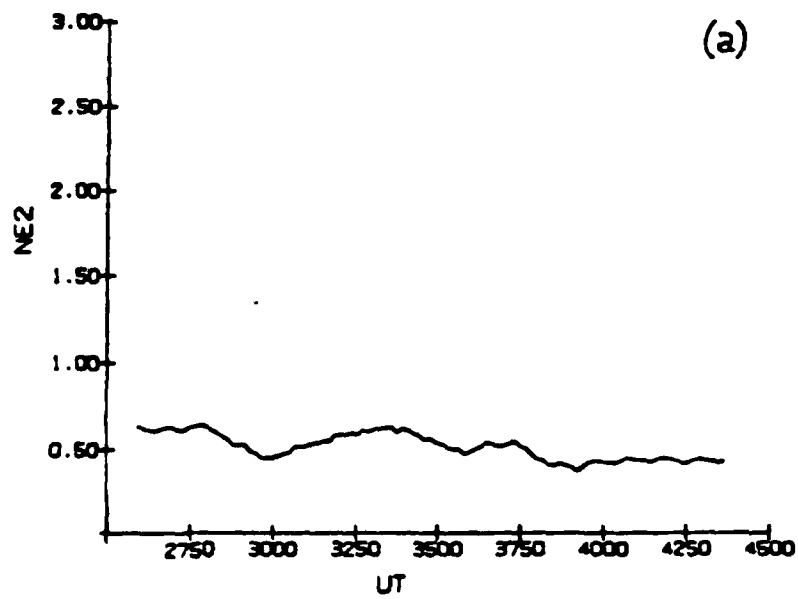


Figure 1.14 Corrected and Smoothed Electron Density and Temperature (Single Maxwellian)

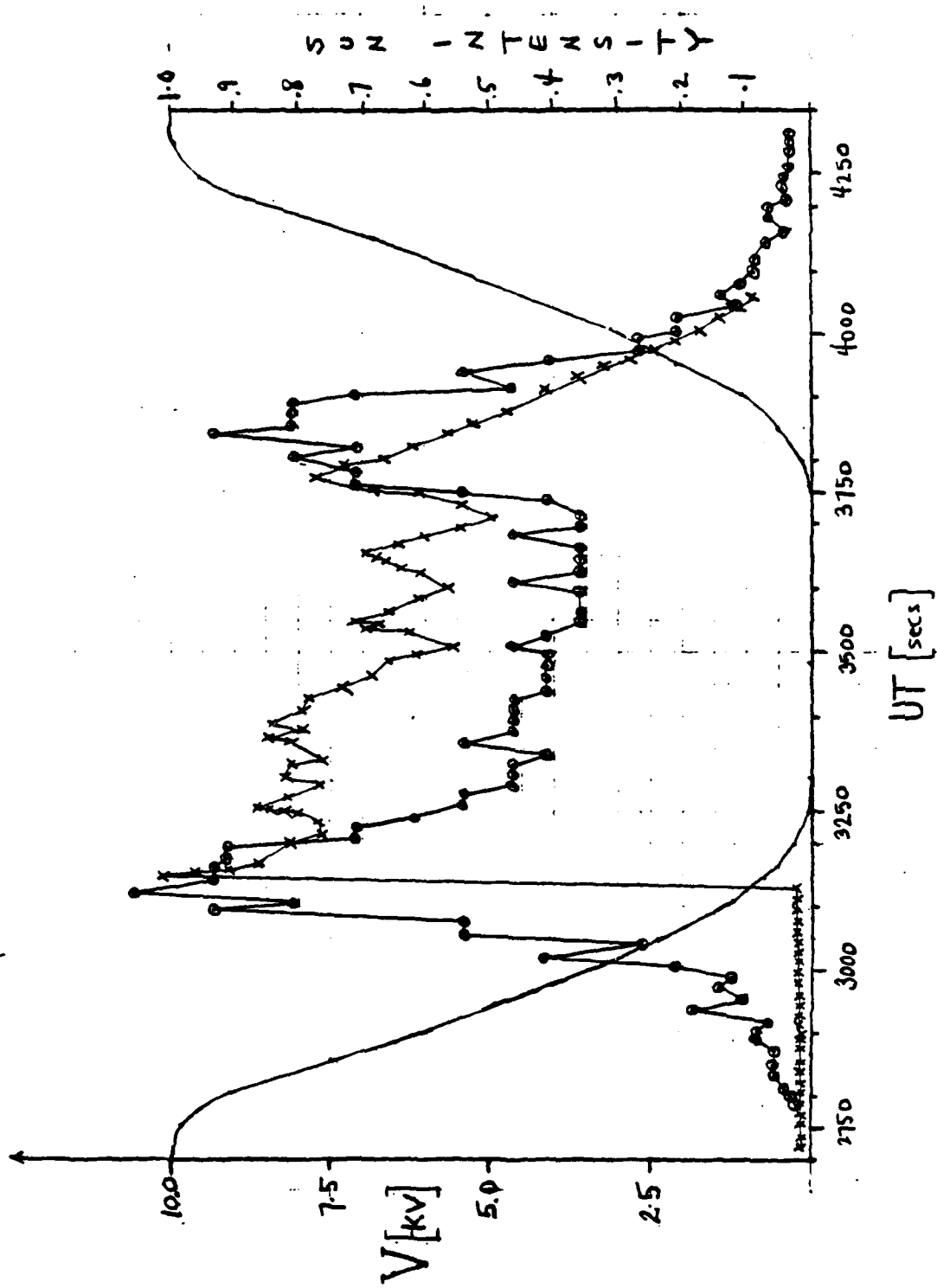


Figure 1.15 NASCAP Ground Potentials vs. UT for Single Maxwellian Fit (Day 113/81)

plot has two peaks; the first peak is correlated with entry to eclipse and the second one occurs in the exit penumbra.

A straightforward physical picture may be used to explain the main features of the day 113 charging event. Assume that there was present a severe charging plasma environment. In sunlight, any shaded surfaces would charge up, but those cells that are exposed to the solar UV would lose photo-electrons, so that the charging would be inhibited. The net effect is that the vehicle ground typically goes a few hundred volts negative. When the spacecraft enters penumbra, the photoemission is reduced and eventually a point is reached where the plasma current dominates. The vehicle then rapidly charges and maintains a high voltage through eclipse. In the exit penumbra region, the photoemission again builds up and the charging is suppressed.

Figure 1.15 gives the NASCAP predictions for the day 113 event assuming a DVLIM parameter of 500 (a comparison run with value 5000 was also done). The following aspects of the simulations are worthy of note:

- a) in sunlight, the vehicle frame potential goes a few hundred volts negative, as expected.
- b) when the sun illumination in the entrance penumbra is sufficiently reduced (to $\approx 25\%$) there is rapid charging. With the smaller DVLIM setting (500), the charging peak is $\approx 10\text{KV}$, in agreement with measurements.
- c) in the full eclipse region, the vehicle frame falls to $\approx 6\text{KV}$, which is a few kilovolts higher than the measurements. This result is independent of DVLIM.

- d) the second peak structure in the data is too high when $DVLIM = 5000$, and slightly low for $DVLIM = 500$.
The latter case should be more accurate.
- e) in the exit penumbra, the solar UV brings down the frame potential, roughly in accordance with measurements. The region is almost independent of $DVLIM$ even though there are frequent cut-backs with $DVLIM = 500$ and none with $DVLIM = 5000$.

The primary weakness in the simulation appears to be near the entrance penumbra region where the NASCAP frame potential starts to rise later than for the measurements and then goes up much more rapidly. This is an inherently difficult part of the event to model, requiring precise values of the sun illumination and correlated plasma environment.

The SPIN approximation, which averages the sun intensity over many cycles is probably inadequate here (the jogs in the measured voltage during charging are probably due to rotational effects). Also, neglecting the low energy electrons is less valid in this region where the vehicle potential is low. For these reasons, it is not surprising that the NASCAP code does not track the measurements better through the initial charge-up phase.

The overall agreement of the 1-grid frame potential with the SC9 voltages is quite good considering that:

- 1) we have neglected the low energy Maxwellian components
- 2) there are uncertainties in the materials properties

- 3) there are approximations in the model (truncated booms, SPIN mode instead of ROTATE)
- 4) there is uncertainty in the O_2 content of the environment
- 5) there were large fluctuations in the charging strength from one plasma spectrum to the next.

The first point above is the most crucial one. The low energy electrons, in particular, form a critical part of the plasma specification. But the low energy part of the SC9 spectra is not known during periods of strong charging because these particles are repelled by the electric field surrounding the vehicle. Thus some guess has to be made as to the shape of the low energy electron spectrum. If we use extrapolated fits to the region (the double Maxwellian fit) then we find that the charging is suppressed. If we neglect the low energy components entirely (the single Maxwellian) then we get charging that is a few kilovolts too high in the central eclipse region. A definitive test of the NASCAP program can only be made if a complete specification of the particle spectrum is available.

References

1. Katz, I. et al, "Extension, Validation and Application of the Nascap Code", Final Report, SSS-R-79-3904, January 1979.
2. Mullen, E.G. et al, "A Worst Case Spacecraft Environment as Observed by SCATHA on 24 April 1979", AFGL-TR-81-0231.
3. Rubin, A.G., Bhavnani, K.H., and Tautz, M.F., "Charging of Spinning Spacecraft", AFGL-TR-79-0261
4. Stannard, P.R. et al, "NASCAP Programmer's Reference Manual", SSS-R-82-5443, March 1982.
5. Tautz, M.F. et al, "Prediction of Materials Charging in Magnetospheric Plasmas", AFGL-TR-81-0088
6. Tautz, M.F. et al, "SSPM Experiment Simulation Study for the April 24, 1979 Charging Event", AFGL-TM #23
7. Tautz, M.F., Rubin, A.G., and Saflekos, N.A., "Preliminary Simulation of Electron Emitter Events on March 29, 1979", AFGL-TM #33
8. Tautz, M.F. et al, "SSPM Experiment Simulations for 1979 Day 87 and Day 114 Charging Events", AFGL-TM #39
9. Tautz, M.F., Rubin, A.G., and Saflekos, N.A., "NASCAP Simulation of Charging Event for Temporal Plasmas of April 24, 1979", AFGL-TM #58
10. Tautz, M.F., Rubin, A.G., and Saflekos, N.A., "NASCAP Simulation of Helios 1 Antenna Boom Potentials", AFGL-TM #61
11. Tautz, M.F., Rubin, A.G., and Saflekos, N.A., "NASCAP Simulation of SCATHA Charging in Worst Case Plasma of April 24, 1979", AFGL-TM #70
12. Tautz, M.F., Rubin, A.G., and Saflekos, N.A., "Preliminary NASCAP Model of the Space Based Radar", AFGL-TM #71
13. Tautz, M.F., Rubin, A.G., and Saflekos, N.A., "NASCAP Model of GEOS Satellite and SPA Sensor Unit", AFGL-TM #72
14. Tautz, M.F., and Rubin, A.G., "Threshold Conditions for Materials Charging in Maxwellian Plasmas", (in publication)
15. Tautz, M.F., Rubin, A.G., and Saflekos, N.A., "NASCAP Simulation of SCATHA Charging on Transit through Eclipse for Day 113, 1981", AFGL-TM #80

2.0 Ionization and Charging Effects of Beam Currents

When a charged probe is placed in a plasma environment, it draws from the plasma a current of oppositely charged particles. Since particles of like charge are repelled by the probe, a sheath develops, depleted to some degree in the repelled species. The application of this system to the charging of beam emitting spacecraft was first detailed by Beard and Johnson.⁽¹⁾ Later, the physics of the probe sheath was studied in depth by Lam.⁽³⁾ More recently, Leadon, et.al.⁽⁴⁾ developed a numerical model to introduce into the Lam model the effect of ionization of neutral gas molecules by current returning to the probe. Figure 2.1 illustrates schematically the physical processes in the sheath region. The case of a spherically symmetric electron beam emitter was considered and it was found that ionization served to reduce probe charging. This was significant in that experimental results then available indicated low probe potentials at high beam currents. However, the study by Leadon, et.al. was not entirely conclusive in that the PLAS3 program developed to implement the model failed to converge at high beam currents. The work on this project was initiated with the aim of determining the origin of the convergence problems and extending the model to higher currents.

The further development of the PLAS3 code is a step towards a synthesis of spacecraft charging models. PLAS3 is an intermediate level program which treats the basic physical processes without dealing with the complications of spacecraft structural detail. Thus it can be used to generate benchmark cases, for comparison with much slower particle pushing methods, or with complex existing codes such as NASCAP and POLAR that do not address the low altitude ionization problem.

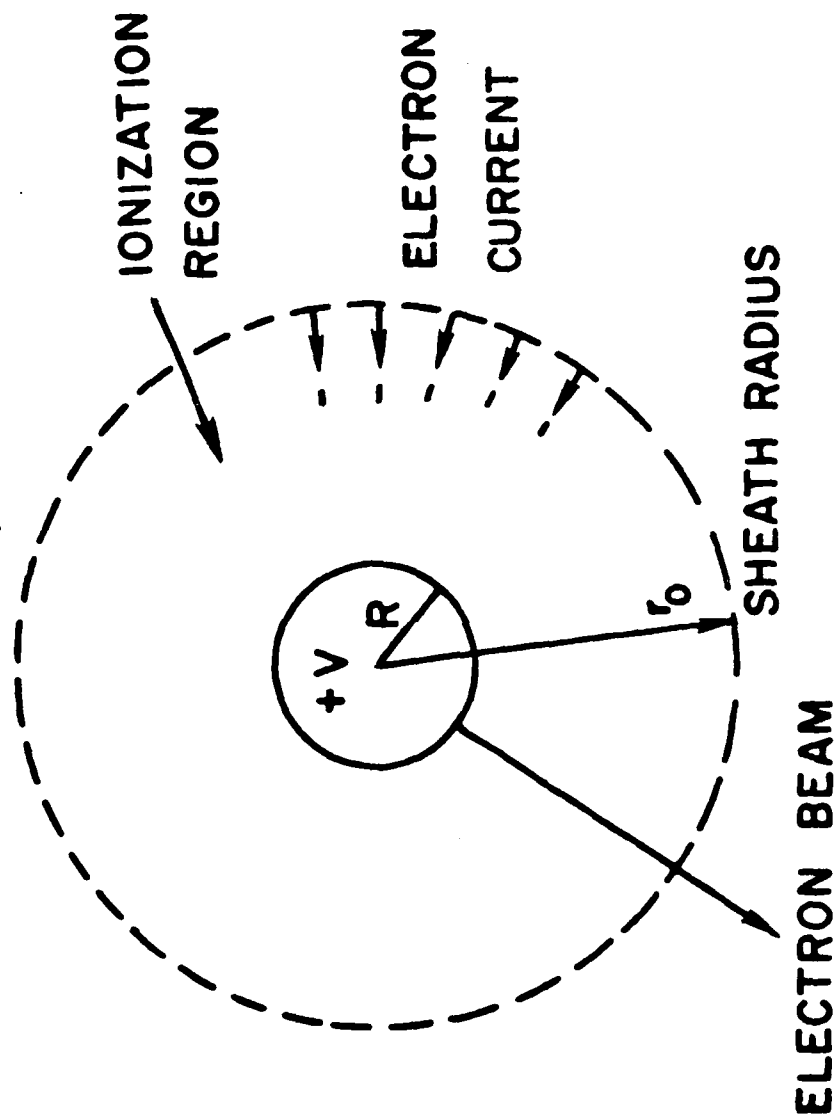


Figure 2.1 Schematic of Ionization Process

2.1 The PLAS3 Model

The model is essentially the same as that used in the previous studies. (3,4) The spherical probe is assumed to be surrounded by a sheath of radius R_0 . At the sheath boundary, the field and potential are set to zero, and electron density is equal to the ambient plasma density n_e . Ambient ions, however, are assumed to be repelled from the probe so that their density is zero both inside the sheath and at the boundary. The sheath boundary is determined by the condition that the inward thermal electron flux is equal to the beam current I_b , thus

$$4 \pi q R_0^2 U_{th} n_e = I_b \quad (1)$$

Once inside the sheath, the electrons are assumed to travel by free fall toward the probe. Conservation of energy then gives

$$\frac{1}{2} m U^2 = \frac{1}{2} m U_{th}^2 + q \Phi \quad (2)$$

On their way to the probe surface, electrons strike neutrals, at a density n_0 , and ionization occurs with frequency

$$P(U_e)/n_0 \sigma \quad (3)$$

Where $P(U_e)$ is a velocity dependent probability curve, normalized to unity, and σ is the maximum cross section for ionization, around $2 \times 10^{-16} \text{ cm}^2$ for O_2 targets, with a peak around 76 eV. The ion pairs thus created are accelerated away by the field and give rise to a secondary electron and ion flux. The number of secondary pairs produced per second throughout the sheath is

$$N = 4 \pi \int_{R_b}^{R_0} r^2 \left(\frac{dn}{dr} \right) dr \quad (4)$$

where R_b is the probe radius.

The potential inside the sheath is related to the charge density by Poisson's equation

$$-\nabla \cdot \nabla \phi = \frac{-1}{r^2} \frac{d}{dr} \left(r^2 \frac{d\phi}{dr} \right) = \frac{e}{\epsilon_0} (n_s^+ - n_p^- - n_s^-) \quad (5)$$

To use (5) we need another equation relating ϕ and n . The charge density is derived from three sources.

(1) The primary electron density is found by equating the flux at a point r to the primary flux, thus

$$r^2 n_p^- v_p(r) = R_0^2 n_e v_{th}$$

Using (2) for $v_p(r)$,

$$r^2 n_p^-(r) = \frac{n_0 v_{th} R_0^2}{\left(v_{th}^2 + \frac{2q}{m_e} \phi(r) \right)^{1/2}} \quad (6a)$$

(2) The secondary contribution to electron density is found by examining the flux at r from electrons originating at ρ .

$$r^2 n_s^-(r) v_s(r) = \left(\frac{dn}{dt} \right) \rho^2 d\rho$$

From energy conservation,

$$\frac{1}{2} m v_s^2(r) = q (\phi(r) - \phi(\rho))$$

since pairs are assumed to originate with zero initial velocity. Summing contributions to n_s from all $R_0 > \rho > r$ gives

$$r^2 n_s^-(r) = \int_r^{R_0} \frac{\left(\frac{dn}{dt} \right) \rho^2 d\rho}{\left(\frac{2q}{m_e} (\phi(r) - \phi(\rho)) \right)^{1/2}} \quad (6b)$$

(3) A treatment equivalent to (2) for secondary ions gives

$$r^2 n_s^+(r) = \int_{R_0}^r \frac{\left(\frac{dn}{dt}\right) \rho^2 d\rho}{\left(V_s^2 + \frac{2q}{m_i} (\phi(\rho) - \phi(r))\right)^{1/2}} \quad (6c)$$

Here the ions are assumed to be swept out by the motion of the probe at velocity V_s so that energy conservation appears as

$$\frac{1}{2} m V^2 = \frac{1}{2} m V_s^2 + \frac{2q}{m_i} |\phi - \phi_b|$$

where ϕ_b is the potential at which the ion was created.

When Eqns. (6a - 6c) are substituted for the RHS of (5) and the boundary conditions

$$\phi(R_0) = 0, \quad \phi'(R_0) = 0$$

are imposed, we arrive at a closed integro-differential equation for ϕ , which we solve by the following numerical scheme.

In order to solve Eq. 5, we define

$$E = -\nabla\phi \quad (7)$$

and consider a corresponding difference equation. The sheath region is divided into N shells of width

$$\Delta r = (r_0 - r_b)/N$$

Each shell begins at a radius $\rho_i = r_b + (i-1)\Delta r$

and has as its midpoint the radius $r_i = r_b + (i-1/2)\Delta r$

At each P_i we define a field variable E_i and at each n_i we define a potential ϕ_i and a space charge n_i . The potential is related to the field by

$$\phi_{i+1} - \phi_i = (E_i + 2E_{i+1} + E_{i+2}) \Delta r / 4 \quad (8)$$

The densities are found by replacing the integrals in Eq. 6 by trapezoidal rule approximates.

To include the effects of ionization in cell 1 to the charge density in that same cell, we divide the cell into general subcells and approximate the field as a constant over each region. The integrals in Eq. 6 can then be done analytically.

With the knowledge that

$$E_{N+1} = 0, \quad \phi_{N+1} = 0$$

We arrive at a set of N non-linear equations in N unknown field points. These we solve by Newton-Raphson iteration as follows. Define

$$f_i(E_1, E_2, \dots, E_N) = \frac{2}{P_{i+1}} E_{i+1} - \frac{2}{P_i} E_i - \frac{e \Delta r n_i}{\epsilon}, \quad i=1, N \quad (9)$$

Guess an initial vector

$$\begin{pmatrix} (0) & (0) & \dots & (0) \\ (E_1) & (E_2) & \dots & (E_N) \end{pmatrix}$$

and modify the initial vector in a direction which will minimize the residuals of Eq. 9.

3.2 Method of Approach and Results

After investigating both the model and the previous numerical implementation, the code was rewritten using a different and more straightforward method (Newton-Raphson) to solve the equations. This program was thoroughly cross-checked with the original for cases where the original converged. Using the new algorithm, we were able to obtain solutions for arbitrarily high beam currents. The nature of the potential contours was rather unusual and SUATEK graphics capabilities were added to the program to facilitate understanding of the underlying physics. Plots of potential, electric field and total and partial charge distributions such as are shown in Figures 2.2 and 2.3 were made available. A series of runs have been made to calculate the dependence of the probe charging on the model parameters, namely, the electron temperature and density, the mean ionization length and ionization profile, and the beam current.

The effect of mean ionization distance λ on the potential of a spacecraft emitting a beam is shown in Figure 2.4. In the region where ionization is negligible ($\lambda = 10^8$ approximately), the potential curves are flat, and the potential increases with beam current. As the ionization distance decreases (i.e., ionization is more probable) the potential curve turns down, and stays constant approximately as the ionization distance λ decreases further.

The main result from the parameter studies was that the curve of the probe potential versus current was very similar to that measured experimentally. For low electron beam currents, the potential increases monotonically with the current. Beyond a critical current, the returning electrons from the environment cause ionization, and the potential drops to a lower value.⁽⁵⁾

ions electrons electrons
deplete accumulate accelerate

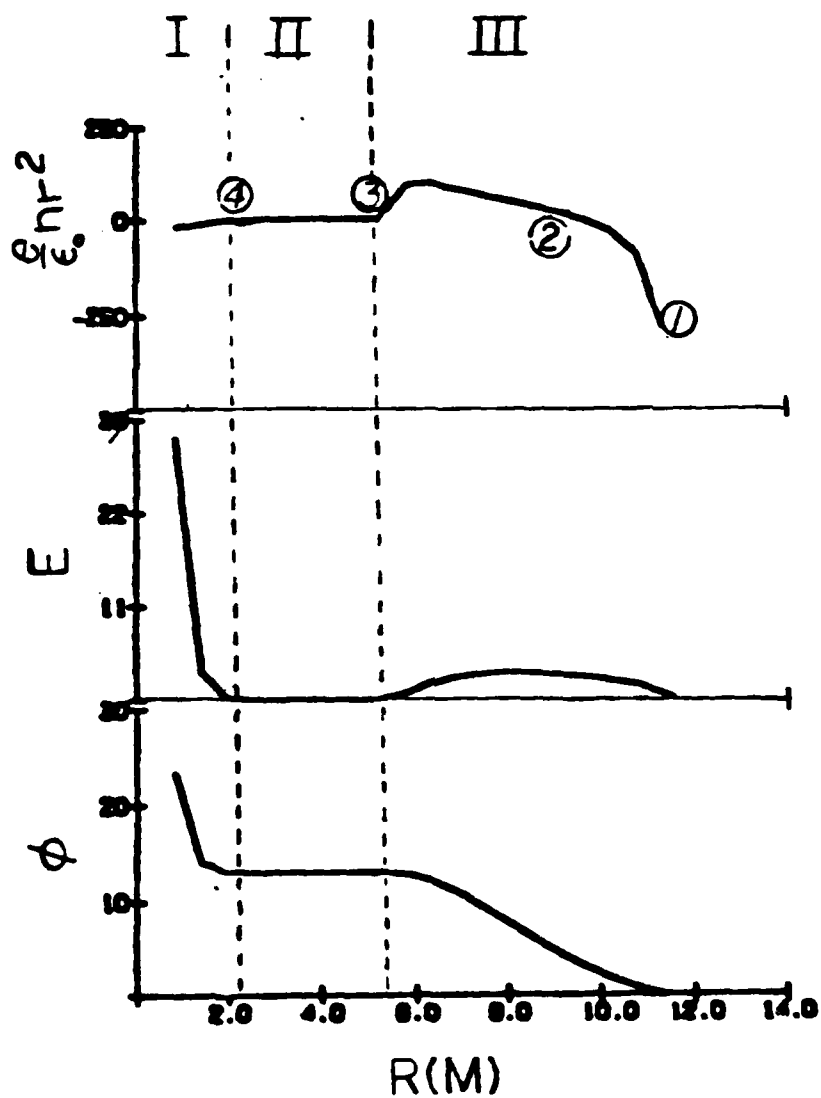
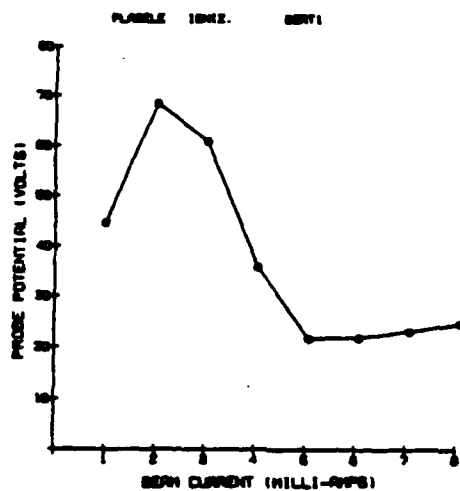


Figure 2.2 Profiles of (a) Total charge density, (b) Electric field, (c) Potential for a beam of 10 ma and $\lambda = 53$ meters



$T_e = .037 \text{ eV}$
 $n_e = 1150/\text{cc}$
 $\lambda = 53 \text{ meters}$

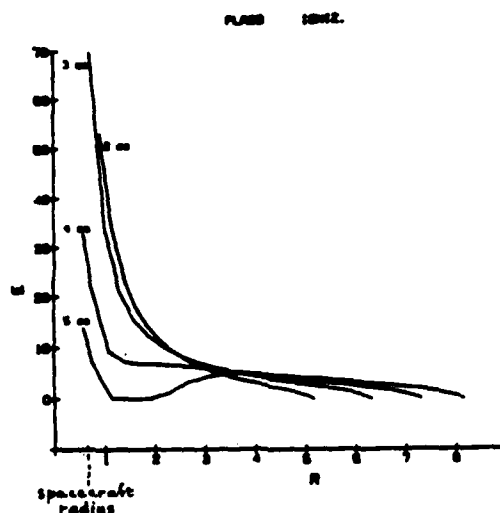
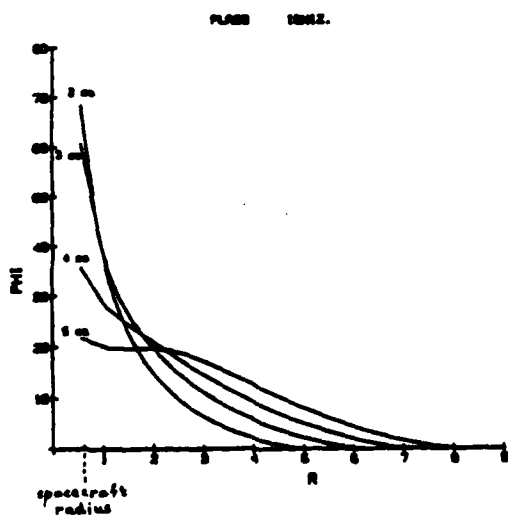


Figure 2.3 Potential and Field Profiles for a Current Sweep

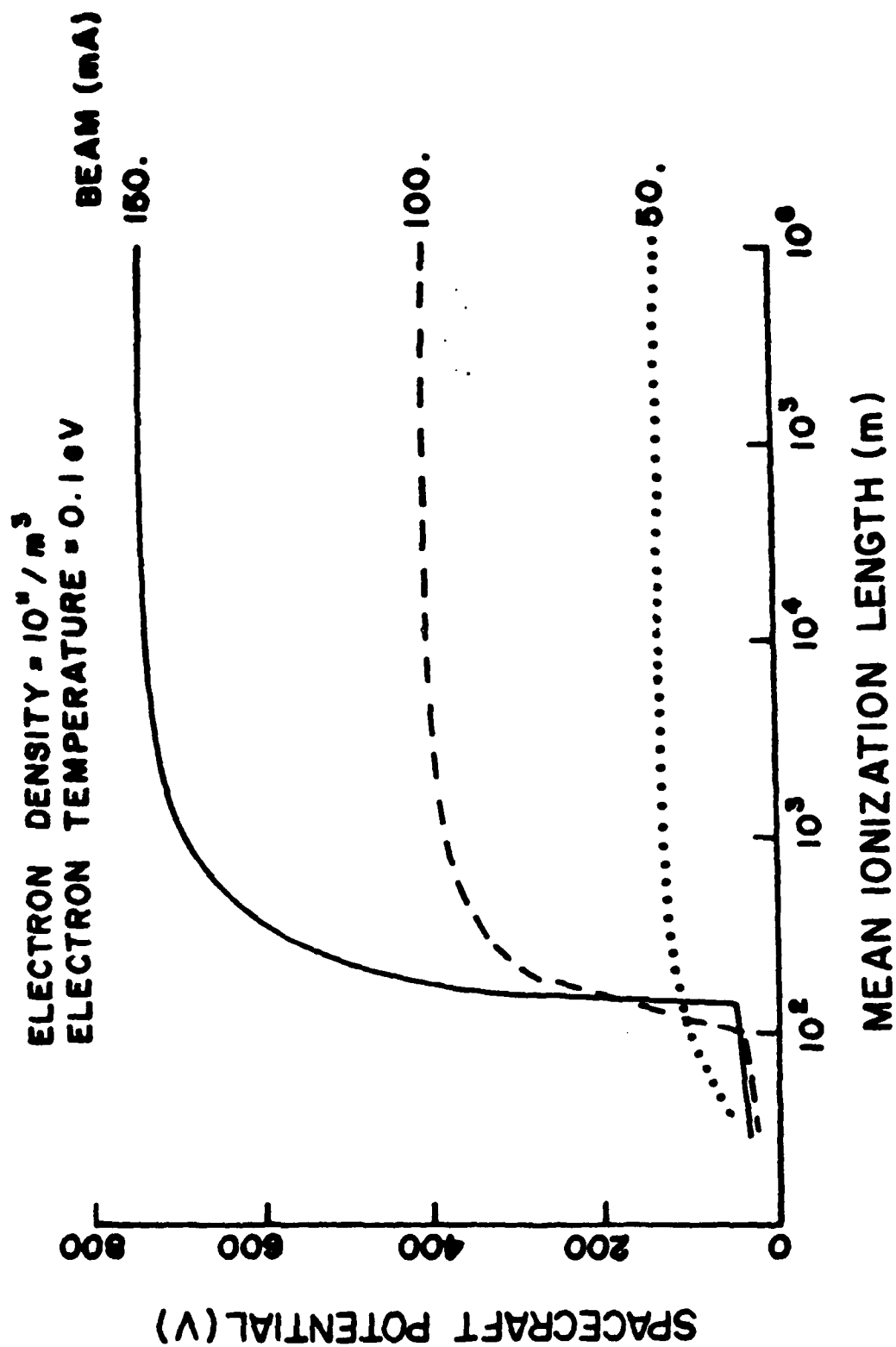


Figure 2.4 Effect of Mean Ionization Length

2.3 Extensions of the Model

The model was applied to two further systems. First, the case of an infinitely long, cylindrically symmetric electron beam emitter was considered. The necessity that the cylinder be infinitely long arises from the fact that this renders the model one-dimensional, whereas use of further dimensions introduces problem complications which should initially be avoided. Results from this study were quite similar to the spherical case. This shows that the spherical nature of the probe is not essential in determining charging characteristics.

A case of more immediate interest was the ion emitter.⁽⁶⁾ Here we needed to include one further effect of secondary electron emission from the probe surface by primary ion collision. We found that, for ion guns, ionization was less important in determining charge than for electron guns. In fact, the major determiner was the enhancement of the return current, mostly from secondary emission, to increase the effective beam current. The result of this was to bring down the magnitude of probe charge, as with electrons, but it became clear that no maximum in the $I-V$ curve would be encountered for ions.

An analytical model was constructed, based on the Lam solution and including secondary emission but not sheath ionization. It was found that this model reproduced the results of the full model quite nicely for environments of greatest interest to experimenters. This indicates that ionization may not be important for typical ion gun experiments.

2.4 Flight Simulation

Studies have been carried out to give an indication of the predictive usefulness of the model.⁽²⁾ The goal was to duplicate as nearly as possible the environmental conditions to which an upcoming test flight, BERT-1, would be subjected. Simulations were carried out at altitudes between 100 and 250 km for the two electron gun models, spherical and cylindrical, as well as the spherical ion emitter. The major findings were the following, assuming a maximum beam current of 20 mA:

- a) for electron guns the potential-current curve will exhibit a local maximum for low altitudes but remain monotonic at higher altitudes, and
- b) for ion guns, the potential will reach the limiting value of the energy of the ion beam itself for all altitudes.

Figure 2.5 shows the computed results of spacecraft potential as a function of electron beam current at various altitudes. The non-monotonic behavior of potential current curves is apparent. At low currents, the potential increases with beam current. When the current increases further, ionization occurs inside the sheath, and the potential then turns around.

In addition to the atmospheric simulation, a study was carried out for electron guns at conditions similar to those in a recent ground based test chamber. In this case, it was shown that the peak voltage and peak current could be matched with reasonable choices of plasma density and temperature in the model.

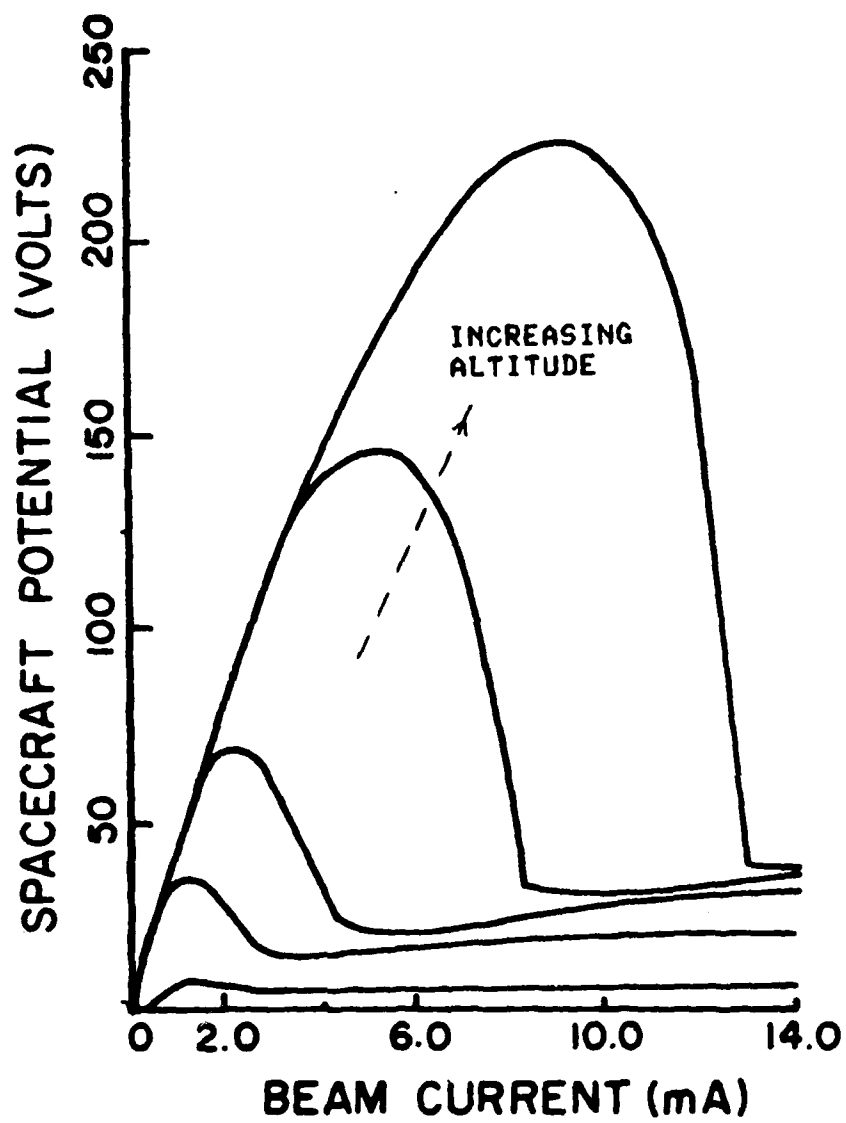


Figure 2.5 Flight Simulation Charging Characteristics

References

1. Beard, D.B. and Johnson, F.S., "Ionospheric Limitations on Attainable Satellite Potential", J. Geophys. Res. Vol. 66, pp. 4113-4122, 1961.
2. Cohen H.A., Lai S.T., McNeil W.J., Wenaas E.P., Leadon R.P., "Spacecraft Charging with Beam Emissions in an Ionizable Environment", EOS Vol. 64, No. 18, p.381, 1983.
3. Lam, S.H., Phys. Fluids 8, 73 (1965)
4. Leadon, R.E. et al, "Analytical investigation of Emitting Probes in an Ionized Plasma", AFGL-TR-81-0138, April 1981.
5. McNeil, W.J., Cohen, H.A., and Lai, S.T., "Effects of Ionization on Charging of Electron Emitting Spherical Probes" AFGL-TM #75, January 1983.
6. McNeil, W.J., Cohen, H.A., and Lai, S.T., "Effects of Ionization on Charging of Ion Emitting Spherical Probes", AFGL-TM #79, February 1983.

3.0 Particle Tracking Studies

3.1 Particle Tracking near Differentially Charged Surfaces

An important aspect of the beam emitter problem is the dynamics of the beam particles themselves. If a differentially charged spacecraft is placed in an environment such that little current is drawn from the surrounding plasma and no sheath develops, Laplace's equation holds and we can calculate the potential at all points outside the spacecraft knowing only the charge on the surface. Once this is known, calculation of the trajectories of emitted charged particles will answer the question of what fraction of an emitted beam will escape the probe, or return and thereby neutralize some of the charge.

A number of investigations were conducted to calculate both the potentials around differentially charged spacecraft and the trajectories of emitted beams. The major results of these studies have been the presentation of potential and particle trajectory plots, and the determination of escape energy as a function of beam angle for several different charging configurations. Contour plots were used to aid in the presentation of these data. The final objective of this work is to determine the time dependence of self-neutralization in a probe which traps some of its emitted beam. Configurations studied included quadrupoles, circular concentric disks, and spheres with a circular cap -- all of which were treated essentially as two-dimensional problems.

3.1.1 Quadrupole Problem

The potential for two like charges at a distance 'd' on either side of a central charge 'f' is given by

$$\phi(x,y) = \frac{f}{(x^2 + y^2)^{3/2}} - \frac{1}{((x+d)^2 + y^2)^{3/2}} - \frac{1}{((x-d)^2 + y^2)^{3/2}}$$

The equations of particle motion are given by

$$\frac{d^2 x}{dt^2} = - \frac{\partial \phi}{\partial x}$$

$$\frac{d^2 y}{dt^2} = - \frac{\partial \phi}{\partial y}$$

and were solved computationally using Hamming's modified predictor-corrector method. (subroutine HPCG from the IBM Scientific Subroutine Library)

Particle trajectories were plotted using SUATEK with appropriate scaling to overlay on transparencies of the associated potential contour plots. These contour plots were generated using routine CONREC from the NCAR graphics package. Figure 3.1 shows a typical plot with four different trajectories for different beam energies. Other parameters that were studied were quadrupole separation and net charge, beam polarity, and beam origination and angle.

Total Energy = $-.56, -.06, +.44, +.94$
 Initial KE = $1.5, 2.0, 2.5, 3.0$

QUADRUPOLE MODEL

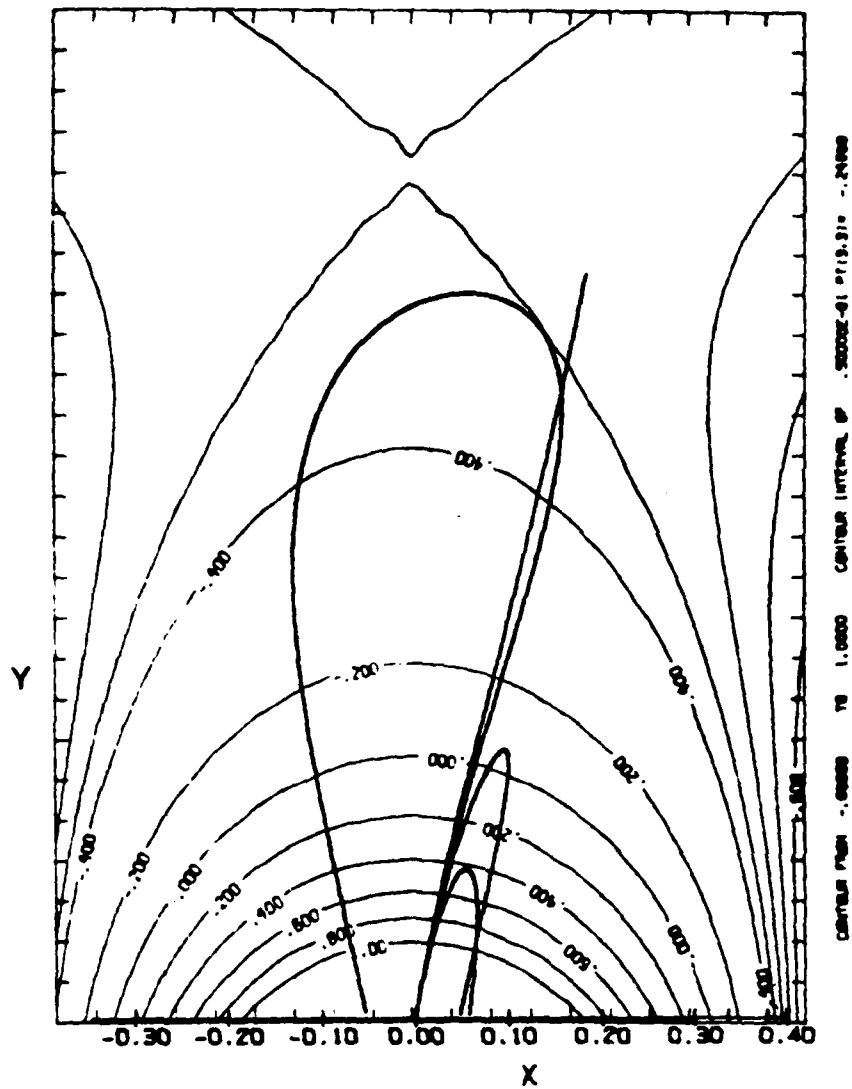
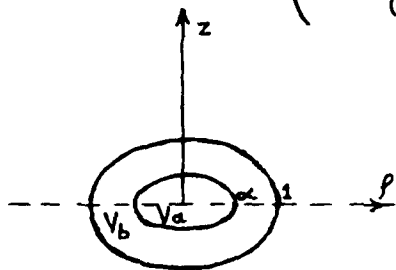


Figure 3.1 Potential Contours and Particle Trajectories in a Quadrupole Field.

3.1.2 Circular Double Disk Problem

The potential for a circular double disk has been derived analytically⁽¹⁾ as follows:

$$V(\rho, z) = \frac{2}{\pi} \left[\gamma \tan^{-1} \left(\sqrt{2} \{ \rho^2 + z^2 - 1 + [(\rho^2 + z^2 - 1)^2 + 4z^2]^{1/2} \}^{-1/2} \right) \right. \\ \left. + \frac{1-\gamma}{\sqrt{2}} \int_{\infty}^1 \frac{s}{(s^2 - \alpha^2)^{1/2}} \right. \\ \left. \times \left(\frac{z^2 - s^2 + \rho^2 + [(z^2 - s^2 + \rho^2)^2 + 4z^2 s^2]^{1/2}}{(z^2 - s^2 + \rho^2)^2 + 4z^2 s^2} \right)^{1/2} ds \right]$$



Radii $\alpha, 1$
Potentials V_a, V_b
 $\gamma = \frac{V_a}{V_b}$

ANALYTICAL CHECKS FOR BOUNDARY CASES

$$V(0, z) = \frac{2}{\pi} \left\{ \gamma \tan^{-1} \left(\frac{1}{z} \right) + (1-\gamma) \left[\frac{z}{(z^2 + \alpha^2)^{1/2}} \right] \right. \\ \left. \times \tan^{-1} \left[(1-\alpha^2)^{1/2} (z^2 + \alpha^2)^{-1/2} \right] \right\}$$

and for $\rho > 1$

$$V(\rho, 0) = \frac{2}{\pi} \left\{ \gamma \tan^{-1} (\rho^2 - 1)^{-1/2} \right. \\ \left. + (1-\gamma) \tan^{-1} \left[(1-\alpha^2)^{1/2} (\rho^2 - 1)^{-1/2} \right] \right\}$$

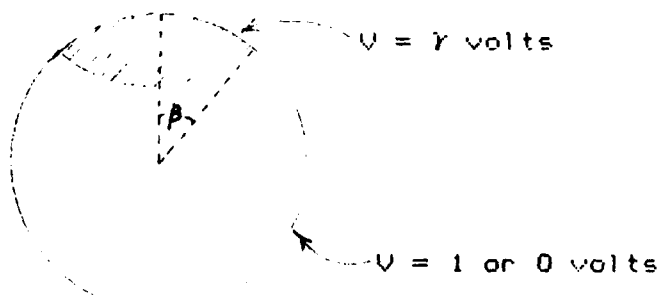
If beam orientation is initially in a plane normal to the disk surfaces, we can take $x = \rho$ (radius) and $y = z$ (normal to disk) and consider the problem in rectangular coordinates.

The inner disk to outer disk radius ratio α , and the potential ratio γ provide parameters that are similar to the quadrupole problem. The main complexity is due to the integral which must be computed for the potential at each location ρ, z .

Figure 3.2 shows overlaid potential and trajectory plots for positively charged inner and outer disks, with 0.1 radius ratio. Ion beams with three different energies, originating at a distance of 0.2 above the disks are considered. The saddle point introduces the question of beam trapping for many of the studies described in this section.

3.1.3 Circular Cap Problem

The problem is to track particles in the vicinity of a spherical probe with a differentially charged surface.



The potential is calculated by noting that the series

$$V(r, \theta) = \sum_{n=0}^{\infty} \left(\frac{a}{r}\right)^{n+1} \alpha_n P_n(\cos \theta) \quad (1)$$

solves Laplace's equation, where a is the probe radius.

CIRCULAR DOUBLE DISK

CIRC. DISKION

A= .1 B=1. VA= .1 VB= 1.0

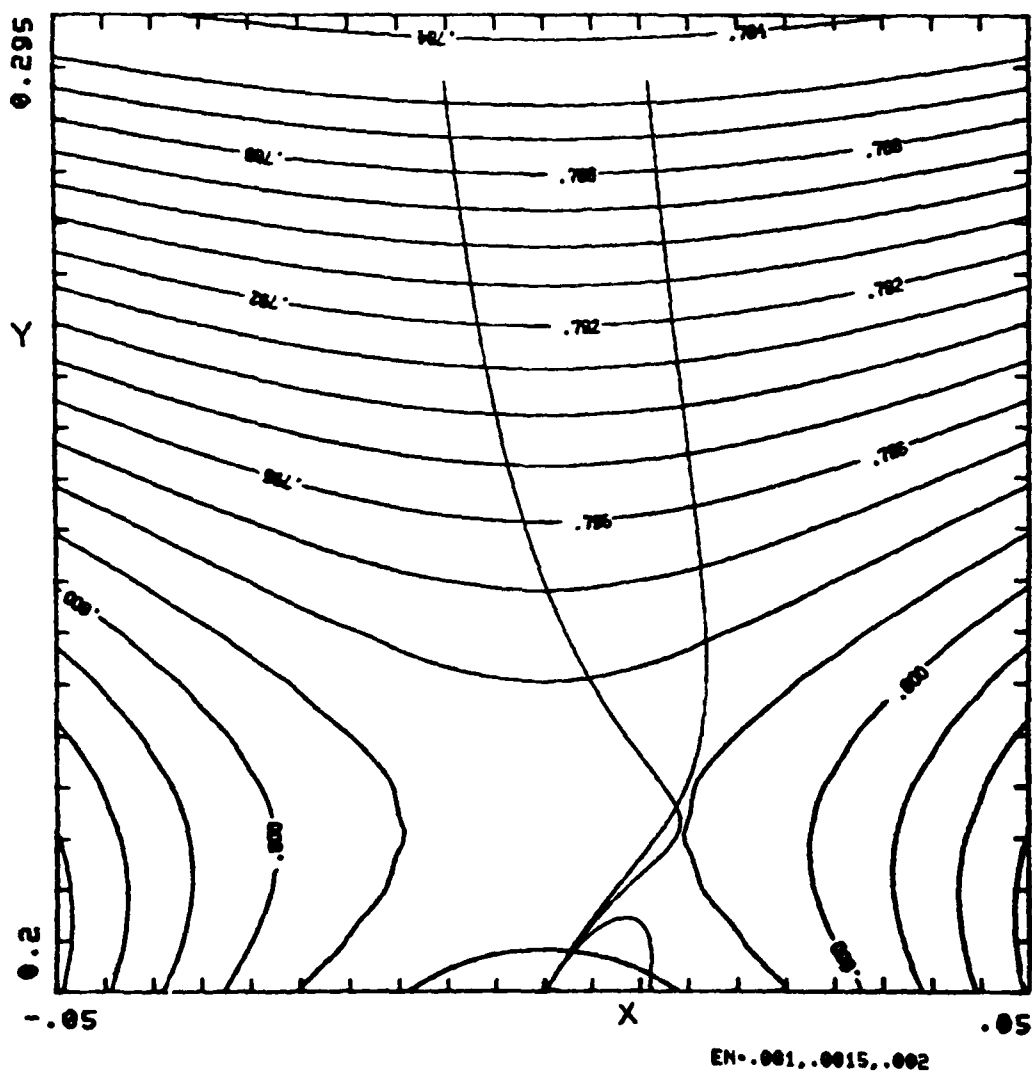
$$\gamma = +0.1$$


Figure 3.2 Potential Contours and Particle Trajectories in the Field of a Circular Double Disk.

The coefficients are easily found since

$$V(a, \theta) = \begin{cases} \gamma & \theta < \beta \\ 1 \text{ (or } 0) & \theta > \beta \end{cases}$$

and

$$\alpha_n = (n + \frac{1}{2}) \int_0^\pi f(\theta) P_n(\cos \theta) d(\cos \theta)$$

by orthogonality.

Program TRKCOEF calculates these coefficients. It is run interactively and requires the following inputs:

NTerm = # of terms in the series

RRR = cutoff distance for "nearness" to the probe.

(good convergence is obtained for RRR = 1.1 when NTerm=38)

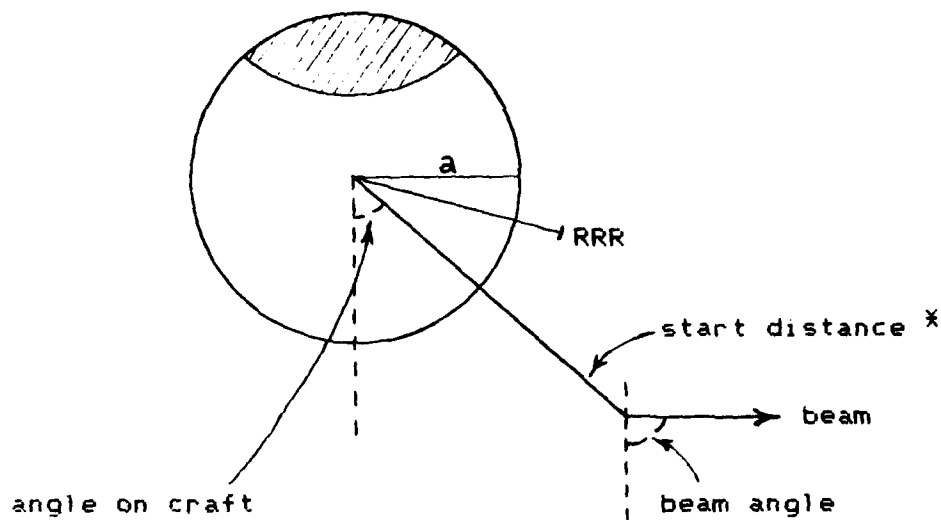
B = the angle β in degrees

G = the charge on the cap

The integrals involved are evaluated analytically; the limit on NTerm is around 50 due to the difficulty of calculating high order Legendres.

Whether the charge on the lower portion of the probe is 1 or 0 is determined by the parameter GAB in subroutine CHECK. Program TRKPLOT sets up a file for contour plotting. TRKCOEF saves the coefficients on TAPE5 and must be run (or TAPE5 saved) before other programs are run.

Program TRKIONS uses HPCG to track particles from a previously generated potential. It allows various starting positions, on or off the probe, and various beam energies and angles. They are defined as follows:



* start distance = 0 will start the particle at $r = RRR$.

Every 600 timesteps, the program asks whether you wish to stop. Thus, in its present form it has to be run interactively.

The status of this problem was that the "hot spot" did not seem to trap the beam when it is released from a point near the craft. This means, at least, that the situation is more complicated than was originally imagined.

3.2 Evaluation of Geomagnetic Field Models

Introduction

An important feature in the application of particle beam emitters is the accuracy with which the beam can be delivered from the spacecraft to the selected target. Since the beam is charged, its trajectory is strongly influenced by the geomagnetic field it must traverse. Thus accuracy of timing is contingent on an accurate knowledge of the geomagnetic field itself. This study determines directly the effect of uncertainties in the geomagnetic field model on targeting by calculating the trajectories of beam particles with various geofield models. Since the discrepancy within different models is expected to be at least as large as the difference between the "best" model and the true field, the study should provide a rough upper bound on the accuracy with which beams can presently be targeted.

Models

The models are based upon fits of experimental data to an expansion of spherical harmonics. The coefficients are referred to a specific year and correction terms are sometimes provided for subsequent years. The study was conducted for the year 1980. In addition to yearly variation, there is also a dependence in the field on time of day and sunspot activity. These effects were investigated by using additional sets of coefficients, consisting of correction terms to the reference IGRF80 set, for 0900 and 1300 hours and for noon at sunspot minimum. The models used and the size of the coefficient sets are given in Table 3.1.

Table 3.1 Geomagnetic Field Models

Model	Order (NMAX = ORDER + 1)
1) IGRF80	10x10
2) Barraclough 80	10x10
3) Barraclough 75	12x12
4) Magsat	13x13
5) WC80	12x12
6) Sq mods (to IGRF80)	

Simulations were carried out for two particle types, two starting altitudes, three initial beam energies and three aiming directions. Thus a total of 36 trajectories were calculated for each model. Trajectories were followed through one gyro rotation and stopped 20 km below the starting altitude. The IGRF80 trajectory was used as the target definition, and deviation of other trajectories from this one was calculated as the nearest approach of a target and test trajectory, without regard to correlation in time.

Procedure

In order to add a set of coefficients to the existing system of programs, the following sequence of runs is carried out:

- 1) The program CNGMAG is used to convert the Gauss normalized coefficients to Schmidt normalized form and to correct the coefficients to the desired epoch. The correction terms are input along with the coefficients and currently extend to second order in time. The program creates a data block containing the renormalized coefficients to be injected into subroutine NEWMG10 of the trajectory generating program.

2) The simulator⁽²⁾ was provided by D. Smart (AFGL) and was transferred to a program library called TJPL. There are several copies therein of the field generating subroutine NEWMG10. The highest order spherical harmonic to date is $N=14$. If a higher order is desired, the program CONMAG will write a new NEWMG10 subroutine. Some problems in the format statements of CONMAG, causing intermediate zeros in constants to be eliminated, have been encountered and care should be exercised in any future use. If the dimension of the new coefficient set is 14 or less, one of the existing NEWMG10's in TJPL can be used directly.

3) The data statements written by CONMAG are injected into NEWMG10 and the program library is updated.

4) The simulation is carried out for a given starting configuration and field model using TJPL. Figure 3.3 shows a typical trajectory for a few gyro rotations.

5) Results from this and previous IGRF80 calculations are compared using program TJCALC, which finds the minimum distance discrepancy between test and reference trajectory.

Results

The longest distances travelled occurred for high energy lithium ions at high altitude and were on the order of 700 km. The shortest were for low energy protons at low altitude and were around 15 km. The miss distances from the IGRF 80 trajectory, as a percent of total distance travelled, were 0.08% for WC 80 and 0.01% for MGST 4181 at high altitudes, and 0.14% for WC 80 and 0.025% for MGST 4181 at low altitude. The daily solar corrections added to the IGRF 80 model gave target deviations on the same order of magnitude.

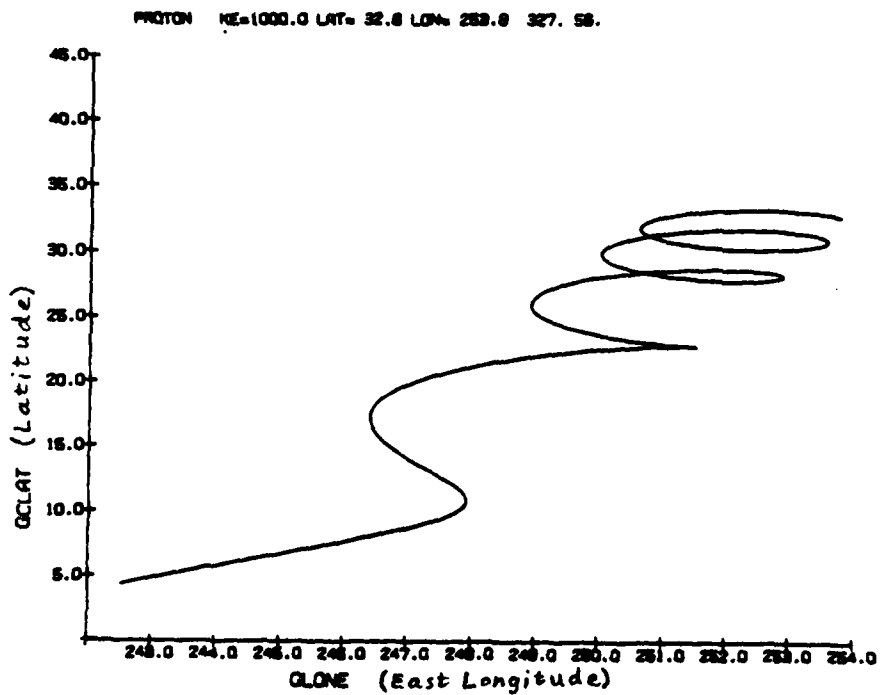
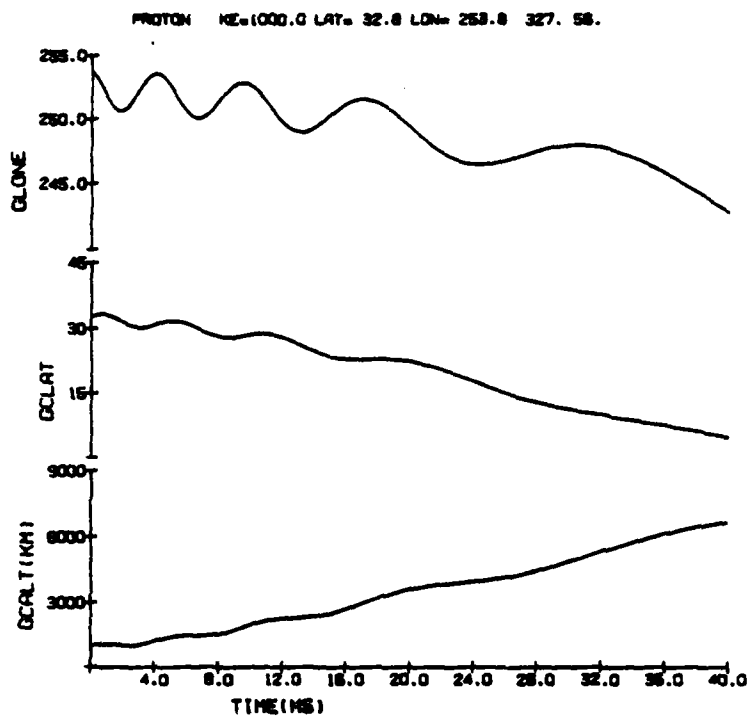


Figure 3.3 Particle Beam Trajectory in the Geomagnetic Field

References

1. Sherman, C. and Parker, L.W., "Potential Due to a Circular Double Disk", J.A.P. Feb. 1971, Vol. 42, No. 2.
2. McCracken, K.G., Rao, U.R., and Shea, M.A., "Trajectories of Cosmic Rays in a High Degree Simulation of the Geomagnetic Field", MIT TR No. 77 (NYO-2670), August 1962.

4.0 Atmospheric Density and Winds from Accelerometer Data

Triaxial accelerometers capable of measuring accelerations in the tenths of micro-g's are released in rocket launched spinning spheres. Once the sensor system is not subject to the large propulsive forces, the sensitive devices are uncaged and, being in continuous free fall in the earth's gravitational field, are able to detect the remaining forces acting on the sensors. These forces are primarily due to the drag of the sphere in the earth's atmosphere, but may include centrifugal forces arising out of module spin and precession. Since the objective of these experiments is the study of atmospheric structure in the lower thermosphere, eccentric forces are an undesirable contaminant, and are eliminated by design by locating the sensors close to the dynamic center of the spinning spheres. Any residual imbalanced signals are attenuated by special notch filters when the expected contaminant frequencies are known e.g. spin frequency for spin axis Z-sensors. Other undesirable modulation signals must be totally removed by computational filtering prior to any detailed processing for analyses of atmospheric density and wind structure.

In the case of the rocket launched experiments, the sensor unit resides within a sphere that is released after launch, and includes the telemetry for transmitting the sensor signals. The trajectory is geographically "local", and analyses have been performed in launcher referenced coordinates in which the spin axis orientation stays inertially fixed. Earth curvature must be accounted for when equating upleg and downleg densities and wind vectors, and can be accomplished by using actual trajectory altitudes at all times. Figure 4.1 shows the coordinate systems which are appropriate for rocket sphere studies. The X" system

is in the spinning sphere reference frame, with Z'' the spin axis direction. The X' and X systems are non-spinning and embedded in the trajectory plane, with $Z' (=Z'')$ coincident with the sphere axis, tilted forward at angle α relative to launcher vertical Z .

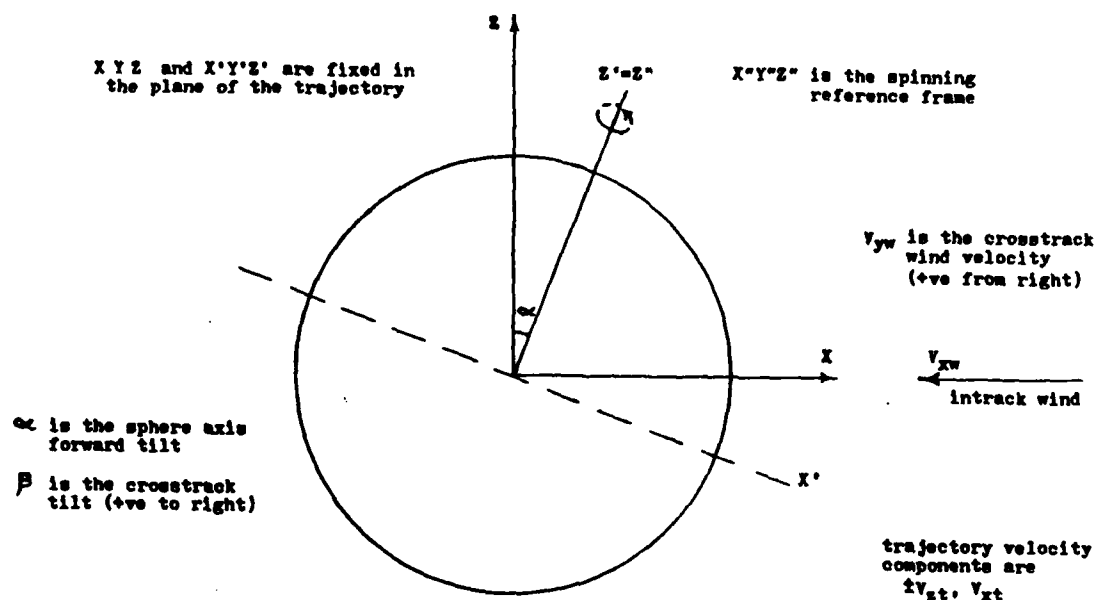


Figure 4.1 Coordinate Systems for the Rocket Sphere

Important functions that the data processing system performs are:

- 1) Telemetry data compaction and splicing
- 2) Sensor calibrations
- 3) Signal demodulation and conditioning
- 4) Trajectory evaluation and integration
- 5) Maintenance of an evolving Resource File
- 6) Resolution of sensor orientation and transverse and in-track winds

- 7) Resolution of consistent density and temperature profiles
- 8) Tables and graphical presentations in interactive or batch mode
- 9) Comparison with other concurrent experiments
- 10) Evaluation of reliability of results
- 11) Studies of auxiliary associated phenomena

A schematic of the program flow and intermediate files is shown in Figure 4.2, starting from the DECOMM tape and calibration and trajectory data. In addition to the final density and wind profiles in file SPIR, tables, plots and supporting analyses are end products. The scope of each functional area is now discussed. The AC13 sphere experiment at Esrange on Dec.1, 1980 serves as the prototype for the sample results in this report.

4.1 Telemetry Data Compaction and Splicing

The 12-bit PCM coded sensor signals are available over the duration of the flight, after sphere release. It is advantageous if the complete data are available on-line during the initial splicing, calibration, and sensitivity and phase adjustment studies. PACKER routines available in the SUNY program library allow all the data for four X and Y channels, plus three Z and a Nutation channel over the 300+ second span of the experiment to be resident on about 2000 PRU's of perm file. The DECOMM tape is checked for sync losses, and the packed file is augmented from alternate telemetry channels for any missing data. Time track errors of nearly 1 second between channels from different radars have been identified during the splicing process; thus such procedures have enhanced quality control over the data base. Once sensor calibrations and signal demodulation results are completed and saved on reduced files, this large packed file need not be resident on permanent file.

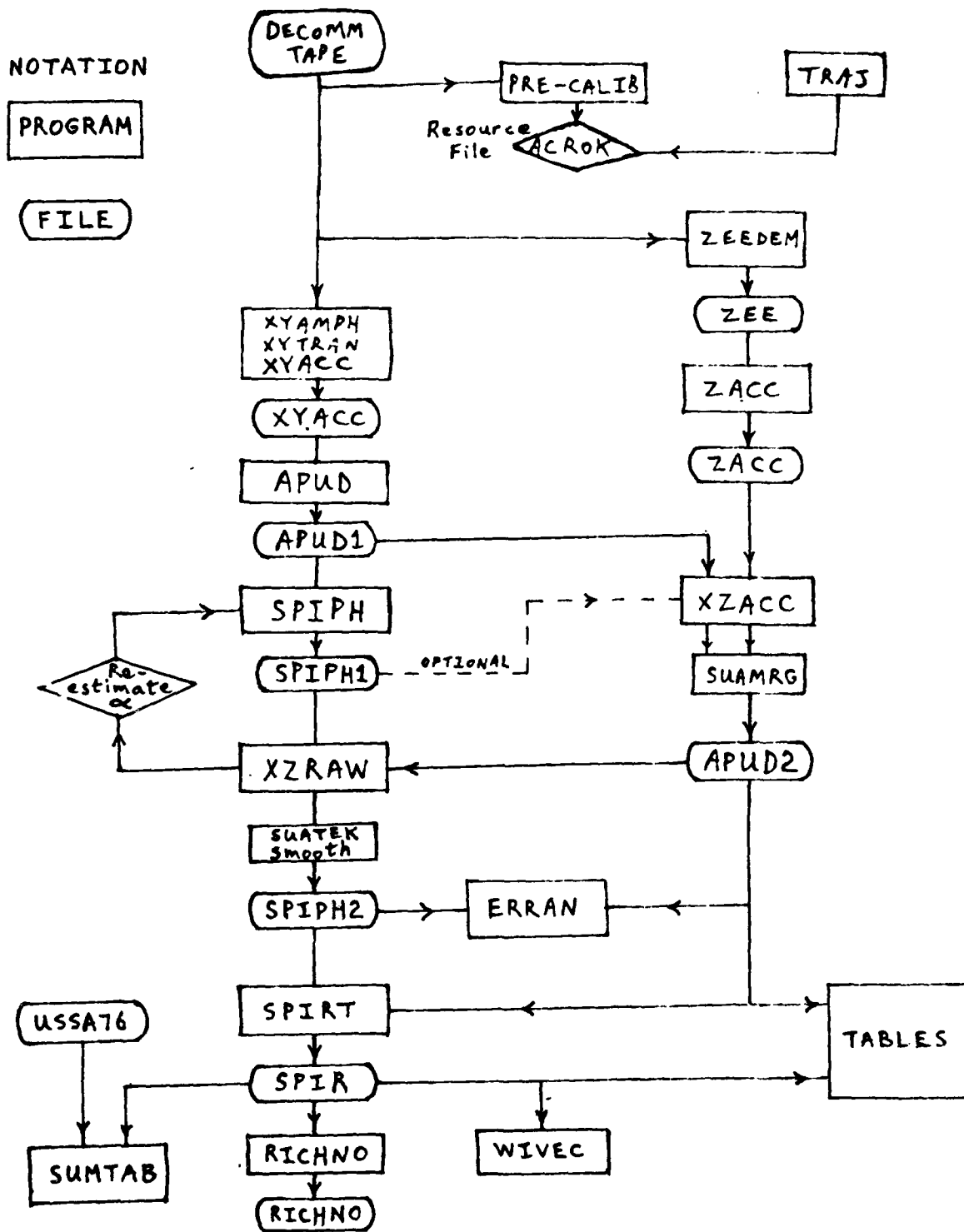


Figure 4.2 Schematic of the Rocket Sphere Processing System

4.2 Sensor Calibrations

Uncaging of the sensors after sphere release initiates a damped resonant response in all the accelerometer bimorphs. These resonant frequencies are invaluable in fixing the calibrations, because the vibrations are produced within the centrifugal force field being experienced by the sensors, and the resultant stiffness and sensitivity calibration estimates improve on the values obtained during lab tests. Correction factors are applied by the researcher, based on the ratio of in-flight and ground based resonant frequencies. Optimized function fitting techniques are used to converge on a best fit solution for each damped oscillation frequency. The Z-axis cases, where the resonance is superposed on the precession modulated signal, have also been implemented and solved using the appropriate extended expressions. A different type of procedure is necessary to determine a calibration correction that accounts for the attenuated slow time constant response of the Z-sensors as the sphere experiences exponentially higher densities on re-entry. Z-signal time constants are determined from log plots, and are applied to lab tests that were performed using various exponential driving functions. A pre-calibration package of results and supporting plots have been provided for each sphere flight.

4.3 Trajectory Evaluation and Integration

In general the trajectory velocity is the greatest contributor to the drag forces experienced by the sphere. Since drag is given by $\frac{1}{2} \rho C_d \frac{\text{Area}}{2m} V_R^2$ where V_R is the velocity of the sphere relative to the atmosphere, it can be seen that inaccuracies in

V_R are amplified. A simplified sphere trajectory calculating routine was installed, a) to create good quality quick look trajectory velocities before refined results become available, and b) to evaluate initial trajectories provided by the range. Launcher referenced trajectory velocity components are formatted and entered at 2 to 5 second intervals in the experiment Resource File. Velocities at any time or altitude upleg or downleg are obtained by cubic interpolation.

4.4 Evolving Resource and Profile Files

In addition to trajectory information, the concept of the Resource File is to collect all initial parameters and intermediate results that are required for processing of subsequent stages of the analysis. Thus, sphere mass, cross-section area, original sensor calibrations, etc. are initially entered. The nominal spin rate is established early and is entered manually. Calibration adjustments to give continuity and consistency are determined later, and are then entered and called by subsequent programs. Figure 4.3 shows a sample segment of the Resource File for the AC13 flight. This presentation provides the investigator and the program user with an up-to-date status of the investigation for each experiment. Profile wind, density, and related solutions per altitude step form a much larger data base, and are not stored on the Resource File, but on successively augmented binary files for ready processing and plotting. Since many rocket sphere flights continue to be studied through improved multi-stages of processing which generate intermediate profiles, a logistics control procedure must be maintained. Figure 4.4 shows a recent chart which, using established input from the Resource File, permits any of the program modules to be rerun with minimum effort.

```

AC13      12/01/80      540.00 SEC.      ESRANGE
SMASS,SAREA (KG, M**2)
10.262, 0.05199
ALAT,FLAZ (LATITUDE, FLIGHT AZIM.)
68., -10.5
FRATE      (FRAME RATE PER SEC.)
.008
CALV      (CALIB. VOLTS PER COUNT)
.009775
RPS      (SPIN RATE, OFFSET, DRIFT REVS. PER SEC.)
5.93340, -.0008, .20E-4
ALPHA,BETA (AXIS TILTS DEG.)
14., 0.
MXV      (1=USE X-SENSOR 2=USE Y-SENSOR)
2
TXV      (3-2, 2-1, 1-2, 2-3, 3-4 CROSS-OVER TIMES X AND Y)
82.,94.,285.,312.,331.5, 80.,93.5,286.,313.5,333.5
CALXY      (ORIG. CAL. M/S**2 PER VOLT FOR X1,X2,X3,X4, Y1,Y2,Y3,Y4)
6.8375E-6,1.8071E-4,4.7216E-3,.1451
9.233E-6,2.489E-4,6.4410E-3,.1926
CRXY      (EST. SENS. RATIOS X1/X2/X3/X4/Y4, Y1/Y2/Y3/Y4/Y4)
26.45,25.90,31.16,1.23, 30.25,24.75,29.92,1.00
CPXY      (EST. PHASE DIFFS X1-X2-X3-X4-X4, Y1-Y2-Y3-Y4-X4)
-7.,45.,-56.,0.0, -3.,42.2,-60.5,-88.2
PHC      (PHASE BIAS X-SENSOR AND Y-SENSOR)
270.,270.
PHS      (PHASE ADJUSTMENTS X1,X2,X3,X4, Y1,Y2,Y3,Y4)
18.,11.,56.,0., -66.8,-69.8,-27.5,-88.
CPH      (LOW ALT. SPIN-DOWN PHASE ADJ. = B*(A-ALT)**2)
85., .045
CAL      (REV. CAL. M/S**2 PER VOLT FOR X1,X2,X3,X4, Y1,Y2,Y3,Y4)
7.190E-6,1.902E-4,4.926E-3,.1535
8.425E-6,2.550E-4,6.3100E-3,.1888
PREF      (PRECESSION FREQUENCY)
.7248
TTST      (START TIMES FOR Z1,Z2,Z3,NUT SENSORS)
300.,310.,325.,340.
TTND      (END TIMES FOR Z1,Z2,Z3,NUT SENSORS)
322.,335.,350.,359.9
TRANS      (Z1-Z2, Z2-Z3, Z3-NUT TRANSITION TIMES)
318.,322.,331.,335.,350.,350.
TCROSS      (Z1, Z2, Z3, NUT CROSS-OVER TIMES)
320.,333.,350.,350.
BG      (BIAS-COUNTS AND GAIN-M/S**2/VOLT FOR Z1,Z2,Z3,NUT)
510.,5.942E-3, 510.71,.05608, 510.36,.7012, 512.,0.
BIAS      (REV. BIAS COUNTS)
510.,510.41,510.22,512.
ZCAL      (REV. CALS. M/S**2/VOLT FOR Z1,Z2,Z3,NUT)
5.838E-3,5.721E-2,.6996,0.
ZTST,ZTND (START,END OF Z-NUT-SENSOR PROCESSING)
300., 345.
BOT,HND      (BOTTOM ALT. FOR XYUP, END ALT. FOR PROCESSING)
85., 55.
ENDROK ***** END OF ROCKET RECORD

```

Figure 4.3 Evolving Resource File (sample segment)

PROCEDURE	PROGRAM	FILES	
		INPUT	OUTPUT
DEMODULATE Z-SENSOR SIGNALS USING KNOWN PRECESSION FREQ. TO GIVE COUNTS/SENSOR	ZEEDEM	AC??TAP	ZEEDEM
DETERMINE OPTIMUM BIAS AND GAIN RATIOS BETWEEN Z-NUT CHANNELS, USING Z2 BIAS ESTIMATE FROM INSPECTION OF PLOTS. ADJUST Z-CALS LEAVING Z2*Z3*Z4 PRODUCT UNCHANGED. APPLY Z-CALS AND BIASES TO CREATE ZACC FILE FROM ZEEDEM COUNTS	ZACC	ZEEDEM	ZACC
ESTABLISH REVISED CALS AND PHASE ADJUST TO GIVE CONTINUITY OF XYACC AND PHASE BETWEEN X-SENSORS, Y-SENSORS, AND X-Y	XYAMPH FOLLOWED BY XYTRAN	AC??TAP AC??TAP	NONE XYTRAN
COMPLETE XYACC RUN USING FINAL GAIN AND PHASE CALS WITH ZERO PHASE ADJUST	XYACC	AC??TAP	XYACC
SMOOTHING AND 1/4 KM. INTERVAL DATA GENERATION FROM FULL XYACC FILE. THIS IS THE ZERO PHASE ADJUST FILE	XYAPUD	XYACC	APUD1
INTERACTIVE SOLUTION FOR RPS, PHC, BETA, ALPHA, SPIND, SALT, DELRPS TO MATCH UPLEG-DOWNLEG CROSSWINDS (UPDATE SPIPH1 AFTER FIXING ALPHA USING XZACC, XZRAW, AND ERRAN)	SPIPH	APUD1	SPIPH1
GENERATE 1/4 KM. INTERVAL XZACC FILE FROM ORIGINAL ZACC FILE, USING APUD1 AND OPTIONAL SPIPH1 FILE	XZACC	ZACC APUD1 (SPIPH1)	XZACC
USE SUAMRG TO MERGE XZACC FILE WITH APUD1 FILE GIVING COMMON DATA FILE	SUAMRG	XZACC	APUD2
USE OVERLAPPING XY AND Z DATA TO SOLVE FOR FURTHER DOWNLEG WIND PROFILE, AND TO RE-ESTIMATE ALPHA	XZRAW	SPIPH1 APUD2	XZRAW
SMOOTH UP-DOWN PHASE AND DOWNLEG WIND SOLUTIONS BEFORE DENSITY-TEMPERATURE CALCULATIONS, AND FOR FINAL PLOTS	SUATEK	XZRAW	SPIPH2
ERROR ESTIMATION PROGRAM MAY BE RUN HERE TO OBTAIN SENSITIVITY ESTIMATES FOR EFFECTS OF CALS, TRAJ VELS, ALPHA, AND PHASE ON RHOD, VXW, VYW	ERRAN	SPIPH2 APUD2	NONE
ITERATIVE RUN TO SIMULTANEOUSLY SOLVE FOR RHO, TEMP, CD CREATING THE FINAL SOLUTION FILE FOR DENSITY, TEMPERATURE, AND WINDS (N-S AND E-W USING FLT.AZ.)	SPIRT	SPIPH2 APUD2	SPIR
DETERMINE RICHARDSON NUMBER VS. ALT. (TURBULENCE)	RICHNO	SPIR	RICHNO
WIND VECTOR PROFILE PRESENTATION	WIVEC	SPIR	WIVEC

Figure 4.4 Processing System for Density, Temperature, Winds
(programs to calibrate, plot, tabulate not shown)

4.5 Signal Demodulation and Conditioning

The equatorial plane (X-Y) sensors are spin frequency modulated, with the amplitude of the signal a direct measure of the lateral drag forces experienced by the sphere. Sine wave function fitting is employed to determine the modulating lateral force amplitude and phase. Calibration sensitivities between sensor channels usually turn out to be somewhat inconsistent, so that sensed acceleration values between, say, X3 and X4, exhibit a jump discontinuity. A program package was developed to adjust all initial calibration sensitivities so that the net percent change for all sensors is minimized, while imposing continuity in the transition regions, and overlap between X and Y sensors. Care is needed in this trimming operation, to avoid interpreting transition discontinuities as density profile features.

The Z-axis sensors are not sensitive to the sphere spin, but the signals are modulated at the precession frequency, which here must be rejected and not demodulated. The resulting signal for each channel starts from near zero and builds up exponentially, with the channel gains set to overlap while providing maximum dynamic range, as for the X-Y sensors above. Gain optimization is again employed for continuity, but special attention is required to estimate and subtract a built-in non-zero bias. Figure 4.5 is a composite plot of the final clean accelerations sensed by the Z-sensor downleg, and the X-Y sensors upleg and downleg. For the X-Y sensors in particular, the high frequency spin modulated acceleration signal ($\approx 6\text{Hz}$) results in excellent bias free data. Demodulation is performed at $\frac{1}{2}$ spin cycle, or at less than 0.1 sec steps. At the lower altitudes where the sphere fall velocity exceeds 1 km/sec, this still allows solutions about 100 m apart. Analyses to date have been conducted conservatively at 1/4 km intervals, but this extension to higher resolution can be readily implemented, for more detailed studies of atmospheric wave and structure patterns.

ZACC * 1.15

Y-SENSOR AC13

0.0.000 M=5.93340 PHC= 0.0

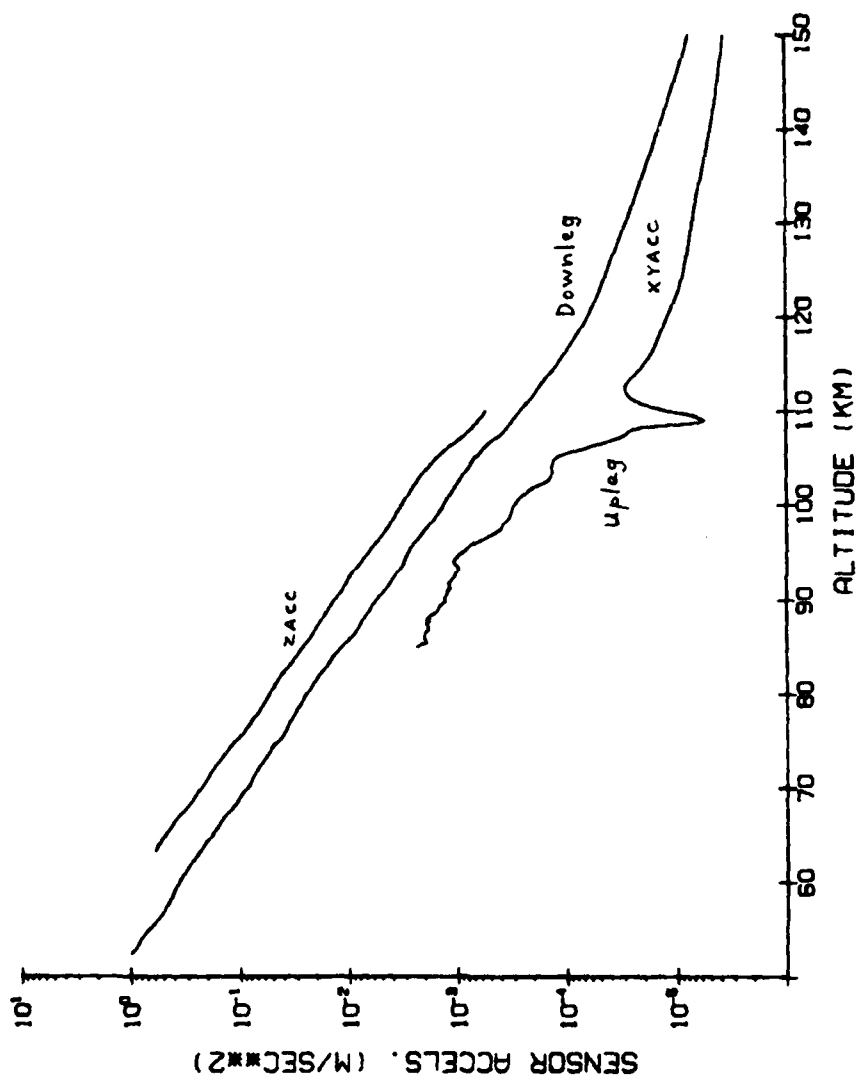


Figure 4.5 Z-sensor and XY-sensor Accelerations

4.6 Sensor Orientation and Winds

Use of a nominal sphere spin rate results in a stable solution for acceleration as a function of altitude. The phase or apparent direction of the acceleration force on the spinning sphere is, however, extremely sensitive to any offset between true and nominal spin rate. The difference is evident as a runaway condition where the apparent peak of the acceleration does not remain locked in the general direction of the trajectory. An effective procedure has been devised to optimize for true spin rate and reference phase, so as to result in transverse wind velocity solutions that are as close as possible on upleg and downleg. The transverse wind is given by

$$V_{yw} = \frac{1}{R(h)} EACC \sin \theta \quad (4.1)$$

where

$$R(h) = V_R \rho C_d \frac{\text{Area}}{2m} \quad (4.2)$$

EACC is the X-Y or equatorial sensed acceleration,

θ is the phase to be optimized,

V_R is roughly the trajectory velocity, and

ρ approximates the true density profile after a few iterations.

The phase θ obtained originally using the nominal spin rate becomes modified according to

$$\theta' = \theta - \epsilon T + \phi \quad (4.3)$$

where ϵ is the spin rate vernier offset, T is trajectory time, ϕ is the reference phase adjustment, and θ' is the corrected phase.

Upleg and downleg transverse wind sensitivities

$$\frac{\partial V_{yw}}{\partial \epsilon} \quad \text{and} \quad \frac{\partial V_{yw}}{\partial \theta}$$

are then used to adjust ϵ and θ for closest upleg-downleg match.

Low altitude spin down is also estimated in this manner by optimizing an altitude dependent polynomial, and in fact introduces the possibility of investigating spin deceleration models. A significant achievement was the identification and quantification of an internal damping spin deceleration for AC13, showing up as a parabolic phase deviation.

Figure 4.6 shows the development steps at this stage. Figure 4.6(a) shows typical upleg-downleg phase solutions for a good fixed nominal spin rate. Figure 4.6(b) shows the final revised spin-phase after the optimization process, which gives the crosswind match of Figure 4.6(c).

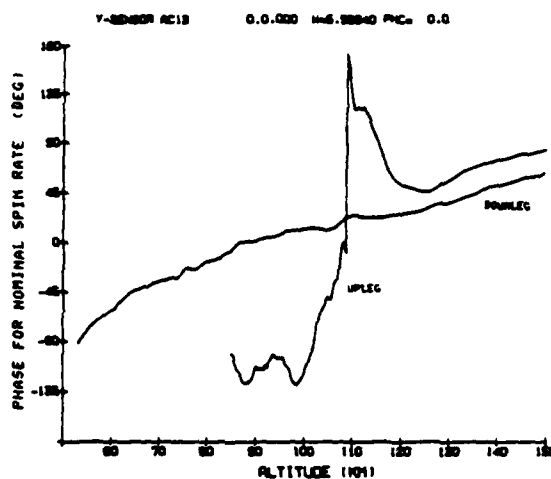
A crucial part of the atmospheric profile analysis is the determination of the forward tilt α of the sphere axis in the trajectory plane. The basic sensed acceleration equations in the non-rotating coordinate system of the sphere fixed in the trajectory plane are

$$XYZ_{acc} = [\vec{V}_t + \vec{V}_w] \vec{B}(\beta) \vec{A}(\alpha) [V_R \rho C_d \frac{Area}{2m}] \quad (4.4)$$

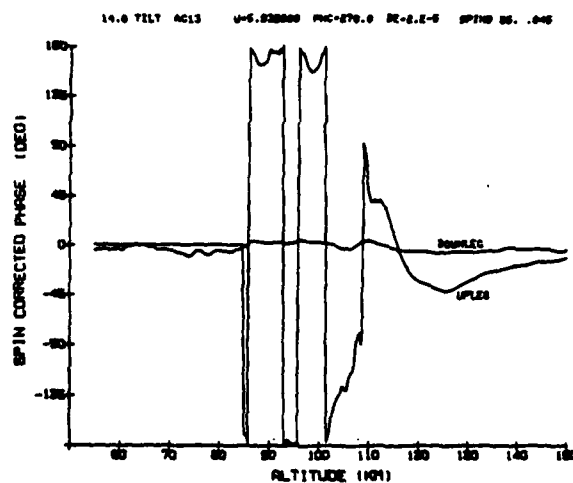
where subscripts t and w refer to the trajectory and wind respectively, $A(\alpha)$, $B(\beta)$ are spherical coordinate transformations corresponding to sphere axis tilt in-, across- the trajectory plane.

The cross tilt β is almost indistinguishable from a small difference in spin rate, in its effect on the sensed accelerations. When sun sensors are installed on daytime flights, this parameter can be further studied along with spin-down. The procedure for establishing α consists of assuming low winds in the 60-80 km region where X-Y as well as Z sensor accelerations are available, and then applying Eq. 4.4. Once α is fixed, the above equation is also applied as follows:

a) Phase obtained using fixed spin rate. With spin orientation not established, upleg-downleg wind solutions differ.



b) Phase obtained with spin rate, damping and drag spin-down, and reference phase optimized for closest cross-wind match.



c) Upleg & downleg cross-winds obtained from phase optimization of (b) above. Downleg values below 85 km. were set to approach Robin sphere test results.

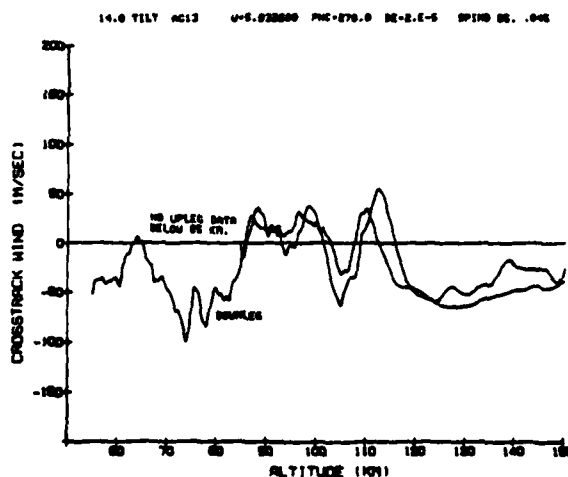


Figure 4.6 Determination of Spin Phase and Crosstrack Wind (AC13)

- a) In the region above 80 km, in-track winds and density are solved simultaneously using upleg-downleg X-Y data.
- b) In the 80 km and lower region, in-track winds are solved using downleg X and Z data for the fixed α , and then with winds known, density is solved using downleg X data alone.

Figure 4.7 shows the final estimated in-track wind profile. Problems of reliability of Z-sensor calibration and filter time response, and therefore uncertainty in the 80 km transition region have been encountered. Overlapping upleg X-Y and downleg Z data are usually available in the 80-100 km region, but unfortunately the Z data are least reliable here. Improved recovery of the true Z-accelerations should be feasible by a procedure that inverts the sensor response transfer function.

4.7 Resolution of Density-Temperature Profiles

Equation 4.4 shows that once trajectory, wind velocity vectors, and the sphere orientation are known, ρC_D is also solved simultaneously and forms the next stage irreducible data base. C_D is a function of Reynolds number (R_e) and Mach number (M), which in turn depend on temperature and the density profile. Given ρC_D and V_R profiles, this interrelationship necessitates an iterative solution procedure as shown in Figure 4.8.

The temperature profile T_m is obtained by integrating along the density profile under the assumptions of the ideal gas law and hydrostatic equilibrium. The drag coefficient C_D is obtained using Whitfield's model for low R_e ,⁽⁶⁾ and provides smooth transition between the free molecular flow and the continuum regions.⁽¹⁾ Figure 4.9 profiles the density ratio to the US Standard Atmosphere (1976), and the associated temperature, that was obtained for AC13.

SPIPH2
NF . 9

14.0 0.0 AC13 65. .045 W=5.932600 PHC=270.0

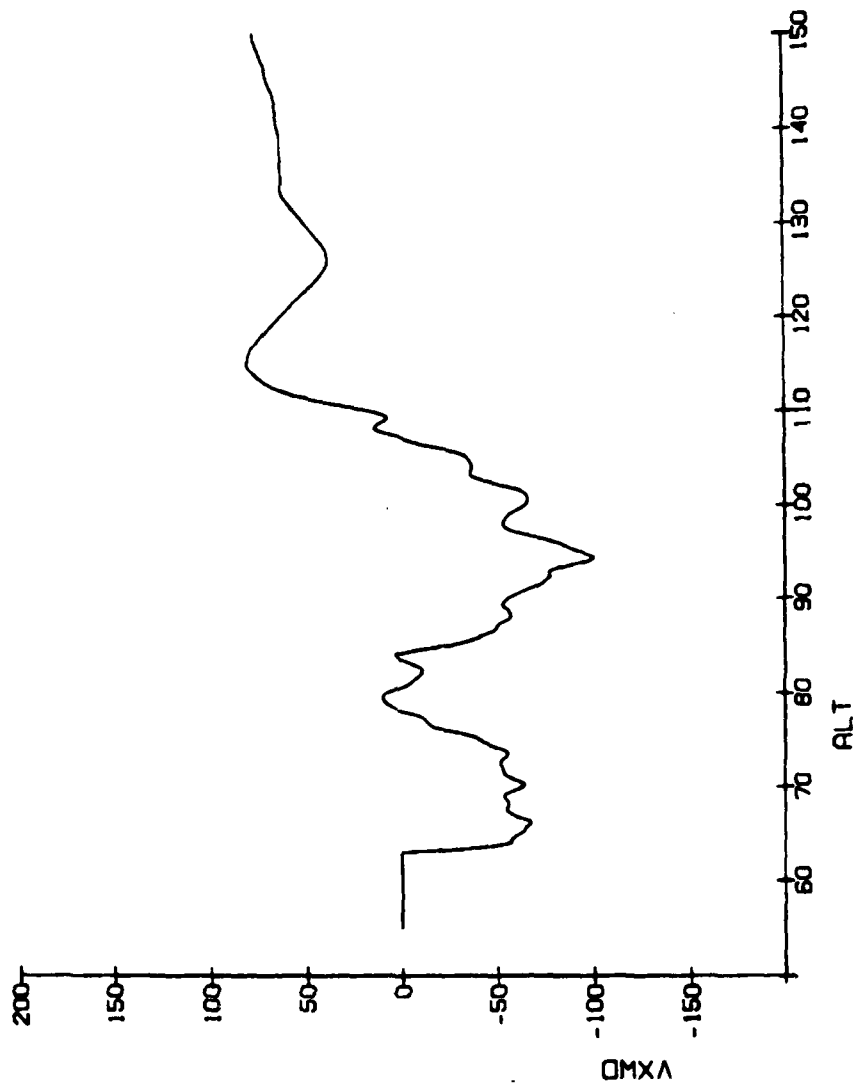


Figure 4.7 Composite Estimate for In-track Wind Profile

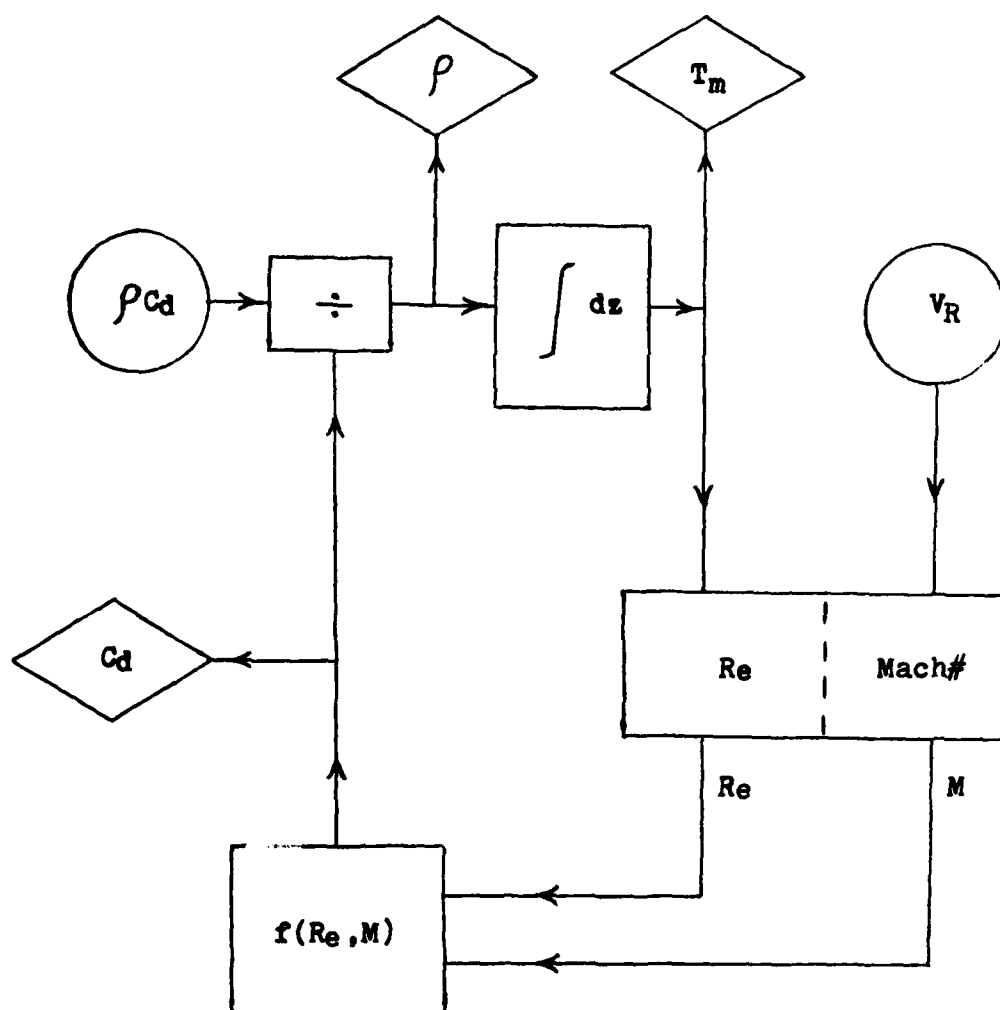


Figure 4.8 Density-Temperature Profiles from ρC_d and V_R
 (the nonlinear dependence of C_d on these parameters
 necessitates an iterative solution procedure)

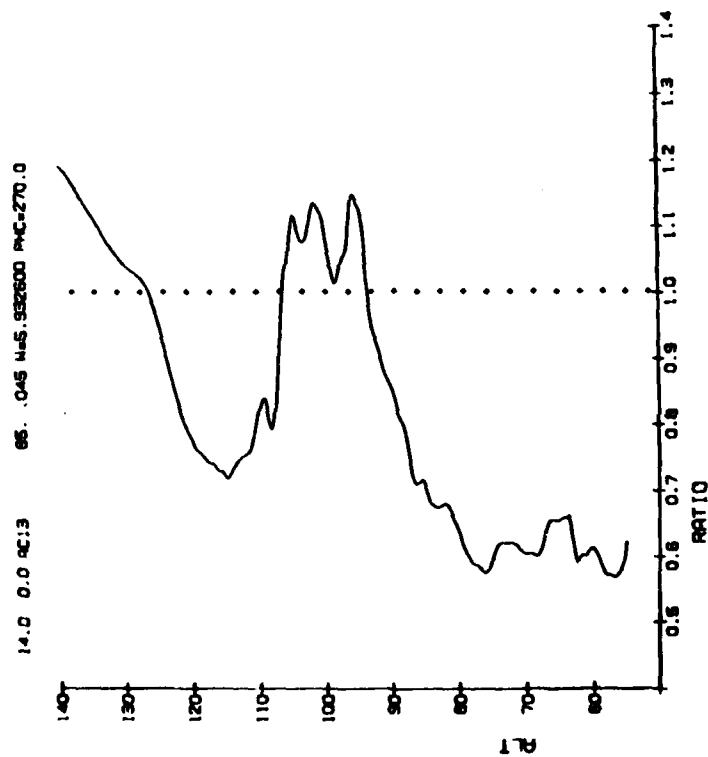
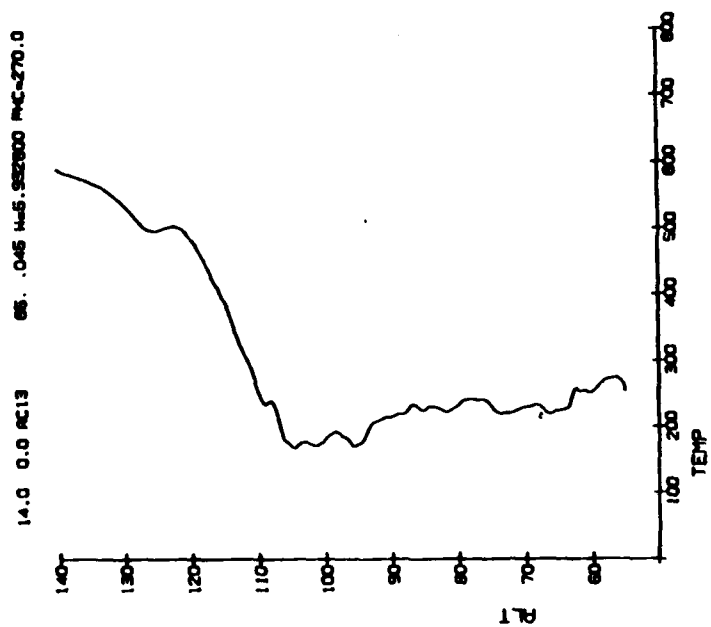


Figure 4.9 Solved Density Ratio (to USSA76), and Temperature Profiles (AC13)

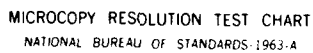
AD-A138 632 ANALYSIS OF SPACECRAFT CHARGING PARTICLE BEAMS AND
GEOPHYSICAL DATA BASES. (U) ARMY SIGNALS WARFARE LAB
VINT HILL FARMS STATION VA K H BHAVNANI ET AL.

2/2

UNCLASSIFIED 31 JUL 83 AFGL-TR-83-0140 F19628-80-C-0127 F/G 22/2

NL

END
DATE
FILED
4 - 84
DTIC



MICROCOPY RESOLUTION TEST CHART
NATIONAL BUREAU OF STANDARDS-1963-A

4.8 Tabular and Graphical Presentations

The processing system propagates augmented profile solution results in SUATEK binary format, and tabulations of desired results are accomplished by simple print-out programs. The Tektronix plotting capability inherent with the files permits intensive interactive operation and evaluation of results of successive processing programs. This capability has permitted the incorporation of many of the analytical features described before, which otherwise would be extremely tedious in a batch processing mode. The present system allows for repeated refining passes after the investigator evaluates results, e.g. revised axis tilt, calibration modification, spin-down model adjustment, consideration of improved drag coefficient model, or installation of other processing modules.

We include here a tabular summary (Table 4.1) of atmosphere and wind profiles. The latter is also depicted in a specialized plot (Figure 4.10) which combines altitude and wind vector data.

4.9 Comparison with Other Concurrent Experiments

Robin sphere and chemical release experiment results become available as the final results for all aspects of a test or campaign are collected for coordination. Good density and wind profile estimates are usually provided from Robin sphere analyses performed around 60-70 km. altitude, which is where the rocket sphere spin deceleration and therefore the wind and density profile is least reliable. Improvement of the spin deceleration model, and even the sphere axis tilt may be warranted if the consensus from the other tests so dictates. These test wind velocities are provided in geographic coordinates, and are converted to the sphere trajectory system for direct comparison.

Table 4.1 Summary of Atmosphere and Wind Profile (AC13)

ALTITUDE (KM)	S-N WIND (M/S)	W-E WIND (M/S)	TEMP (DEG K)	TEMP-US78 (DEG K)	DENSITY (KG/M**3)	DENSITY RATIO TO USSA78
140.	-58.4	34.1	590.4	30.7	4.570E-09	1.193
139.	-58.3	28.8	584.5	33.1	4.855E-09	1.184
138.	-57.9	30.1	581.2	38.3	5.135E-09	1.168
137.	-58.8	30.0	577.9	43.6	5.427E-09	1.162
136.	-54.4	48.0	574.1	48.5	5.784E-09	1.138
135.	-53.3	52.9	569.8	53.1	6.121E-09	1.120
134.	-53.3	52.9	565.2	57.7	6.504E-09	1.103
133.	-52.8	54.5	560.8	62.6	6.911E-09	1.084
132.	-49.5	57.3	553.6	64.9	7.349E-09	1.070
131.	-44.9	60.3	545.8	66.7	7.818E-09	1.057
130.	-40.8	60.4	537.2	67.9	8.310E-09	1.044
129.	-37.3	57.4	526.2	67.0	8.197E-09	1.035
128.	-34.1	52.8	513.8	64.8	9.065E-09	1.028
127.	-30.8	51.1	503.1	64.5	1.083E-08	1.016
126.	-28.4	55.0	497.0	69.0	1.165E-08	.995
125.	-28.0	61.5	488.1	78.9	1.241E-08	.967
124.	-30.7	65.9	479.3	93.1	1.312E-08	.919
123.	-35.6	64.9	502.3	107.4	1.388E-08	.875
122.	-41.4	61.9	502.5	119.0	1.475E-08	.835
121.	-47.2	58.9	497.2	125.3	1.587E-08	.803
120.	-52.0	57.1	484.8	124.8	1.734E-08	.769
119.	-57.1	56.7	470.4	122.4	1.909E-08	.761
118.	-61.7	57.1	450.8	114.5	2.124E-08	.750
117.	-66.0	58.9	428.8	104.8	2.410E-08	.742
116.	-69.9	53.2	409.8	97.8	2.719E-08	.721
115.	-72.8	43.0	389.6	89.6	3.094E-08	.722
114.	-73.4	31.8	361.8	73.8	3.631E-08	.730
113.	-70.1	19.0	332.5	56.5	4.332E-08	.748
112.	-62.2	8.6	308.0	44.8	5.161E-08	.755
111.	-49.0	-14.4	284.3	32.3	6.242E-08	.770
110.	-26.9	-29.0	262.9	12.9	7.816E-08	.818
109.	-12.8	-27.4	235.1	4.7	8.726E-08	.838
108.	-15.0	-6.4	239.0	15.7	1.005E-07	.764
107.	2.0	14.7	207.9	-9.8	1.455E-07	.888
106.	21.6	25.2	178.3	-34.8	2.014E-07	1.031
105.	39.2	24.0	168.8	-40.0	2.563E-07	1.103
104.	39.8	10.9	174.1	-31.2	3.011E-07	1.068
103.	35.9	-5.2	177.3	-24.9	3.558E-07	1.078
102.	50.3	-16.6	172.4	-27.1	4.411E-07	1.121
101.	61.9	-25.0	174.0	-23.2	5.290E-07	1.127
100.	61.0	-28.7	181.9	-13.2	6.097E-07	1.088
99.	52.9	-29.2	180.7	-2.5	6.936E-07	1.031
98.	48.4	-32.1	190.0	-1.7	8.272E-07	1.025
97.	53.8	-38.8	183.4	-7.0	1.024E-06	1.057
96.	72.9	-42.8	171.2	-18.1	1.322E-06	1.138
95.	87.6	-29.8	174.2	-14.2	1.576E-06	1.131
94.	94.9	-27.2	186.8	-1.0	1.769E-06	1.059
93.	76.1	-23.3	206.2	19.0	1.896E-06	.948
92.	72.2	-29.3	216.0	23.0	2.185E-06	.913
91.	83.4	-28.0	214.3	27.5	2.504E-06	.878
90.	53.4	-22.2	215.5	28.8	2.808E-06	.851
89.	50.1	-24.6	218.5	32.7	3.325E-06	.815
88.	52.9	-28.4	221.1	34.2	3.841E-06	.788
87.	44.2	-35.7	233.2	48.3	4.216E-06	.724
86.	38.7	-21.2	226.6	41.8	4.963E-06	.713
85.	28.0	10.8	226.4	37.5	5.807E-06	.706
84.	3.3	35.3	230.6	39.8	6.589E-06	.680
83.	13.9	42.9	227.9	35.1	7.708E-06	.676
82.	18.6	51.3	222.7	28.0	9.143E-06	.681
81.	11.5	51.5	226.8	30.1	1.047E-05	.661
80.	2.3	49.0	232.9	34.3	1.172E-05	.635
79.	6.1	57.0	240.5	40.0	1.308E-05	.608
78.	15.4	61.3	242.2	39.6	1.489E-05	.590
77.	25.9	71.9	240.7	38.2	1.720E-05	.584
76.	30.9	42.1	240.5	34.1	1.877E-05	.578
75.	51.2	46.8	228.5	20.1	2.397E-05	.601
74.	64.1	75.8	220.7	10.4	2.881E-05	.621
73.	84.5	82.1	221.3	8.0	3.343E-05	.621
72.	62.3	51.6	222.1	7.8	3.872E-05	.621
71.	62.7	40.8	227.2	10.4	4.393E-05	.610
70.	72.5	29.0	230.2	10.6	5.016E-05	.608
69.	58.8	21.2	232.2	9.9	5.745E-05	.604
68.	59.8	24.2	231.7	8.7	6.445E-05	.609
67.	58.1	13.3	221.8	-8.0	8.046E-05	.644
66.	69.6	3.4	221.2	-8.3	9.386E-05	.656
65.	61.1	-11.5	225.1	-8.2	1.071E-04	.657
64.	49.8	-14.1	227.7	-8.4	1.228E-04	.660
63.	3.3	1.4	248.0	10.3	1.397E-04	.611
62.	2.0	10.6	254.3	12.8	1.446E-04	.601
61.	5.2	28.1	254.0	9.8	1.651E-04	.604
60.	7.4	39.9	252.8	5.8	1.895E-04	.612
59.	8.7	38.2	263.5	13.8	2.070E-04	.591
58.	7.8	40.4	272.3	19.8	2.270E-04	.573
57.	6.8	36.9	274.1	18.8	2.549E-04	.570
56.	8.8	38.7	271.6	13.5	2.908E-04	.578
55.	9.8	51.3	283.4	-7.4	3.638E-04	.623

14.0 0.0 AC13 85. .045 N=5.932600 PHC=270.0

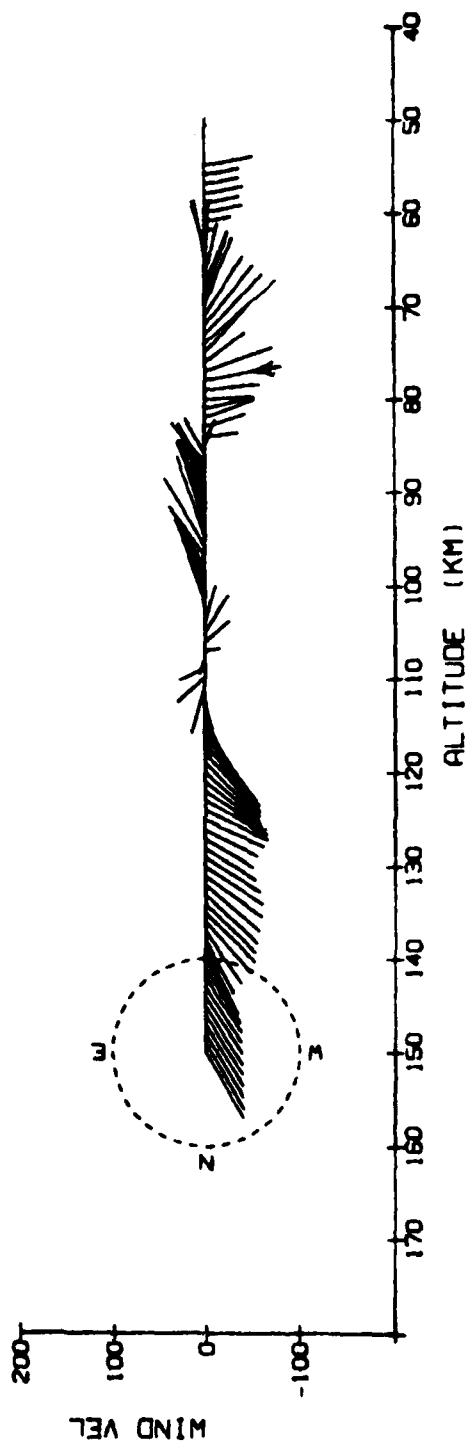


Figure 4.10 Plot of Geographic Wind Vector Profile (AC13)

In this manner it was concluded that the AC12 and AC13 Z-acceleration values were about 15% low, and the revised calibrations jointly improved in-track wind and low altitude densities. Chemical release measurements provide good wind velocity estimates at the higher altitudes, with greatest confidence placed on these tests under conditions of uniform winds, particularly in directions transverse to the lines of sight. Refinement of the rocket sphere spin rate, suggesting a cross-track axis tilt, would be possible using these data.

4.10 Evaluation of Reliability of Results

Uncertainties in the density and wind solutions arise as discussed above, primarily from

- a) Calibration coefficients
- b) Trajectory velocity provided
- c) Spin axis tilt estimate
- d) Spin phase orientation estimate

The equations that have been described in Section 4.6 for the inversion of Eq. 4.4 are also directly useable for determining the sensitivity of the solutions to variations in the above four parameters. An error analysis program has evolved in parallel with the complete solution algorithm, and turns out to be most useful, not only to establish error-bars, but also to determine whether any combination of adjustments of the parameters would bring results closer to values from other sources. (Table 4.2) Further advances in these sensitivity estimating programs are possible in order to include other variables such as cross-track tilt, and for implementation of alternate solution procedures in the 80 km transition region.

Table 4.2 Solution Sensitivity Error Analysis (AC13)

14.0 0.0 AC13 86.045 U-5.938000 PHC-870.0

ERROR ANALYSIS FOR RCD, UVW, UVS, DUE TO
1% ERROR IN CAL, 1 R/S ERROR IN UXT, UZT,
AND 1 DEG. ERROR IN ALPHA, PHASE.

ALT	CAL	UXT	UZT	ALF	PHI	CAL	UXT	UZT	ALF	PHI	CAL	UXT	UZT	ALF	PHI
150.0	1.00	-.56	-.26	-0.64	-.13	0.00	.01	.23	23.61	.89	0.00	-.12	-.03	-1.04	7.07
149.0	1.00	-.53	-.25	-0.48	-.04	0.00	.85	.81	23.59	.79	0.00	-.12	-.03	-1.04	7.17
148.0	1.00	-.51	-.25	-0.34	-.07	0.00	.79	.20	23.45	.88	0.00	-.11	-.03	-1.04	7.21
147.0	1.00	-.49	-.25	-0.21	-.14	0.00	.73	.18	23.32	1.01	0.00	-.11	-.03	-1.04	7.25
146.0	1.00	-.47	-.24	-0.08	-.18	0.00	.68	.17	23.18	1.08	0.00	-.10	-.03	-1.04	7.29
145.0	1.00	-.45	-.23	0.09	-.15	0.00	.64	.16	23.12	.99	0.00	-.10	-.03	-1.04	7.34
144.0	1.00	-.44	-.23	0.30	-.13	0.00	.60	.15	23.04	.97	0.00	-.10	-.02	-1.04	7.38
143.0	1.00	-.43	-.23	0.50	-.15	0.00	.56	.14	22.82	1.01	0.00	-.10	-.02	-1.04	7.41
142.0	1.00	-.41	-.22	0.73	-.16	0.00	.53	.13	22.75	1.06	0.00	-.09	-.02	-1.04	7.46
141.0	1.00	-.40	-.22	0.86	-.16	0.00	.50	.13	22.72	1.05	0.00	-.08	-.02	-1.04	7.52
140.0	1.00	-.39	-.21	0.99	-.18	0.00	.48	.12	22.66	1.07	0.00	-.08	-.02	-1.04	7.57
139.0	1.00	-.38	-.21	0.83	-.27	0.00	.45	.11	22.59	1.15	0.00	-.06	-.01	-1.27	7.64
138.0	1.00	-.37	-.21	0.47	-.22	0.00	.43	.11	22.58	1.16	0.00	-.06	-.01	-1.37	7.68
137.0	1.00	-.36	-.20	0.43	-.16	0.00	.41	.10	22.56	1.12	0.00	-.06	-.01	-1.05	7.71
136.0	1.00	-.35	-.20	0.39	-.09	0.00	.39	.10	22.53	1.08	0.00	-.11	-.01	-2.68	7.78
135.0	1.00	-.36	-.20	0.36	-.07	0.00	.37	.09	22.52	1.09	0.00	-.12	-.01	-3.04	7.84
134.0	1.00	-.34	-.19	0.32	-.07	0.00	.36	.09	22.58	1.18	0.00	-.12	-.01	-3.04	7.89
133.0	1.00	-.33	-.19	0.29	-.06	0.00	.34	.08	22.61	1.12	0.00	-.12	-.01	-3.16	7.95
132.0	1.00	-.32	-.19	0.24	-.05	0.00	.32	.08	22.89	1.17	0.00	-.13	-.01	-3.41	8.01
131.0	1.00	-.31	-.18	0.19	-.05	0.00	.29	.07	21.98	1.19	0.00	-.14	-.01	-3.69	8.04
130.0	1.00	-.31	-.18	0.14	-.04	0.00	.27	.07	21.37	1.20	0.00	-.14	-.01	-3.74	8.09
129.0	1.00	-.31	-.18	0.09	-.04	0.00	.24	.06	21.37	1.21	0.00	-.13	-.01	-3.67	8.09
128.0	1.00	-.30	-.18	0.04	-.04	0.00	.22	.06	21.04	1.21	0.00	-.12	-.01	-3.49	8.07
127.0	1.00	-.30	-.18	0.00	-.09	0.00	.20	.05	20.79	1.24	0.00	-.12	-.01	-3.21	8.06
126.0	1.00	-.29	-.17	0.07	-.06	0.00	.19	.05	20.65	1.21	0.00	-.12	-.01	-3.52	8.09
125.0	1.00	-.29	-.17	0.06	-.02	0.00	.18	.04	20.70	1.16	0.00	-.14	-.01	-3.98	8.06
124.0	1.00	-.28	-.17	0.06	-.02	0.00	.18	.04	20.97	1.09	0.00	-.15	-.04	-4.26	8.08
123.0	1.00	-.28	-.17	0.06	-.02	0.00	.18	.04	21.31	1.04	0.00	-.14	-.03	-4.12	8.21
122.0	1.00	-.27	-.16	0.06	-.01	0.00	.18	.05	21.70	1.01	0.00	-.13	-.03	-3.83	8.34
121.0	1.00	-.27	-.16	0.07	-.00	0.00	.19	.05	22.10	.98	0.00	-.12	-.03	-3.55	8.47
120.0	1.00	-.27	-.16	0.07	-.00	0.00	.19	.05	22.43	.93	0.00	-.11	-.03	-3.46	8.58
119.0	1.00	-.26	-.16	0.08	-.02	0.00	.19	.05	22.82	.82	0.00	-.10	-.03	-3.25	8.72
118.0	1.00	-.26	-.16	0.08	-.06	0.00	.19	.05	23.17	.69	0.00	-.10	-.03	-3.23	8.86
117.0	1.00	-.26	-.16	0.08	-.12	0.00	.20	.05	23.49	.50	0.00	-.10	-.02	-3.16	9.00
116.0	1.00	-.26	-.16	0.08	-.19	0.00	.20	.05	23.79	.30	0.00	-.09	-.02	-2.85	9.12
115.0	1.00	-.25	-.15	0.08	-.23	0.00	.19	.05	23.81	.18	0.00	-.07	-.02	-2.15	9.17
114.0	1.00	-.25	-.15	0.03	-.26	0.00	.18	.04	23.68	.04	0.00	-.04	-.01	-1.29	9.17
113.0	1.00	-.25	-.15	0.00	-.26	0.00	.18	.04	23.18	-1.09	0.00	-.01	-.00	-.48	9.10
112.0	1.00	-.24	-.15	0.04	-.20	0.00	.13	.03	22.67	-1.02	0.00	.01	.00	.44	8.95
111.0	1.00	-.24	-.15	0.06	-.06	0.00	.09	.03	21.16	-.64	0.00	.05	.01	1.66	8.68
110.0	1.00	-.23	-.15	0.06	-.08	0.00	.03	.01	19.27	-.32	4.06	.07	.02	2.39	8.37
109.0	1.00	-.23	-.15	0.01	-.10	0.00	-.00	-.00	18.87	-.15	0.00	.06	.04	2.11	8.15
108.0	1.00	-.23	-.15	0.02	-.17	0.00	.01	.00	18.88	.01	0.00	.02	.00	.88	8.34
107.0	1.00	-.23	-.16	0.07	-.08	0.00	-.03	-.01	17.59	.61	0.00	-.03	-.01	-1.07	8.04
106.0	1.00	-.22	-.14	0.02	-.06	0.00	-.08	-.02	16.61	.80	0.00	-.06	-.01	-2.07	7.84
105.0	1.00	-.22	-.14	0.04	-.11	0.00	-.10	-.02	15.10	1.07	0.00	-.06	-.02	-2.21	7.55
104.0	1.00	-.22	-.14	0.05	-.13	0.00	-.12	-.03	14.77	.88	0.00	-.04	-.01	-1.29	7.52
103.0	1.00	-.21	-.14	0.05	-.13	0.00	-.11	-.03	14.04	.60	0.00	-.00	-.00	-.11	7.62
102.0	1.00	-.21	-.14	0.08	-.08	0.00	-.15	-.04	13.63	.18	0.00	.01	.00	.51	7.77
101.0	1.00	-.21	-.14	0.07	-.03	0.00	-.18	-.04	12.79	-.14	0.00	.01	.01	.96	7.80
100.0	1.00	-.21	-.14	0.01	-.04	0.00	-.18	-.04	12.72	-.41	0.00	.03	.01	1.23	7.23
99.0	1.00	-.20	-.14	0.05	-.05	0.00	-.17	-.04	13.36	-.58	0.00	.04	.01	1.37	7.41
98.0	1.00	-.20	-.14	0.04	-.04	0.00	-.17	-.04	13.62	-.60	0.00	.04	.01	1.64	7.48
97.0	1.00	-.20	-.14	0.05	-.05	0.00	-.18	-.04	13.06	-.32	0.00	.05	.01	2.02	7.43
96.0	1.00	-.20	-.13	0.03	-.09	0.00	-.22	-.05	11.58	-.18	0.00	.05	.01	2.06	7.16
95.0	1.00	-.19	-.13	0.01	-.06	0.00	-.24	-.06	10.72	-.02	0.00	.02	.01	.96	6.98
94.0	1.00	-.19	-.13	0.07	-.07	0.00	-.26	-.07	9.91	.08	0.00	.02	.00	.68	6.84
93.0	1.00	-.19	-.13	0.02	-.04	0.00	-.22	-.06	11.61	-.01	0.00	.02	.00	.65	7.25
92.0	1.00	-.19	-.13	0.02	-.04	0.00	-.22	-.06	11.69	-.16	0.00	.03	.01	1.12	7.30
91.0	1.00	-.19	-.13	0.04	-.02	0.00	-.21	-.05	12.46	-.23	0.00	.03	.01	1.15	7.51
90.0	1.00	-.19	-.13	0.05	-.01	0.00	-.19	-.05	13.34	-.15	0.00	.02	.01	.87	7.71
89.0	1.00	-.19	-.13	0.04	-.04	0.00	-.19	-.05	13.63	-.48	0.00	.03	.01	1.08	7.80
88.0	1.00	-.19	-.13	0.06	-.06	0.00	-.20	-.05	13.00	-.57	0.00	.01	.01	1.32	7.72
87.0	1.00	-.19	-.13	0.04	-.04	0.00	-.18	-.05	13.92	-.36	0.00	.05	.01	1.24	7.97
86.0	1.00	-.19	-.13	0.01	-.04	0.00	-.18	-.04	14.10	-.18	0.00	.02	.01	1.00	8.09
85.0	1.00	-.19	-.12	0.00	-.00	0.00	-.17	-.04	14.82	-.20	0.00	-.03	-.01	-1.11	8.21
84.0	1.00	-.01	-.17	0.04	-.14	0.00	-1.00	.10	21.81	0.00	0.00	.00	.00	.16	8.92
83.0	1.00	-.01	-.17	0.03	-.18	0.00	-1.00	.10	21.89	0.00	0.00	.00	.00	.16	8.94
82.0	1.00	-.01	-.16	0.02	-.22	0.00	-1.00	.18	22.00	0.00	0.00	.00	.00	.25	9.05
81.0	1.00	-.01	-.16	0.02	-.21	0.00	-1.00	.18	22.18	0.00	0.00	.00	.00	.24	9.07
80.0	1.00	-.01	-.16	0.03	-.19	0.00	-1.00	.19	22.36	0.00	0.00	.00	.00	.22	9.08
79.0	1.00	-.01	-.16	0.03	-.23	0.00	-1.00	.18	22.48	0.00	0.00	.00	.00	.25	9.15
78.0	1.00	-.01	-.16	0.03	-.18	0.00	-1.00	.18	22.68	0.00	0.00	.00	.00	.34	9.20
77.0	1.00	-.01	-.16	0.03	-.20	0.00	-1.00	.17	22.63	0.00	0.00	.00	.00	.31	9.28
76.0	1.00	-.01	-.16	0.03	-.19	0.00	-1.00	.16	22.79	0.00	0.00	.00	.00	.19	9.20
75.0	1.00	-.01	-.15	0.04	-.23	0.00	-1.00	.14	22.73	0.00	0.00	.00	.00	.68	9.67
74.0	1.00	-.01	-.15	0.04	-.27	0.00	-1.00	.13	22.80	0.00	0.00	.01	.00	.37	9.46
73.0	1.00	-.01	-.15	0.04	-.31	0.00	-1.00	.13	22.97	0.00	0.00	.00	.00	.28	9.41
72.0	1.00	-.01	-.15	0.04	-.28	0.00	-1.00	.13	23.06	0.00	0.00	.00	.00	.24	9.39
71.0	1.00	-.01	-.15	0.03	-.28	0.00	-1.00	.13	23.18	0.00	0.00	.00	.00	.19	9.37
70.0	1.00	-.01	-.14	0.03	-.19	0.00	-1.00	.12	23.25	0.00	0.00	.00	.00	.15	9.37
69.0	1.00	-.01	-.15	0.03	-.13	0.00	-1.00	.13	23.22	0.00	0.00	.00	.00	.12	9.37
68.0	1.00	-.01	-.14	0.03	-.14	0.00	-1.00	.13	23.54	0.00	0.00	.00	.00	.13	9.40
67.0	1.00	-.01	-.14	0.02	-.19	0.00	-1.00	.12	23.66	0.00	0.00	.00	.00	.10	9.41
66.0	1.00	-.00	-.14	0.01	-.07	0.00	-1.00	.11	23.73	0.00	0.00	.00	.00	.06	9.43
65.0	1.00	-.00	-.14	0.01	-.00	0.00	-1.00	.12	23.87	0.00	0.00	.00	.00	.01	

4.11 Auxiliary Associated Phenomena

As described in the previous sections, studies of AC10, AC12 and AC13 have been completed; and initial processing for flights AC14 thru AC16 has begun. Results and procedures as now implemented have been of sufficient resolution quality to lead to the reporting of basic phenomena,^(2,3) the identification of gravity waves,⁽⁴⁾ and the association of density gradient reversals with supersonic auroral fronts.⁽⁵⁾ The experiment also provides a fertile source for other unscheduled but important measurements in the lower thermosphere, such as estimating the drag and spin down processes. A special study of the telemetry AGC signal was conducted for the sphere's spinning antenna, in order to fix spin orientation. It was shown that the antenna side-lobes introduced unexpected non-uniform spin modulation, rendering phase analysis unreliable. Future daytime flights will include a sun-sensor, and accurate spin down phase determination should be possible.

Atmospheric turbulence studies were also performed through calculation of Richardson number profiles from the solved atmospheric density-temperature profiles. This parameter indicates where the gradient becomes too steep to sustain a stable density profile.

References

1. Philbrick, C.R., Faire, A.C., and Fryklund, D.H., "Measurements of Atmospheric Density at Kwajalein Atoll, 18 May 1977", AFGL-TR-78-0058, January 1978.
2. Philbrick, C.R., McIsaac, J.P., and Bhavnani, K.H., "Atmospheric Structure Associated with Dynamical Processes in the Mesosphere and Lower Thermosphere", IAGA Symposium, Edinburgh, Aug 81
3. Philbrick, C.R. et al, "Vertical Density and Temperature Structure over Northern Europe", Adv. Space Res., 1983, Vol. 2, No. 10.
4. Philbrick, C.R. et al, "Mid-Latitude Measurements of Atmospheric Waves and Structure", EOS Vol 63, 45, Nov 1982.
5. Philbrick, C.R. et al, "Density and Temperature Structure over Northern Europe", JATP (to be published).
6. Whitfield, D.L., "Mean Free Path of Molecules from a Surface in Rarefied Flow with Application to Correlating Drag Data", AIAA Paper No. 73-198, January 1973.

5.0 Interactive Graphics Systems for AFGL Applications

5.1 Graphical Functions

Plotting capabilities very similar to those for conventional static plotters such as Calcomp or microfiche are valuable to a broad range of investigators, for interactive use on the CDC-6600 system at AFGL. This includes

- a) Stacked or overlaid X-Y plotting i.e. more than one plot displayed.
- b) Linear or logarithmic axes scales.
- c) Symbol and connected line plotting to distinguish the graphs.
- d) Additional X-axes for concurrent parameters.
- e) Range of data plotted controlled by record count or dependency variable limits.
- f) Flexible heading and axis labelling.
- g) Running average and other simple plot smoothing options.
- h) Compatability between off-line and on-line data base requirements and procedures.

These capabilities have been implemented for conventional X-Y plots as well as for special pictorial presentations. An integrated interactive graphics package SUATEK^(1,3) incorporates the above and other useful specialized features. Figures 5.1 and 5.2 show the range of options that are available to the SUATEK user in menu form. Figure 5.1 lists the items that may be set by the user in order to select variables to be plotted, or to lay out the plot frame, or to enable options. Activated options may work in extended combinations, and Figure 5.2 describes each one briefly.

BRIEF DESCRIPTION OF THE TERMS

NXU - NUMBER OF THE X-VARIABLE
 NY1 - NUMBER OF THE FIRST Y-VARIABLE
 UPTO 4 Y VARIABLES NY1-NY4 PER PLOT
 XL - LENGTH OF X-AXIS IN INCHES (TEKTRONIX COPY IS 50X)
 Y1L - LENGTH OF Y1-AXIS
 XMIN,XMAX - LEFTMOST, RIGHTMOST ENDS OF X-AXIS
 Y1MIN,Y1MX - BOTTOM, TOP END VALUES OF Y1-VARIABLE
 XOFF - LEFT(-VE) OR RIGHT(+VE) X-AXIS OFFSET IN INCHES
 Y1OF - DOWN(-VE) OR UP(+VE) Y1-AXIS OFFSET
 IPLX - X-AXIS SCALE LINEAR(0) OR LOG(1)
 2 STARTS LINEAR SCALE FROM XMIN MARKED AS ZERO
 IPL1 - Y1 SCALE AND PLOT OPTIONS LINEAR(0,2,4) OR LOG(1,3,5)
 0-1 PRODUCES SYMBOLS AT DATA POINTS
 2-3 PRODUCES A LINE THROUGH DATA POINTS (DEFAULT)
 4-5 PRODUCES CONNECTED SYMBOLS THROUGH DATA POINTS

 NX1 - NUMBER OF FIRST EXTRA X-AXIS VARIABLE (UPTO 4 ALLOWED)
 IST,ISP,IREP - START,STOP, AND REPEAT FACTOR FOR RECORDS
 IREP-1 RECORDS ARE SKIPPED (DEFAULT-1)
 IPARM....NCHK - PLOT AND DATA HANDLING OPTIONS
 -0 DEACTIVATED, -1 ACTIVATED
 NDPN - NUMBER OF DEPENDENCY PARAMETERS (UPTO 5 ALLOWED)
 IDP1 - NUMBER OF THE FIRST DEPENDENCY VARIABLE
 P1MN,P1MX - MIN-MAX ACCEPTANCE RANGE FOR VARIABLE IDP1
 BEFORE CORRESPONDING DATA IS PLOTTED

Figure 5.1 SUATEK Menu of Facilities

DESCRIPTION OF OPTIONS IPARM.....NCHK

IPARM - OVERLAY PLOTS FOR SPECIFIED RANGES OF A PARAMETRIC VARIABLE.
 USE DEPENDENCY PARAMETERS OR PROMPTING TO FIX
 OTHER SIGNIFICANT VARIABLES. INCLUDES OPTION TO

ISORT - SORT UP TO 512 DATA POINTS ON X(*1) OR Y(*2)

IRAV - RUNNING AVERAGE FOR WINDOW OF 'N' DATA POINTS
 VALUE OF 'N' WILL BE REQUESTED

IPOLF - MAKE N'TH ORDER POLYNOMIAL FIT TO DATA IN PLOT RANGE (N*20)
 VALUE OF 'N' WILL BE REQUESTED

ISING - SINGLE PLOT (1-4) FROM MULTIPLE PLOT SPEC

ILBL - REVISE PLOT AXES AND HEADER LABELS
 PROMPTING FOR REVISION WILL OCCUR

IRANGE - REVISE X AND Y PLOT MIN-MAX RANGES
 DEFAULT IS THE PLOT FRAME RANGES

ICOMB - PLOT LINEAR COMBINATION OF UP TO 4 VARIABLES (D(NU)*FACTOR +)
 PROMPTING FOR NU,FACTOR WILL OCCUR

ICON - Z-CONTOUR PLOT VS. X-Y VARIABLES (Z IS A NUMBER DEFINED BY ASU+B)
 PROMPTING FOR NU,A,B WILL OCCUR

ICURF - RUNNING CUBIC FIT FOR WINDOW OF 'N' DATA POINTS
 VALUE OF 'N' WILL BE REQUESTED

IEDIT - DELETE, REPLACE, INTERPOLATE, OR SMOOTH DATA
 (VALUE OF DELETE VARIABLE IS SET TO -9.999)
 PRIOR TO EDITING, PROMPTING GUIDE WILL BE DISPLAYED

IMERG - REPLACE Y-VARIABLE DATA BY EDITED AND CURVE FIT RESULTS
 OPTION TO MERGE WILL BE OFFERED AFTER PLOTTING

NSPEC - UPDATE PLOT SPEC FROM 'NSPEC'TH RECORD ON SUSPEC
 RECORDS MUST BE SEPARATED BY / IN COLUMN 1
 AFTER UPDATING NSPEC WILL BE RESET TO ZERO

NCHK - OPTION TO ABORT AFTER PLOTTING 'NCHK' POINTS
 PROMPTING TO ABORT OR CONTINUE WILL OCCUR

Figure 5.2 Description of Activatable SUATEK Options

5.2 Analytical Functions

The following functions can be performed on the data base for direct graphical evaluation and revision:

- a) Data may be selectively edited, replaced, and filtered.
- b) Data may be plotted conditionally, depending on its range or that of some other significant concurrent variable (dependency parameter).
- c) Data may be sorted according to one or more variable prior to viewing.
- d) Functional combinations of variables may be formed as the variable to be plotted.
- e) Polynomial fits to segments of the data stream can be applied and viewed.
- f) Running polynomial fits over the whole data set may be applied and viewed.
- g) Parameters determined during any of the above analysis procedures may be presented for recording and evaluation.
- h) New data formed by any of the above procedures may replace or augment the original data base.

5.3 Data Base Structure

The philosophy for a basic format for the data base for SUATEK has been the capability of handling data streams of indeterminate length, where each variable to be considered appears in each record, in standard floating binary format. The only other information necessary on such a file is a header containing

- a) Number of variables per record.
- b) Alphanumeric (axis label) per variable.

An optional plot heading label may be added. Figure 5.3 gives the specification for SUATEK files.

DESCRIPTION OF SUATEK FORMAT FILES

SUATEK FORMAT FILES FOR USE ON THE CDC-6600 ARE BLOCK TYPE 'I', RECORD TYPE 'U', BINARY FILES. THEY CONSIST OF ONE TO THREE HEADER RECORDS DESCRIBING THE DATA, FOLLOWED BY UNIFORM DATA RECORDS EACH CONSISTING OF ONE REAL NUMBER PER VARIABLE. THESE DATA ARE GENERALLY THE RESULTS OF VARIOUS ANALYSIS AND PROCESSING PROCEDURES, AND MAY BE READILY MANIPULATED AND PLOTTED USING SUATEK WITH THE SYSTEM FACILITIES AT AFGL.

THESE FILES MAY BE ACCESSED AS FOLLOWS (ASSUMED TAPE1 HERE)

```
READ(1) NOV,MN,LAE,MMA,((LBL(I,J),I=1,3),J=1,NOV)
IF(LAE.NE.0) READ(1) (MLBL(I),I=1,5)
IF(MMA.NE.0) READ(1) ((DMNX(I,J),I=1,2),J=1,NOV)
```

```
READ(1) (D(J),J=1,NOV) ..... ALL SUBSEQUENT RECORDS
```

WHERE

```
NOV - NUMBER OF VARIABLES
MN - FLAG (PRESENTLY UNASSIGNED)
LAE - -1 IF HEADER LABEL 'MLBL' FOLLOWS
MMA - -1 IF PLOT MIN-MAX RANGES FOLLOW
LBL - 3 WORD HOLLERITH DESCRIPTOR PER VARIABLE
MLBL - 5 WORD HOLLERITH LABEL (IF LAE=1)
DMNX - MIN AND MAX PLOT RANGE PER VARIABLE (IF MMA=1)
```

D - ARRAY OF REAL NUMBERS

NOTE ...

```
-9.9E99 REPRESENTS AN IGNORABLE VALUE
E.G. SAMPLE NOT PRESENT WHEN MERGING DATA
-9.0E99 INDICATES A DELIBERATELY DELETED VALUE,
FOR POSSIBLE SUBSEQUENT REPLACEMENT
```

Figure 5.3 General Specification for a SUATEK File

This specification is the simplest possible, and places the fewest constraints on the organization and development of new functional options. The header records turn out to be self-descriptive if the file needs to be examined. An important aspect of this file design is that it frequently corresponds to the sequence in which experimental data are telemetered and stored on tape. A variable that might appear say once in 64 records is identified by another subcom frame number variable, which is necessarily available in the transmission. Dependency plotting with the appropriate subcom number then achieves the desired separation.

The only additional restrictions placed on the file structure relate to two special values for each variable. Since a variable value may not exist in concurrence with others in a record, a dummy fill or IGNORE value is required to which the processing must be completely transparent. In other cases a variable value may be absent or consciously removed, and where the system is required to be aware of this break in the data. Here a DELETE value is required, which causes a break while plotting, and which may be automatically replaced during certain curve fitting procedures. The numbers assigned to DELETE and IGNORE are $-9.E99$ and $-9.9E99$ respectively, values which are extremely unlikely to be encountered.

The main objection to the above data base structure may be the inefficient use of disk file storage when a few bits worth of information is floated and stored in a full 60-bit CDC word. SUATEK could be modified to handle either the conventional or a packed file format automatically through a flag bit in the header. A packed file processing package available in the SUNY library could be adapted for this implementation.

5.4 Implementation of the Internal File Processing

The processing functions outlined in Section 5.2 are generally required to act on only two variables (X,Y), even though other dependency variables may determine which records are accepted or rejected. Subsequent stages for any complex process, e.g. edit followed by curve fit, are handled by two auxiliary files which contain only the accepted X,Y values and their record number, and which are used solely for internal reading, processing, and plotting by SUATEK. A processing pass on one of these files creates the next stage data on the other file, and this see-saw procedure is continued. Details of each analytical procedure will not be discussed, as they are extensions of conventional techniques. During a pass such as curve fitting, DELETE records are skipped, additional data are read in order to form an adequate window for the fit, and the DELETE records are replaced to form a continuous plot. Merging of the final reworked data into the original file is readily accomplished using the record number saved on the auxiliary files.

5.5 Implementation of the Interactive Modules

Acceptance of the graphics capabilities by researchers for their own use is a significant consideration. A self-prompting plot specification is displayed and forms the initial menu. The user may enter a "?" for a short description of any parameter displayed. Plot spec modification is accomplished by entries that are nearly identical to the spec display. This special input section has the virtue of permitting gradual build up of each plot specification, and of readily becoming habitual and unnoticed by the typical SUATEK user. Figure 5.4 is a summary guide for interactive input. This scheme has also been adopted for the SUACON contour plotting system. (Section 5.6)

SUATEK INPUT GUIDE

TO ENTER OR CHANGE PARAMETER VALUES:

**MAKE ENTRIES EXACTLY AS DISPLAYED.
FOR EXAMPLE: XMIN=80,XMAX=160.,NY1=3 ETC.
EMBEDDED BLANKS ARE IGNORED**

**SEPARATE ENTRIES BY ',' OR BY 'CR',
WITH A MAXIMUM OF 80 CHARS/LINE,
AND EACH ENTRY FULLY CONTAINED IN A LINE.**

**TERMINATE ENTRY BY '/' IN ANY POSITION,
OR BY '1' IN POSITION ONE.**

CONTROL IS AS FOLLOWS:

- / IN POSITION ONE INITIATES PLOTTING.**
 - / IN ANY OTHER POSITION GIVES A SUMMARY
"PLOT SPEC" STATUS PRINT-OUT, AND
IN POSITION TWO ALSO PRESENTS ALL OPTIONS.**
 - 1 IN POSITION ONE INITIALIZES PLOT MIN-MAX VALUES
FROM TAPE1 FOLLOWED BY "PLOT SPEC" STATUS SUMMARY.**
 - 1/ ADDITIONALLY DISPLAYS ALL VARIABLES AND OPTIONS.**
 - // IN POSITIONS ONE-TWO STOPS THE PROGRAM.**
-

**AN OPTION IS ACTIVATED WHEN SET TO NON-ZERO.
(SUBSEQUENT PROCEDURES ARE SELF-PROMPTING)**

Figure 5.4 Summary Guide for SUATEK Interactive Input

Output prior to and after plotting freely uses prompting requests to interact with the user, and calls for specific data or actions as the function that has been activated progresses. Cross hairs adjustment for editing proceeds in a similar manner, with the appearance of the cross hairs being the signal for user action.

Realization of some of the above functions requires interchangeable use of list directed and formatted print statements, as well as the PLOTLIB and TEKSIM libraries. Compatibility of usage between these utility packages was explored with the systems group at AFGL, and a calibration pass that was originally incorporated is now not required.

Realization of any of the interactive graphics packages must be through the CDC-6600 INTERCOM system. This system is limited to 70K_g memory, and therefore calls for an Overlay or Segmented organization of routines that need not be co-resident. This is optimized in SUATEK by branching into one of

- i) the input section
- ii) the analytical processing sections (which may have their own sub-branches)
- iii) the plot section

Data file handling and common blocks are resident at all times. File buffer sizes are set at the 64 word size of the mass storage PRU's.

The NOS/BE job control procedure language has been implemented, and the user can begin to plot with minimal effort -- viz. one command: BEGIN,SUA,TEK,M,HISFILE,ID=HISNAME.

where M is the Tektronix unit number and may also be PEN or MIC for off-line plotting purposes.

As mentioned above, pen-and-ink or microfiche plots, identical to those displayable on the Tektronix, may be initiated using SUATEK files. The data input plot requested is also identical to the entries that are keyed in on-line. Thus the user does not have to learn a second plotting system. Figure 5.5 gives the sample deck set-up for initiating these plots. Four cards for special data and labelling precede the normal SUATEK type input. Other differences are that the off-line (SUAPEN) version does not allow interactive input; values such as N for an N-point running average must be input where the prompt would normally occur. Off-line plotting is also likely to consist of multiple plots from successive files, possibly with identical plot specifications. These extra facilities are implemented in SUAPEN.

The requirement for versatile file extraction and merging capabilities, arising out of the proliferation of SUATEK format files for analyses or plots, has been supported specifically by program SUAMRG. Specific segments and variables may be selected, relabelled, and merged with or without acceptance of special variable control values such as DELETE. Figure 5.6 summarizes SUAMRG options, and shows a sample execution.

5.6 Three Dimensional Graphical Systems

Other graphical presentation capabilities are valuable for multivariable files, particularly

- i) Contour plotting
- ii) Isometric plotting

Employing different approaches, these plot forms permit introduction of another dimension for viewing and interpreting data.

```

JOBNN,CM77777.      SUATEK OFFLINE PENPLOTS      ????  YOURNAME
BEGIN,SUA,TEK,PEN,YOURSUFILE,ID=YOURID.
EOR
SCALE FAC(DEF=1.)      1  IN COL. 30 USES PLOT SPEC SET REPEATEDLY
  YOURNAME      TEL NO      (BLANK CARD)
                              (BLANK CARD)
XL=180.,XMIN=240,XMAX=420      (PLOT SPECS
NY1=2,Y1MN=0.,Y1MX=8.,Y1L=1.      IN STANDARD
NY2=3,Y2MN=0,Y2MX=.8,Y2L=4,Y2OF=1.25      INTERACTIVE
NY3=4,Y3MN=0,Y3MX=.8,Y3L=4,Y3OF=5.5/      SUATEK FORMAT)
/
      (SIMILAR ENTRIES FOR
      FURTHER PLOTS)
//
EOR

```

Figure 5.5a Sample Deck Set-up for Pen-and-Ink Plots

PENPLOT OR MICROFICHE PLOTS MAY BE MADE FROM
SUATEK FILES. NO NEW INSTRUCTION REPERTOIRE
NEEDS TO BE LEARNED, SINCE PLOT SET-UP INPUT
IS IDENTICAL TO THAT FOR ON-LINE SUATEK.

```

JOBNN,CM77777.      SUATEK MICROFICHE PLOTS      ????  YOURNAME
BEGIN,SUA,TEK,MIC,YOURSUFILE,ID=YOURID.
EOR
SCALE FAC(DEF=1.)      1  IN COL. 30 USES PLOT SPEC SET REPEATEDLY
  YOURNAME      TEL NO
MICROFICHE TITLE1 (42 CHARACTERS)
MICROFICHE TITLE2 (42 CHARACTERS)      1  IN COL. 50 FOR MODULO 7 FRAMES
XL=10.,XMIN=240,XMAX=260      (PLOT SPECS
NY1=2,Y1MN=0.,Y1MX=8.,Y1L=1.      IN STANDARD
NY2=3,Y2MN=0,Y2MX=.8,Y2L=4,Y2OF=1.25      INTERACTIVE
NY3=4,Y3MN=0,Y3MX=.8,Y3L=4,Y3OF=5.5/      SUATEK FORMAT)
/
      (SIMILAR ENTRIES FOR
      FURTHER PLOTS)
//
EOR

```

Figure 5.5b Sample Deck Set-up for Microfiche Plots

SUAMRG OPTIONS FOR MERGING TAPEA AND TAPEB

- OPTION 1 -- INTERLEAVE BASED ON MUTUAL VARIABLE
EQUIVALENCE RECORDS WITHIN TOLERANCE
OPTION 2 -- INTERLEAVE BASED ON MUTUAL VARIABLE
INCLUDE ALL RECORDS
OPTION 3 -- STACK WRITE TAPEA RECORDS
FOLLOWED BY TAPEB RECORDS
OPTION 4 -- STACK SEPARATED BY 'DELETE' RECORD

SELECT OPTION (DEFAULT 0=1) *** 0

TAPEA VARIABLES FILTER 0 DOWN LEG
1 TIME
2 ALTITUDE
3 IG
4 FILTER
5 COUNTS

TAPEB VARIABLES FILTER 3 DOWN LEG
1 TIME
2 ALTITUDE
3 IG
4 FILTER
5 COUNTS

TO MERGE ENTER NOVA, NOVB (0,0 TO EXIT)
ONE COMMON VARIABLE (NOVA.NE.0 AND NOVB.NE.0) ALLOWED

ENTER NOVA, NOVB 1,1
ENTER TOLERANCE AND RANGE (DEFAULT=0,0,0) 0.,0.,0.
ENTER NOVA, NOVB 2,0
ENTER NOVA, NOVB 5,0
ENTER NOVA, NOVB 0,5
ENTER NOVA, NOVB 0,0
TOLERANCE FOR EQUIVALENCING RECORDS SET AT .05

ENTER ALPHANUMERIC LABEL
MERGED R0D AND R3D FILES

REVISE VARIABLE LABELS? (0=NO) 0
REVISE PLOT MIN-MAX RANGES? (0=NO) 0

1 TIME
2 ALTITUDE
3 COUNTS
4 COUNTS

502 RECORDS WRITTEN TO TAPEI
END SUAMRG

Figure 5.6 SUAMRG Options and Sample Execution

5.6.1 Contour Plotting

Characteristics of the interrelationship between measurements and causal parameters can be highlighted through these presentations. NCAR (Boulder, CO) has developed a comprehensive package that offers many versions of these capabilities which are suitable for off-line use but, due to their computer memory requirements and large range of options, cannot be operated in on-line (70K₈) mode. Contour plotting is, however, a presentation that offers valuable insight in many applications, and the CONREC routines as adapted by Aiken (AFGL), were implemented for on-line Tektronix plotting. This system, SUACON, allows interactive adjustment of simple options such as frame size, axes scales and labels, and selection of contour levels to be plotted. Figure 5.7(a), (b) are two pages from the current user's guide. The binary data file must consist of a header and successive records of a fixed number of X,Z data pairs:

Record 1 - MLBL(5),LBL(3,2)

where, MLBL is a 50 character alphanumeric plot label

LBL contains 30 char X and Y axes labels

Record 2 ... NX,(X(I),Z(I),I=1,NX)

where, NX = number of X,Y pairs in each record

X(I) = X values, must be equally spaced

Z(I) = function of X,Y being contoured

Successive records represent equally spaced Y values.

A maximum of 50 records with NX < 50 is presently allowed.

This format is compatible with program ISOTEK which produces isometric plots of the same data.

SUACON - INTERACTIVE CONTOURING

Following an audit of the input data file, SUACON offers the user a number of default or activatable options for generating contour plots of the data. The options and the interaction are described using a sample session, as reproduced on the following pages.

Audit and Initial Presentation

X and Z min-max values are as encountered on the input file. Y values corresponding to each record do not occur on the file and may therefore be redefined during the plotting session. Default Y min-max values are set to the X min-max values. Entering Z directly produces the default plot of Example 1.

Options default values may be retained, or changes may be keyed in as shown underlined in the examples.

XL,YL specify the plot frame i.e. the length of the X- and Y- axes in inches (default = 8 inches)

XMIN,XMAX are the minimum and maximum for the frame range and
YMIN,YMAX establish the plot scale, given the axes lengths

XOFF,YOFF are the offsets for positioning the plot frame

Options below are off(=0) but may be selectively activated(=1)

ILABC labels the contour levels
IDASHN draws negative level contours dashed
IMOXN labels local maxima-minima levels
ILBL allows modification of header and axes labels

IPICK,NCONT are used for Contour Level Specification as follows:

Desired contour levels to be drawn must always be identified, and may also be interactively revised after viewing the plot.

With IPICK off, NCONT evenly spaced contour levels may be automatically selected as in Example 2.
With IPICK on, contour levels may be individually specified as in Example 3,
or, previously set contour levels may be listed and selectively revised as in Example 4.

Figure 5.7(a) Excerpt from SUACON User's Guide

EXAMPLE 4. ENTRIES TO PLOT WITH REVISED CONTOUR LEVELS
(LEVELS 1 & 10 DELETED)

```

***
REPEAT PREVIOUS PLOT? (1=YES)?
REVISE CONTOUR LEVELS AS FOLLOWS
EACH CURRENT LEVEL WILL BE DISPLAYED
ENTER  -1 TO DELETE A LEVEL
        0 TO RETAIN A LEVEL
        1 TO REVISE THE LEVEL

```

```

LEVEL 1 CONTOUR VALUE      .9500E+00 ?-1
LEVEL 2 CONTOUR VALUE      .9000E+00 ?0
LEVEL 3 CONTOUR VALUE      .7500E+00 ?0
LEVEL 4 CONTOUR VALUE      .5000E+00 ?0
LEVEL 5 CONTOUR VALUE      .2500E+00 ?0
LEVEL 6 CONTOUR VALUE     -.2500E+00 ?0
LEVEL 7 CONTOUR VALUE     -.5000E+00 ?0
LEVEL 8 CONTOUR VALUE     -.7500E+00 ?0
LEVEL 9 CONTOUR VALUE     -.9000E+00 ?0
LEVEL 10 CONTOUR VALUE    -.9500E+00 ?-1
DO YOU WISH TO ADD ANY LEVELS? (1=YES)?0

```

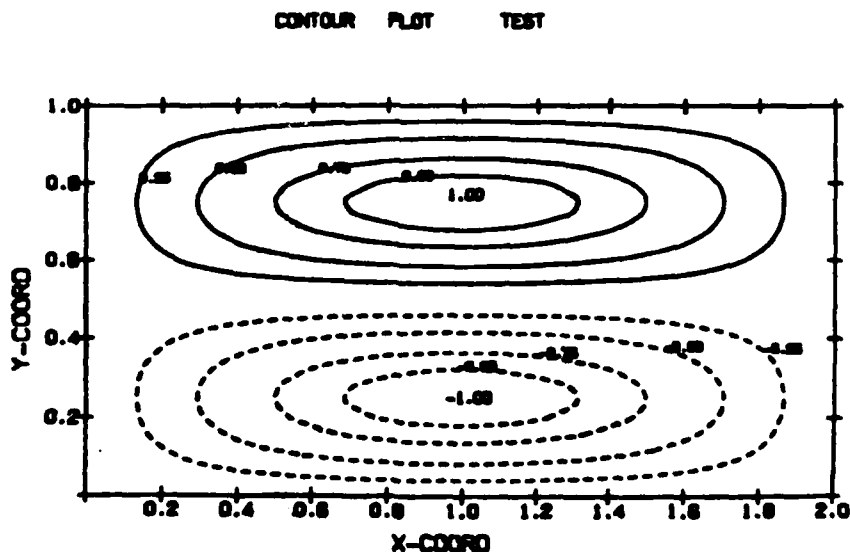


Figure 5.7(b) Excerpt from SUACON User's Guide

The Procedure

After ETL,??? for extended interactive sessions, SUACON may be set up and activated for Tektronix and associated Pen and Ink or Microfiche plotting with a single command as follows:

```
BEGIN,CON,TOUR,MODE,pfn,ID=pfid.
```

where MODE = 1 or 2 (Tektronix #) for Interactive use,
 PEN or MIC (off-line not implemented)
 If ID is omitted a local file "pfn" is assumed,
 and a local file TAPE1 is created.
 If pfn is also omitted, the default lfn is TAPE1.

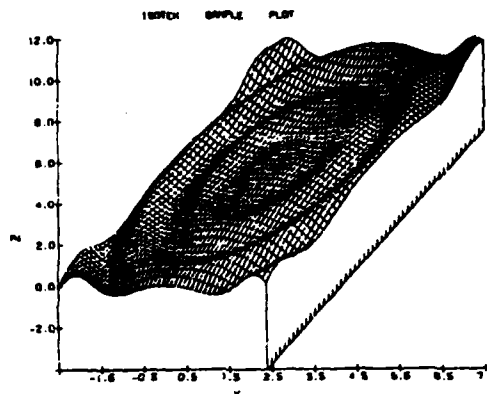
5.6.2 Isometric Plotting

Another package (ISOTEK) developed from basic principles of hidden line removal, and using an identical data base format to the one for SUACON, was developed for isometric presentations of three-dimensional data. The system simplifies the basic approach of Wray⁽²⁾ by allowing interactive selection of block min-max ranges and therefore the viewing orientation and scale. Block depiction, tick marks, cross-hatching, and other simple options are implemented. Figure 5.8 shows sample usage.

```

COMMAND- ISOTEK
ENTER START AND END RECORD NUMBERS (DEF=0,0) >0,0
ENTER PLOT BLOCK LIMITS (DEF=0,0)
XMIN,XMAX >-2.5,7.5
YMIN,YMAX >-4.12
TO HIDE LINES INTERPOLATE WITH EVENLY SPACES POINTS
ENTER NUMBER OF POINTS PER LINE (0=PLOT RAW DATA) >250
ENTER NUMBER OF CROSS LINES WANTED (DEF=0) >50
50 GRID LINES HAVE BEEN COPIED
WITH SUATEK FORMAT ON TAPE 1
STOP
060000 MAXIMUM EXECUTION FL.
7.703 CP SECONDS EXECUTION TIME.
COMMAND- SUATEK2

```



```

COMMAND- ISOTEK
ENTER START AND END RECORD NUMBERS (DEF=0,0) >25,48
ENTER PLOT BLOCK LIMITS (DEF=0,0)
XMIN,XMAX >-5.5,2.5
YMIN,YMAX >-2.6
TO HIDE LINES INTERPOLATE WITH EVENLY SPACES POINTS
ENTER NUMBER OF POINTS PER LINE (0=PLOT RAW DATA) >200
ENTER NUMBER OF CROSS LINES WANTED (DEF=0) >8
24 GRID LINES HAVE BEEN COPIED
WITH SUATEK FORMAT ON TAPE 1
STOP
060000 MAXIMUM EXECUTION FL.
5.368 CP SECONDS EXECUTION TIME.
COMMAND- SUATEK2

```

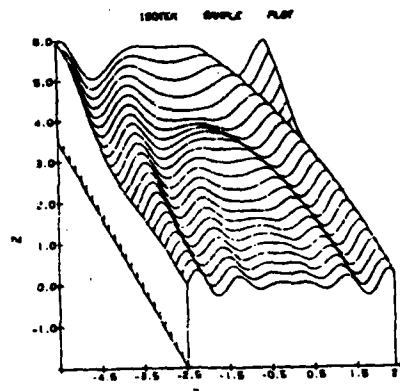


Figure 5.8 ISOTEK - Interactive Isometric Sample Plots
(An intermediate file is created for SUATEK)

References

1. Bhavnani, K.H. and McInerney, R.E., "SUATEK Interactive Graphics User's Guide", (periodically updated guide to latest features and usage).
2. Wray, Jr., W.B., "Fortran IV CDC 6400 Computer Program for Constructing Isometric Diagrams", Univ. of Calif., Berkeley.
3. Ziemba, E.J. and McInerney, R.E., "SUATEK - An Interactive Graphics Program", AFGL-TM #22, August 1979.